



3D Printed Sensor to Detect Muscle Contraction by means of Force Myography

E.A. (Eric) Perez Lorea

MSc Report

Committee:

Prof.dr.ir. G.J.M. Krijnen

Dr. M. Sartori

Ing. R.G.P. Sanders

November 2017

049RAM2017

Robotics and Mechatronics

EE-Math-CS

University of Twente

P.O. Box 217

7500 AE Enschede

The Netherlands

Abstract

With the help of new technologies used to sense signals from the human body, this project aims to design a sensor, manufactured using the 3D printing technology, to detect muscle contractions using Force Myography (FMG). FMG uses force sensors to detect the signals from the muscles during movement, mainly force sensitive resistors (FSR) and strain gauges. These sensors are easier to personalize and manufacture utilizing 3D printing.

This project uses as a reference point the increment in cross-sectional area of the muscle when it is contracting. This way a device that senses stretching like the strain gauge or a pressure sensor such as the FSR can detect the muscle activity measuring mechanical changes in the material. The sensor designed in this thesis is a 3D printed FMG band with four strain gauges that are attached to the upper arm. This band can stretch when the muscle is expanding sensing the movement of the arm.

Experiments on the material, the strain gauges and the band allowed to determine that the sensor can detect the muscle contraction and categorize the muscle movement. The 3D printed sensor presented advantages in customization and reduction on costs due to the ease of manufacture. FMG proved to be a robust indicator of muscle activity, which shows a readings similar to the muscle's behavior.

Preface

The project presented in this report is the work of my Master Thesis to graduate as a MSc. in Biomedical Engineering. I started this project because of my curiosity about the 3D printing and the human body, and I enjoyed every day working and learning about these topics. I would like to thank some people whom without this thesis would have never been possible.

To Gijs Krijnen, thank you for all the teaching, the patience, and the exhaustive feedback, but mostly, for not losing the hope on me. I am thankful for all the things I learned regarding the academic life, and I know I will be using all of them in my upcoming adventures.

To Massimo Sartori, thank you for your insight on my research, with your help my project had the correct approach to accomplish my objectives.

To Remco Sanders, thank you for your patience and your help in the Lab, I would have taken much more time doing those experiments without your help.

To Lorena, you are my cornerstone, and without you, I would not be here today. You are the reason I am motivated every day, my partner on this fantastic journey and the love of my life.

To my family, without your support, your motivation words, and your love I would never be the person I am today. This accomplishment is for you.

To all my friends, those from Mexico and those whom I met here in Enschede. You all made this time unforgettable and one of the best time in my life.

Finally, last but not least, I am grateful to CONACYT- I2T2 who honored me with a full scholarship to engage in this odyssey.

Eric Perez

Enschede, November 2017

Contents

Contents	iv
List of Figures	vi
List of Tables	ix
1 Introduction	1
1.1 Context	1
1.2 Problem Statement	2
1.3 Goals	2
1.4 Approach	2
1.5 Report Organization	3
2 Background	4
2.1 Introduction	4
2.2 Arm Anatomy	4
2.2.1 Upper Arm Muscles	4
2.2.2 Forearm Muscles	6
2.2.3 Muscle Contraction	6
2.3 Stiffness	7
2.4 Electro Myography	8
2.5 Force Myography	8
2.6 Force Sensors	9
2.6.1 FSR	9
2.6.2 Strain Gauge	10
2.7 3D Printing	12
2.7.1 Materials	13
2.8 Conclusion	14
3 Models	16
3.1 Introduction	16
3.2 Muscle Modeling	16
3.2.1 Musculoskeletal Model	16
3.2.2 Circumference Analysis	19
3.2.3 Force Model	22
3.2.4 Circumference as a measure for muscle contraction force	23
3.3 FDM Filament Model	24
3.3.1 Material Properties	24
3.3.2 Strain Gauge Model	28
3.4 Conclusion	30

4	Design	31
4.1	Introduction	31
4.1.1	Material	31
4.1.2	Printing Specifications	31
4.2	3D Printer Configuration	32
4.2.1	Infill	32
4.2.2	Line Width	33
4.2.3	Parallel Lines	33
4.3	Strain Gauge	34
4.3.1	Prototypes	36
4.4	FSR	38
4.4.1	Prototypes	38
4.5	Band	40
4.5.1	Prototypes	42
4.6	Final Design	43
4.7	Conclusion	44
5	Experimentation	45
5.1	Introduction	45
5.2	Filament	45
5.2.1	Setup	45
5.2.2	Results	46
5.3	Printed Filament	49
5.3.1	Setup	49
5.3.2	Results	49
5.4	Strain Gauge	50
5.4.1	Setup	50
5.4.2	Results	50
5.5	FMG Band Sensor	52
5.5.1	Setup	52
5.5.2	Results	53
5.6	Sensor Evaluation in Subjects	55
5.6.1	Setup	55
5.6.2	Experimental Protocol	55
5.6.3	Results	55
5.6.4	Isometric Experimentation	56
5.6.5	Isokinetic Experimentation	57
5.7	Muscle Classification	59
5.7.1	Setup	59
5.7.2	Results	60
5.8	Conclusion	62
6	Conclusions	64
6.1	Future Work	65
	Bibliography	66
	Appendix	70
	A Experimental Protocol	71
	B Ethical Committe Documents	76

List of Figures

2.1	The upper arm is formed by three main muscles: Biceps Brachii, Brachialis, and Triceps Brachii. These muscles are around one single bone, the humerus. Different muscles are activated when different movements are performed. As the arm is being flexed, the biceps and the brachialis are activated, and when the arm is extended, the triceps brachii performs most of the work.	5
2.2	Muscle architecture related to pennation angle. Muscle fibers can be oriented parallel to the muscle axis that generates force, <i>a</i>)Longitudinal, at a fixed angle, <i>b</i>)Pennated, or at multiple angles, <i>c</i>)Multi-pennated. This figure shows idealized view of muscle architecture [1].	6
2.3	Muscle contraction. During the isometric contraction, the muscle contracts without presenting movements. The isotonic contraction is defined as concentric contraction when the muscle shortens, and as an eccentric contraction, when the muscle elongates.	7
2.4	The FSR consist of two membranes separated by a thin air gap, which is maintained by a spacer. When pressed the carbon layer shorts the two traces with a resistance dependent on the applied force. Figure obtained from [2].	9
2.5	Basic design of a strain gauge. The strain gauge is connected through the terminals. The gauge reacts in two different ways, when the area narrows the resistance increases, when the area thickens the resistance decreases.	10
2.6	Effect of stretching and contracting a material.	11
3.1	Hills model configuration illustrating the passive series element (<i>SE</i>) and the contractile element (<i>CE</i>) in parallel with the passive element (<i>PE</i>). The model shows the total force exerted as the summation of the force in the series element and the passive element ($F_{total} = F_{se} + F_{pe}$)[3]	17
3.2	Zajac adaptation of the Hill's model related to the tendon length (L_T), the muscle length (L_M) and the musculotendon length (L_{MT}). It also considers the real pennation angle for the muscles [4]	17
3.3	Active and Passive Force Length Relation. The plot obtained from Garner and Pandy [5] represents the behavior of the muscle isometric force. Active muscle force in a range between $0.5 L_{Mo}$ to $1.5 L_{Mo}$ (solid line), and passive force when muscle is stretched beyond its optimal length L_{Mo} (dashed line).	18
3.4	The diagram shows the importance of the slack length of the tendon, which determines the size and strength range of the muscle. While having a large slack length (1) the muscle excursion is small. On the other hand, when tendon slack is small, the muscle excursion is large. It also shows the relation to the optimal muscle-fiber length (L_{Mo}) and the physiological size of the muscle [5].	19
3.5	Approximation of the upper arm muscles, 1) shows an approximate axial view of the muscles surrounding the humerus (upper arm bone). 2) shows a representation of cylindrical form, two heads of the biceps, one for the brachialis and three heads of the triceps.	20

3.6	Both plots show the increase in circumference while the muscle length is decreasing, the value may differ from real due to the approximation of fat and veins in the upper arm.	22
3.7	Free body diagram of the arm, while holding a load.	23
3.8	Change in force related to the increase in circumference of the upper arm. Left plot shows the absolute values and right plot shows the fractional change.	24
3.9	Various expressions from the Equation 3.13*, calculating $\frac{\Delta R}{R_0}$ assuming $\nu=0.5$ with and without second order term. All results are not considering the piezoresistive effect, except for the lowest curve using Equation 3.16, has a negative piezoresistive coefficient ρ_σ	26
3.10	Geometric and Material inputs in the resistance value when the filament is elongated	26
3.11	Combined contribution in resistance behavior during the elongation of the conductive material.	27
3.12	Strain gauge first model	28
3.13	Diagram that represents the behaviour of the material while stretched based on the poisson strain.	28
3.14	The change resistance considering the linear contribution of the of the strain gauge and the input of the material electrical properties according to Equation 3.16 . . .	29
4.1	A dual Flexion Extruder that allows better control of the flexible filaments. Image obtained from [6].	32
4.2	Object to test the different types of infill.	33
4.3	Comparison of the trial with the desired design for testing different types of linewidth.	34
4.4	Figure of the trial lines that were tested. 1) is the printed structure and 2) is the design desired.	34
4.5	The methodology for the process of designing new objects.	35
4.6	First design of the strain gauge. Dimensions in mm	36
4.7	Strain gauge second design. Dimensions in mm	37
4.8	Strain gauge final design	38
4.9	First prototype of the FSR sensor.	39
4.10	Second prototype of the FSR sensor, with support lines to be later removed	39
4.11	Third prototype of the FSR sensor, printed with a different orientation.	39
4.12	First design of the band proposed using a support base.	42
4.13	First design of the band proposed without support base.	42
4.14	Second design of the band proposed.	43
4.15	Third design of the band proposed.	43
4.16	The selected design for the band contains different extensions allowing the sensor to be adapted to different users.	44
4.17	Measurements of the final band including the optimized strain gauges.	44
5.1	Setup used to stretch the filament while testing the resistance changes.	45
5.2	Resistance measured while filament is stretched 9%	46
5.3	Computed resistivity of the filament tested	46
5.4	Filament measured up to breaking point	47
5.5	Two samples of material tested under the same conditions to determine its repeatability.	48
5.6	Final value of the fractional resistance for both samples of material	49
5.7	Relative resistance changes of the printed filament while stretched.	50
5.8	Resistivity of the material computed for the printed filament.	50
5.9	Measurement of three strain gauges with same dimensions a design. The fractional change is consistent between the three prototypes.	52
5.10	Resistivity of the material computed for the three gauges.	52
5.11	System used to test the band, the tube increases in size uniformly, allowing to test the band stretching and measure the circumference simultaneously.	53

LIST OF FIGURES

5.12	Initial measurement of the band.	53
5.13	Measurement of the band stretching 6 times.	53
5.14	Drift analysis of the band, its absolute resistance values and the relative change.	54
5.15	Hysteresis of the band showing the drift between the first measurement and the sixth.	54
5.16	Sensor signals from Subject #2 while performing an isometric contraction every 8 sec with a 5 kg load. Blue rectangles represent the time during the upper arm contraction.	56
5.17	Mean of the EMG and FMG signals during isometric contraction for each subject and its standard error.	57
5.18	Sensor signals from Subject #1 while performing contraction every 8 sec at 60 BPM with a 3 kg load. Blue rectangles represent the time during the elbow flexion and extension.	58
5.19	Mean of the EMG and FMG signals during isokinetic contraction for all the subjects and its standard error.	59
5.20	Movement to test muscle classification of the FMG sensor, flexing the elbow joint at 50BPM with a 3kg load.	60
5.21	Fractional change of Biceps and Triceps movement during concentric contraction at 60BPM with a 3kg load of subject #3.	61
5.22	Mean values of the measured Biceps and Triceps signals, with the mean subtracted result.	61

List of Tables

2.1	The table shows the specifications of the materials tested to design the device . . .	13
3.1	Muscle architecture of the upper limb. The table presents a recompilation of different authors that obtained information of the upper body through different studies. The measurements are average data from male patients between 25-45 years old . .	21
4.1	The eight different prototypes vary only in line width and line shape. All the models have the same base measurements and the same length for the sensitive material. The conductive material was printed at 1500 mm/min with a layer height of 0.15 mm for a complete thickness of 0.5 mm.	37
4.2	Comparison of force sensing technologies.	40
5.1	The eight different prototypes vary only in line width and line shape. All the models have the same base measurements and the same length for the sensitive material. The conductive material was printed at 1500 mm/min with a layer height of 0.15 mm for a complete thickness of 0.5 mm.	51
5.2	Table with the results of the paired t-test, showing the <i>P</i> -values for the comparison between the strain gauges of each subject while detecting biceps and triceps simultaneously.	62

Chapter 1

Introduction

1.1 Context

There is a steadily increasing research activity dedicated to the development of technologies that enable the acquisition of signals from the human body. This activity is aimed at signals related to the physiology and the biomechanics of the human body, targeting the enhancement of the quality of the interface between the individual and his/her environment.

Muscle contractions physiological activities that have lately been studied in various disciplines with the objective to accurately acquire its corresponding signals. The data obtained from the muscle can be used in many different fields, from rehabilitation and up to human-machine interfaces.

Currently, the most used technology to detect muscle activity by EMG sensing; electromyography (EMG) is the technique to acquire the signal that the skeletal muscles produce when they are active. The convenience of using it, the quality of signal and the costs of the EMG electrodes make this technology an attractive method. However, the signal acquired depends on many characteristics of the patients, e.g. their skin, and the way the electrodes are connected, this can disturb the reading of the signal and add noise or other non-necessary interference to the actual reading.

Force Myography (FMG) features as a more robust alternative to conventional EMG, this type of reading is less susceptible to measurement noise, and it can be as accurate as EMG when correctly designed and used[7]. Essentially, FMG senses the change in shape of the muscles when activated, allowing to easily and conveniently detect contraction or movement of the targeted limb.

Since the sensor technologies are evolving and becoming more complex, new manufacturing technologies are also being developed. The 3D printing, also known as additive manufacturing, is one of the new technologies being investigated to enable the manufacture of devices. Due to its low costs and rapid deployment, applying 3D printing to the medical field has improved the fabrication of prototypes and reduced the lead time.

Using 3D printing to create an FMG sensor takes the advantages of both technologies. It makes possible to create a customizable sensor, comfortable and economical, that can sense the muscle activity without much interference. When the sensor is designed, it allows developing a technology with specific functions and characteristics not found in commercial sensors. Some advantages that a 3D printed sensor for FMG provides are the improvement of features enabling categorization of the muscles, better adaptability to different environments and modifications of the output without the need for complicated electrical interfaces.

The project here presented, aims to combine the innovation of the additive manufacturing and the force myography to develop a sensor able to detect the muscle activity, in an easy way and with reasonable accuracy.

1.2 Problem Statement

Force myography is presented as a robust alternative to detect the muscle activity while reducing the complexity of the signal acquisition. These type of sensors can be adapted to the patient needs, decrease the preparation of its use and ease the post processing of the signal obtained.

The use of 3D printing to manufacture force sensitive devices is a field seldom studied. It is important to explore the use of force sensitive devices, its properties and the configuration needed for them to perform efficiently. The selection of the material used to manufacture the sensor also plays an important role, regarding the mechanical behaviour of the device and its conductivity.

With a proper characterization of the technology and the materials to design the device, it is possible to develop a reliable FMG sensor to detect the muscle activity.

1.3 Goals

This research project focuses in to develop a force sensitive device able to detect the muscle contraction using force myography. The project has two primary objectives. First, to select a proper force sensing technology and use it to design a customizable sensor able to adapt to the muscles of the upper arm. Second, to evaluate the designed sensor to identify the muscle activity correctly, the data obtained has to be analyzed to detect reliability and repeatability of the technology.

To successfully accomplish the second objective, some research questions were established:

- Is it possible to relate the change in resistance of the sensor with the increase in cross sectional area of the upper arm?
- Can the contraction be related to the variation of resistance in the sensor?
- Are the resistance measurements repeatable?

1.4 Approach

The method to successfully answer the research questions is described below.

The force sensors can detect the deformation of the muscle where they are attached. To detect if the arm is going to change its shape enough to deform the force sensors, it is essential to model the behavior of the muscles tested. Based on the biomechanics of the muscles it is possible to evaluate their performance with a proper model that allows comparing the mechanical characteristics of the muscles with the properties of the materials selected to design the device. Due to the limited knowledge about the materials used in 3D printing, several tests have to be conducted. The manufacturer provided some mechanical and electrical specifications, but a characterization of the material will provide complete and actual information about their properties.

Another feature regarding the additive manufacturing is the different parameters that allow the customization of the manufactured prototypes. Since the devices are likely to be multi-material, the 3D printer requires a correct configuration of these properties, such as the temperature, the velocity of printing and the correct filament extrusion. For this purpose, several tests will help to identify the critical parameters needed for an optimum manufacturing.

It is important to select the optimal technology, the sensing principle, the materials and the correct designing protocol to develop a sensor that detects the muscle activity. Therefore, different force sensors are tested and modeled to select an appropriate one. With the material characterized and the sensor selected a model of the device is the next step to determine if the technology will be adequate to characterize muscle behavior.

After understanding the functioning of the material and being sure that it can be adapted to the muscle behavior, the following action is to design the sensor. For this purpose, some requirements, and guidelines are established, supported by a designing methodology.

Finally, with a working sensor that fulfills the requirements, an experimental protocol is proposed to determine if the device can detect the muscle activity correctly in different subjects. The experimentation proposed will help to determine the functioning, the comfort, and the safety of the designed device.

1.5 Report Organization

The introduction chapter of this report presents the motivation of the project and the general approach to fulfill the objectives proposed. Chapter 2 gives a brief introduction to the basic concepts related to the project. Chapter 3 focuses on a description of the mathematical models, regarding the muscles of the arm, the sensors used, and the results after comparing them with real measurements. Chapter 4 explains the methodology used to design the device and describes the characterization of the materials. The requirements and specifications of the sensor are also explained. The experimentation protocol the procedure and its results are presented during Chapter 5. Finally, chapter 6 concludes the project work and comments on the possible future work for this innovative technology.

Chapter 2

Background

2.1 Introduction

To put the project's theoretical framework into perspective, the following background knowledge is presented regarding the techniques and materials employed. The sensor designed in this assignment is aimed at measuring the muscle contraction. Thus, a brief description of the muscles in the upper arm and information about the technologies used in the force myography is also given. In the end, a short literature overview of some previously published work related to the new developments in the area of force myography is presented.

2.2 Arm Anatomy

In the current section, a detailed description of the anatomy, including location and muscle composition of the arm will be provided.

The human arm is the limb attached to the neck in the upper part of the body. Based on its components and joints, it is divided between the shoulder, upper arm, forearm, and hand. The shoulder is the joint attached to the neck and the trunk; the upper arm is the segment between the arm and the elbow joint and contains one bone, the humerus. The forearm is the section between the wrist and the elbow and contains two bones, the lateral bone named radius, and the medial bone, the ulna. Finally, the hand is located after the wrist joint.

The human arm is highly mobile at the moment of positioning the hand in space. The elbow joint located between the upper arm and the forearm has major movements denominated: flexion and extension. At the other end of the forearm, supination and pronation occur. The pronation happens when the hand turns 180 deg due to radius bone going over the ulna, and supination is when the hand goes back to its natural anatomical position from a pronated position. The wrist has major movements being able to perform several movements such as adduction, abduction, extension, and flexion. These movements are possible due to the activation of muscles from the forearm.

The objective of this project is to detect activation of muscles from the upper arm since those muscles, as presented by Gray et al. [8], contain more muscle fibers than other muscles in the human body and are more predisposed to expand further while being contracted.

2.2.1 Upper Arm Muscles

The upper arm is positioned above the elbow joint, and it contains two compartments of muscles: the posterior compartment, with muscles that extend the elbow joint, and the anterior compartment, with muscles that mainly flex the joint.

The anterior compartment contains three muscles, the coracobrachialis, brachialis and biceps brachii. The posterior compartment contains the triceps brachii, as shown in Figure 2.1. A brief

description is now given for each of these muscles.

Anterior Compartment:

- The coracobrachialis is located from the shoulder innervating at the middle of the humerus, and it is in charge of flexing the upper arm at the shoulder joint.
- The biceps brachii is a two-headed muscle that has no attachment to the humerus itself. It is attached to the forearm on one side and to the shoulder on the other. The biceps brachii is a powerful flexor of the forearm at the elbow joint, and an essential supinator of the forearm when the elbow is flexed.
- The brachialis muscle is beneath the biceps brachii muscle, and it flexes the forearm at the elbow joint [8].

Posterior Compartment:

- The triceps brachii is the only muscle in the posterior compartment of the arm. It has three heads that converge into a large tendon inserting into the ulna. The triceps brachii is the muscle in charge of extending the forearm at the elbow joint.

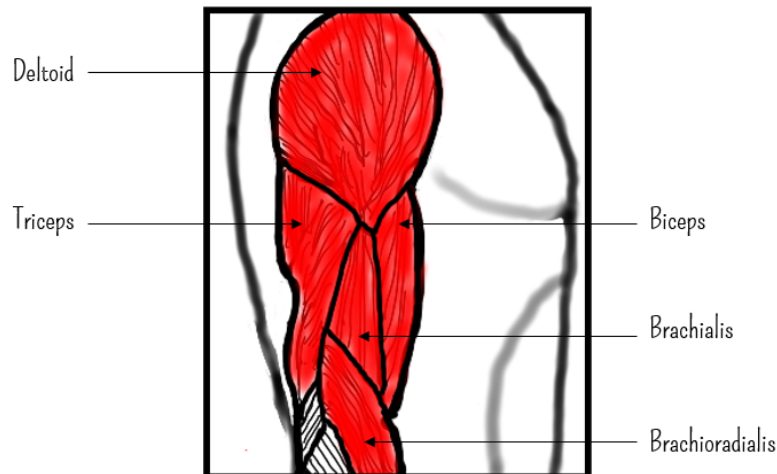


Figure 2.1: The upper arm is formed by three main muscles: Biceps Brachii, Brachialis, and Triceps Brachii. These muscles are around one single bone, the humerus. Different muscles are activated when different movements are performed. As the arm is being flexed, the biceps and the brachialis are activated, and when the arm is extended, the triceps brachii performs most of the work.

The muscles of the upper arm are typically attached to a bone over a significant region known as the line of pull or line of action. This line describes the direction of the muscular force, and its relationship with the axis of rotation of a joint determines the action that the muscle produces. When there is an angle between the line of action and the muscle fibers it is called the pennation angle. This angle can affect the way the muscles are contracted, by elongating or compressing the muscle fibers in different directions. The Figure 2.2 shows the types of pennated muscles in the human body. The muscles contained in the upper arm have a pennation angle. While the biceps brachii and the brachialis have an angle between 1 deg and 3 deg, the triceps is about 15 deg pennated [9].

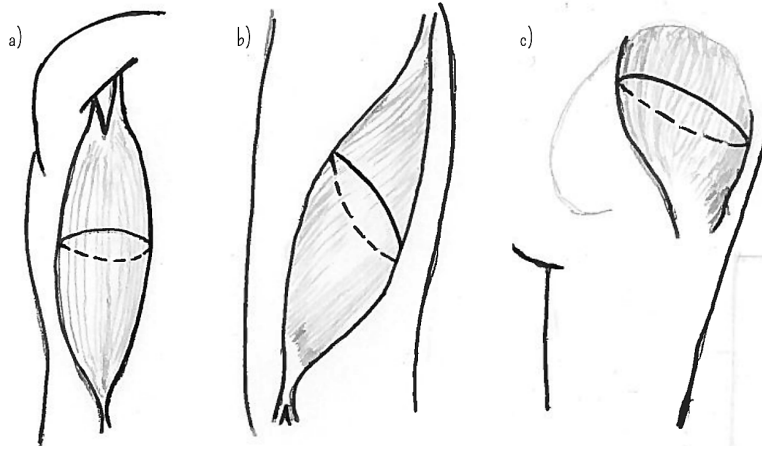


Figure 2.2: Muscle architecture related to pennation angle. Muscle fibers can be oriented parallel to the muscle axis that generates force, *a)*Longitudinal, at a fixed angle, *b)*Pennated, or at multiple angles, *c)*Multi-pennated. This figure shows idealized view of muscle architecture [1].

2.2.2 Forearm Muscles

The forearm is the section of the arm located between the elbow joint and the wrist; it contains the bones ulna and radius. Its muscles are associated with movements of the wrist joint, flexion of the fingers and thumb, and pronation. The forearm is also divided into two compartments, anterior and posterior:

- The anterior compartment contains the muscles related to the flexion of the wrist joint: flexor carpi ulnaris and radialis, pronator teres, palmaris longus, flexor digitorum superficialis and profundus and flexor pollicis longus.
- Muscles in the posterior compartment are mainly in charge of the extension of the wrist joint: extensor carpi radialis longus and brevis, extensor digitorum, extensor carpi ulnaris, anconeus, supinator extensor pollicis longus, and brevis, among others. [8]

Most of the muscles are only activated when the hand performs movements. The high amount of muscles in the forearm is related to the high capacity of the hand to perform delicate movements. [8]

2.2.3 Muscle Contraction

The human arm is denominated as a musculoskeletal system, as it contains mainly muscles and skeleton. A relevant characteristic of these type of systems is they can willingly perform muscle contractions. The phenomenon that describes contractions is presented in the following section.

Muscle contraction happens when the muscle fibers are generating tension. The muscle does not necessarily shorten when contracted and the muscle tension can be produced without a change in length. Frequently, the muscle contraction is described through two factors: length and tension. Based on those factors, it is divided into two categories, isometric contraction, and isotonic contraction [10].

Isometric contractions happen when the muscle produces tension without changing length. On the other side, isotonic contraction occurs when the muscle changes in length but the tension remains constant. Isotonic contraction is at the same time subdivided into eccentric contraction, which happens when the muscle's length increases, and concentric contraction when the muscle's length shortens [10].

According to a research on modeling of muscle tissues made by Spyrou and Aravas [11], the skeletal tissue has a Poisson's ratio between 0.45 and 0.5 thus, is considered incompressible. When

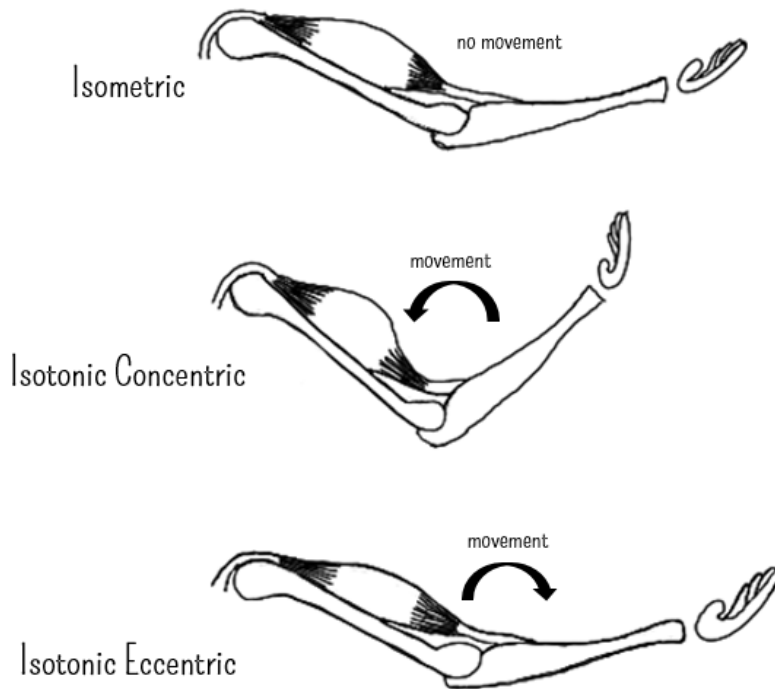


Figure 2.3: Muscle contraction. During the isometric contraction, the muscle contracts without presenting movements. The isotonic contraction is defined as concentric contraction when the muscle shortens, and as an eccentric contraction, when the muscle elongates.

the muscle contracts its cross-sectional area changes, which could be an indication that all the muscle fibers are expanding at the same rate. However, the relation between the size of a muscle and its contraction depends on the muscle architecture.

There are two types of cross-sectional areas, anatomical and physiological. The anatomical cross-sectional area (ACSA) is the area of the muscles widest point and perpendicular to the length of the muscle. When the muscle fibers are in parallel, the ACSA cuts across the muscles indicating the cross-sectional area of the muscle fibers. However, if the muscle is pennated, the ACSA cuts across only one portion of the muscle, without being a uniform cross-sectional cut [12]. The standard measure used to approximate the number of muscle fibers in a muscle is the physiological cross-sectional area (PCSA). The PCSA cuts through all the fibers of a muscle regardless being pennated or not [13].

When there is a change in the cross-sectional area of the muscle, there is an activation of the muscle considered as a muscle contraction. Independent of the type of contraction, the muscle activates every time it performs a movement, which can be tracked by different techniques such as ultrasound, EMG, FMG, among others.

2.3 Stiffness

The human arm has mechanical properties used to stabilize its joints during different movements and tasks. An impedance component used to maintain the stabilization is this stiffness, which is especially important during posture maintenance [14]. When related to the human arm, stiffness can be categorized in two different ways:

- By its relation with the components of the limb, it can be classified in muscle stiffness, joint stiffness, and end-point stiffness. The muscle stiffness is in the connective tissue and the muscle fibers. The joint stiffness is given by the amount of torque increment per unit of joint

angular reflection [15]. Moreover, the end-point stiffness is the one expressed at the limbs extremities.

- Related to the source of forces that create muscle deformation, stiffness can be divided in passive or active. When the muscle deforms due to an external force applied to it, it is known as passive stiffness. When the muscle generates the force is active stiffness; the one produced by the muscle contraction.

The muscle can modify its stiffness over time according to the task that is performing. During an initial strain, the muscle behaves as an elastic spring. At this moment the muscle undergoes an initial length change and presents a high stiffness over a short period of time, which is identified as short-term stiffness. But beyond a certain amount of force, when the variation of length continues, the stiffness drops and the muscles starts presenting a viscous behavior [16].

The stiffness of the muscle affects the velocity of the contraction. As mentioned before there are different techniques targeted to measure the movement in muscles. Below, there is a description of these techniques.

2.4 Electro Myography

Electro Myography or EMG is a technique that records and evaluates the electrical activity produced by the skeletal muscles. EMG uses electrodes to detect the electrical potential from the muscle cells when these are neurologically activated [17].

Currently, there are two types of EMG, surface (sEMG) and intramuscular. The use of sEMG has many advantages providing a safe, comfortable and noninvasive technology for detecting muscle contraction.

This technique allows to observe the muscle energy throughout the movements and with a proper sensor array, to differentiate aspects of the muscle architecture. However, it has also significant disadvantages. The EMG is limited to monitor few muscle sites, and it cannot interpret when another group of muscles activates the same movement. However, the main weakness is the possibility of "cross-talk," a phenomenon where energy from one muscle group travels to the recording field of another group. It may make challenging to isolate the signals from the muscles targeted [18].

Due to these and other limitations on the electromyography, the investigation of muscle sensors is motivated to finding new alternatives to develop better technologies aiming to detect biosignals with robustness and accuracy [19].

2.5 Force Myography

Force myography (FMG) emerges as an alternative technology that utilizes force sensitive devices to detect muscle activity [20]. FMG was proposed under the assumption that it is possible to use pressure sensors around the muscle to map different movements [19] detecting distinct muscles activated at the same time.

The movements of the wrist joint are controlled by the muscles contained in the forearm known as extrinsic hand muscles. When the forearm is activated, some muscles expand outwards and some inwards from the surface. This expansion results in pressure change observable at the skin of the forearm. If categorized, forearm movements can represent specific actions of the hand and the wrist. The same behavior is present in the upper arm muscles when the elbow joint moves. The expansion of the biceps and the triceps are more prominent due to the increased size of the muscles. This expansion is measured by force sensors utilizing the force myography.

Nowadays, FMG is used to detect the shape changes of the muscles during contraction using mainly force sensitive resistors. While the muscles contract and move, the deformation of the muscles exert a force in the sensors fixed to the targeted muscles [21].

FMG has some advantages compared to other myography techniques. Compared to EMG, force myography is robust to external electrical interference, skin sweating or humidity, it is less expensive and easy to implement and use [7]. Using FMG makes it uncomplicated to quantify the muscle activation caused by changes in the muscle shape. It can measure the kinetic activity during the muscle contraction and also senses any external changes and radial pressure occurring.

In the end, FMG does not measure the muscle activity directly, but through mechanical deformations. In that sense, EMG, as a direct representation of the muscle activity, may be expected to be a better way to determine the muscle contraction, as long as the electrical interference and the motion artifacts can be kept controlled. The FMG may also cause some mechanical loading due to the elastic band where the sensors are attached.

2.6 Force Sensors

In the following section, some details about the force sensors utilized in force myography will be laid out.

A force sensitive sensor (FSS) is a device, mainly electromechanical, able to detect changes in force often as a mechanical transducer. FMG is often implemented utilizing force sensitive resistors (FSR). However, there are two main types of sensors that can be used in FMG, the strain gauges, and the FSR.

2.6.1 FSR

FSR is one of the sensors typically used in force myography, mainly because of its ability to measure pressure points caused by a variation of muscle deformations. A force-sensitive resistor described best by its flat shape, which functions by displaying a decrease in electrical resistance when normal pressure is applied on it [22].

FSR typically consists of two polymer layers, a semiconductive film on one side and a conductive pattern on the other. The films are facing together but separated by a thin air coating; this separator allows the device to have a high resistance when no pressure is applied. As more pressure is applied to one layer of the FSR, the contact between the two films increases. Thus, the bigger the acting force, the less resistance the FSR provides [23].

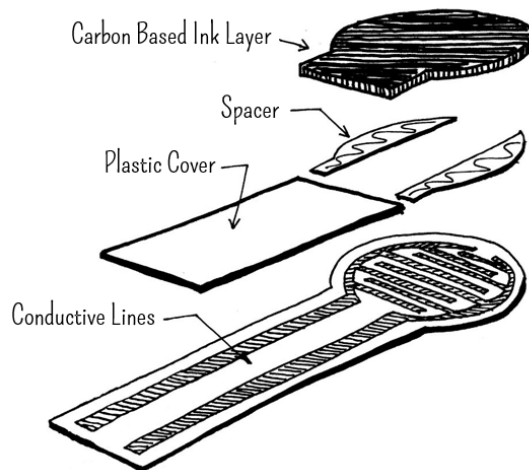


Figure 2.4: The FSR consist of two membranes separated by a thin air gap, which is maintained by a spacer. When pressed the carbon layer shorts the two traces with a resistance dependent on the applied force. Figure obtained from [2].

Unlike other piezoelectric transducers, the FSR is a slow sensor, due to its dependence on force,

which allows it to be insensitive to vibration and acoustic noise. Compared to other force sensors, FSR is advantageous due to its low cost, reduced size, and excellent shock resistance, being also able to operate in moderately under extreme circumstances such as low temperatures or dynamic systems. However, despite its good force sensing, it lacks in terms of providing high accuracy.

The FSR is not a pure force or pressure sensor since its output depends on the part and size of the sensor addressed, the type of actuator, and the ratio of the area of the applied force [22]. A significant advantage of FSR is its impedance, being purely resistive greatly simplifies electrical interfacing. Analog interfaces are simple because the FSR is placed in series with a current source and the voltage measured across the FSR is then computed to determine the resistance using Ohms Law.

FSR is a low-profile, unobtrusive device, with a smooth interface and easily arrayed that has a long life service. However, due to its accuracy limitation ($\pm 15\%$), a strain gauge or a load cell is a more viable option for applications that need better accuracy or detection of small changes of force [22].

2.6.2 Strain Gauge

On the other hand, the strain gauge is a measurement device that calculates the stress in a body

When a force is applied to a body, the body deforms. This deformation is known as a strain. It is possible to define a strain as the deformation of a material or an object per unit length or fractional change in length. This deformation can be positive if the body is stretched or negative if it is compressed. The fundamental relationship between the mechanics of a given the material and its strain is the stress applied to the body. The stress in the material has to be computed through measurable parameters. Thus, with a determined strain and the properties of the material, the applied stress can be calculated using a strain gauge.

The typical metal-foil strain gauge takes advantage of this effect to determine mechanical properties by measuring electrical properties, which depend on the body deformation of the gauge. An essential electrical characteristic that varies in proportion to the strain is the electrical resistance, fundamental in the design of piezoresistive or semiconductor gauges.

The mechanic behavior

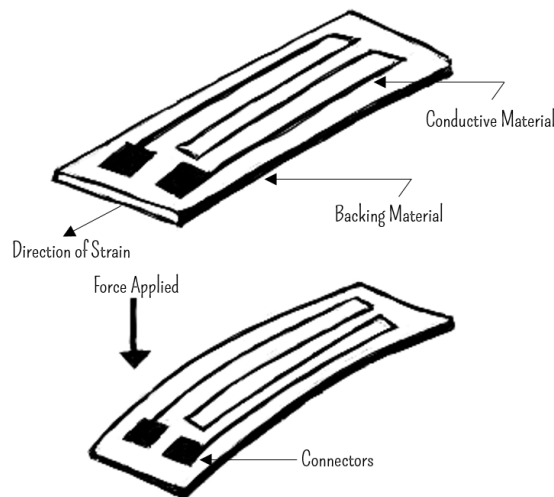


Figure 2.5: Basic design of a strain gauge. The strain gauge is connected through the terminals. The gauge reacts in two different ways, when the area narrows the resistance increases, when the area thickens the resistance decreases.

The semiconductor strain gauge which is the one used in this project considers the piezoresistive effect of specific materials to produce an elastic behavior, this way it is possible to produce positive

or negative resistance changes when is strained. The strain gauge can be physically small while maintaining their high nominal resistance. Semiconductor gauges show a high sensitivity to strain, but the variations in resistance to strain are nonlinear. Their resistance and their output are temperature sensitive [24].

When the conductive material of the strain gauge is deformed in the axial direction, its length will change, and its cross-sectional area will change as well due to the property of the material known as Poisson's Ratio. Figure 2.6 illustrates the behavior of the strain gauge when stretched.

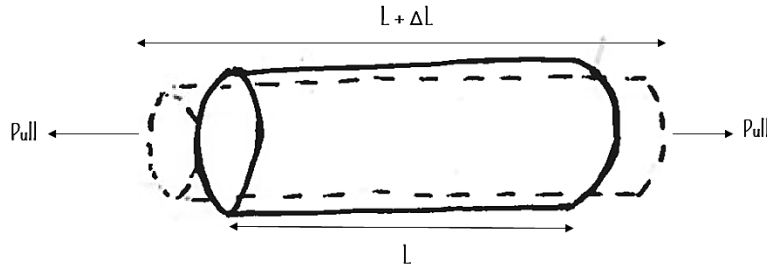


Figure 2.6: Effect of stretching and contracting a material.

The strain gauge will change its form while deformed according to the change in length (ΔL), which is a function of the material properties and the ratios of longitudinal and transverse strain [25].

An essential characteristic which varies in proportion to the strain of the gauge is the electrical resistance. [26].

The strain gauge resistance can be expressed as $R = U/I$ where U is the voltage across the gauge, I is the current passing through it, and R is the gauge resistance. When the resistance changes from R to $R + \Delta R$, the voltage, the current or both, will also be modified. Therefore, change in resistance can be measured in two ways, with constant voltage or with constant current.

- **Constant Voltage.** When the voltage stays constant, the current will change according to the variations in resistance; then it is possible to determine the resistance of the gauge by measuring the current through the gauge.
- **Constant Current.** If the current stays constant, there will be changes in the voltage drop across the gauge while the resistance is changing, thus, determining the electrical resistance of the gauge is possible by measuring the voltage drop in the strain gauge.

Measuring the resistance with a constant current could be most effective when dynamic strain is being measured. If a dynamic force is causing a change in the resistance of the strain gauge, the time between the change in voltage is measured, thus small changes in lead resistance due to temperature variations can be neglected.

Semiconductor gauges with a constant-current measurement are more likely to detect small changes due to muscle deformation. The performance of the strain gauge designed for this project will depend on the materials used, the resistivity of the material has a high input on the resistance changes of the strain gauge.

For the strain gauge used in this project a measurement using constant current suits better. Since the current is more harmful than the voltage to the human body [27], a measurement using a constant current is utilized.

The damage produced by current depends on several factors and can cause a slight sensation in the hands or a heart fibrillation, depending on exposure conditions, current magnitude, and duration. The safe values of current are between 1 mA and 5 mA [27]. It is safer then to have a small value of current constant with standard voltage variations than a variable current due to high resistance values

The properties of its conductive material make the absolute value of resistance of the strain gauge less predictable, being that the material is exposed to high temperatures and is modeled in different shapes and forms, affecting the conductivity of the material. The unexpected behavior of the material can cause high values of current, which can cause discomfort to the users of the sensor.

With a constant current measurement, the voltage values will not exceed the range of volts (v^1) when the resistance reaches values of $1\text{ M}\Omega$ if the current is always $I = 1\ \mu\text{A}$.

Utilizing different materials during the construction of the strain gauge allows obtaining different results conductivity, hence in resistance values. It also depends on the type of manufacture which allows customizing, at a certain extent, the form and size of the gauge.

2.7 3D Printing

Layer manufacturing (LM), also called 3D printing, rapid prototyping (RP) or additive manufacturing, is a technology to create a three-dimensional object. It has been a revolutionary development in the field of manufacturing for the past two decades [28]. Rapid manufacturing uses physical or chemical phenomena to build parts by adding material layer by layer. This process was first introduced in the late 80s according to Kurt [29], with the stereolithography (SL). This technique uses liquid-based process using photosensitive polymer.

From this technique, many others technologies were developed including fused deposition modeling (FDM), ink jet printing (IJP), 3D printing (3DP), selective laser sintering (SLS) laser vapor deposition (LVD), among others. This broad range of technologies makes possible to print in a great variety of materials, from metals and polymers to concrete and even food. According to a sales analysis [30], the most popular and commercial available LM processes are SL, FDM, and SLS.

FDM is the technique used to manufacture the sensor of this project. It was developed by Stratasys, Inc. [31] and offers functional plastic prototypes with Acrylonitrile butadiene styrene (ABS), polycarbonate, polyphenylsulfone (PPSF), and other materials. These materials are produced from custom blends of commercially available thermoplastic resins, making material properties one of this technology's strong points.

The FDM process consists of building by deposition of semi-molten polymeric materials onto a base plate or a previously solidified material. The solidification happens by cooling the material on the colder underlying layers. The material is obtained from a solid filament of thermoplastic material fed into an XY controlled extrusion head. After that, the material is brought near above the melting point to ensure resolidification by natural cooling. The flow rate is adapted to the head traveling speed, to achieve the desired layer thickness and laminate width. When using FDM, some parts still could seem rough and is less suited for small details [29]. However, it provides the resolution necessary to produce the sensor of this project.

The process to build an object using additive manufacturing can be described in nine steps below described.

1. Generation of the geometric model using a computer-assisted design (CAD)
2. The geometric model is then translated into a tessellated version of a CAD, a process where the surface of the CAD is piecewise approximated using one or more geometric shapes [32]. The result is a Standard Tessellation Language (STL) format.¹
3. The STL file is then examined to detect flipped triangles, bad edges or hidden lines that could affect the slicing of the figure.
4. Determine the optimal orientation, considering the surfaces of the object and the capabilities and limitations of the machine, such as the largest and most exact plane at the bottom [34].

¹There are additional formats to tessellate the CAD model, depending on the CAD software and the printer [33].

5. Slice the STL file using software dedicated.
6. Provide support to overhanging features of the object.
7. Define the toolpath for the material deposition for the model and the support.
8. Manufacture of the prototype.
9. Finally, post-processing of the object. Removing and cleaning excess material adhered to the part.

FDM has been rapidly developed in different fields to improve the manufacturing of new objects. New devices are recently adapted for a consumer-oriented use. The advantages of this FDM printers are related to the inexpensiveness of the procedure, its easy maintenance, the few spatial requirements and the low power usage [35]. Desktop 3D printers are well known due to its open-source technology. This feature allows to explore in different customization of the devices or to diversify in the materials used. The advantage to select different materials is the main idea behind the sensor designed in this project, to create with a consumer-oriented 3D printer an electronic sensor able to detect mechanical flexing of the muscles.

2.7.1 Materials

The materials selected to print the sensor are an essential part. Nowadays, flexible materials are more common in different devices printed, and the piezoresistive behavior previously observed in flexible conductive materials [36] indicates that it could add great value to the sensor detecting the muscle activity. The main body of the 3D printed sensor consists of a flexible thermoplastic polyurethane (TPU), and the electrical lines are made of a conductive TPU. Both materials are described below.

Dielectric TPU

NinjaFlex is a flexible dielectric filament made from TPU, resulting in uniquely flexible and robust prints [37]. The mechanical characteristics of this flexible material, are presented in Table 2.1.

According to the manufacturer, when the material is in contact with the skin it is not likely to result in irritation during solid form, and the chemical structure does not suggest a specific alert for any chronic or acute toxicity.

X60 Ultra-Flexible Filament is another option for the dielectric TPU used as a base for the sensor. The material has as specification half the tensile modulus than the NinjaFlex, which implies that the material can be easily deformed.

According to its manufacturer, MakeSharper [38], the material is non-toxic and is perfect for wearable devices which will need to stretch to fit.

	ETPU[39]	NinjaFlex[37]	X60[38]
Tensile Strength	15 MPa	4 MPa	23 MPa
Tensile Modulus	12 MPa	12 MPa	5 MPa
Elongation at break	250 %	660 %	760 %
Hardness	95 Shore A	85 Shore A	61 Shore A
Volume Resistivity	<300 Ω cm	-	-
Printing Temperature	200-230°C	200-230°C	190-210°C

Table 2.1: The table shows the specifications of the materials tested to design the device

Conductive TPU

PI-ETPU 95-250 Carbon Black [39] is a professional conductive and flexible filament. It is made of a rubber-like Thermoplastic PolyUrethane (TPU) compound material with a carbon black filler

bound in the base polymer. In Table 2.1 some mechanical and electrical characteristics of the material are shown.

This material is never in contact with the skin of the user; this is to avoid any current traveling through the users skin when the device is working.

Previous Work

The use of flexible 3D printed materials is a recent application where there are no many technologies yet developed. However, FMG using commercial force sensors is a technique vastly studied. Relevant work related to FMG sensors is presented in this section. Force myography has been adapted for various applications. Philips and Craelius [40] first proposed FMG as a technique to produce topographic maps in a prosthetic socket utilizing pressure sensors. They mapped the pressure exerted against the socket to categorize finger flexion and extension. With this same technique, Craelius and Yungher [41] used an array of force sensors to detect movement generated due to muscle activity on the forearm, being able to accurately differentiate six grasps with the arm in a fixed position. From this point forward, several applications of the FMG used as a premise that the pressure pattern obtained from the array of sensors gives information about the pressure points primarily [40].

Aiming to use force sensor to develop a pressure pattern, occasioned that FMG is now also known as residual kinetic imaging (RKI) or muscle pressure mapping (MPM). Erina et al. [42] used RKI to control a robotic prosthesis. They developed a prototype using a strap and attached FSR sensors from Interlink Electronics evenly spaced on the inner surface. When the prototype is fixed to the arm, it can detect muscle deformation due to the muscles creating pressure against each FSR. This way they could analyze muscle movement. Recently Li et al. [21] used a cluster of 32 FSR sensors combined with a Support Vector Machine (SVM) algorithm to classify finger motion based on distribution MPM. They successfully detected and validated 17 different finger motions. Based on the same procedure, Castellin et al. [43] used FSR attached to the forearm to detect forces in the fingers. They tested in 10 subjects the movement of the muscles while the users were pressing accurate force sensors with their fingers, matching the muscle activity with the recorded forces.

Strain gauges are also used to detect the muscle activity, but only in complex configurations. Salter [44] suggested applying pressure to small metal cantilevers to detect the force applied by each finger, relating it to the muscle activity.

Since the applications of FMG previously discussed are related to the use of FSR and the muscle mapping using FMG, the innovative approaches to these applications can be divided into two branches, ease of use and implementation, or the improvement of the accuracy. An example of the improved accuracy is the high-density force myography (HD-FMG) which Radmand et al. [19] used to detect changes in surface pressure caused by displacement of superficial and deep forearm muscles, and even bone movement to create a map of the limb. This technique uses the basic concept of FMG, encircling the forearm with a high-resolution grid of 128 pressure sensors, thus, increasing the accuracy and quality of the signals acquired. Another example, this time regarding the ease of implementation, Xiao and Menon [45] developed an easy-to-use strap with 8 FSR sensors to extract FMG signals from the posterior compartment of the forearm. Successfully detecting the movement of the fingers when flexed.

2.8 Conclusion

Since FMG utilizes, force sensitive devices to measure the force exerted by the muscles. Therefore, it is highly related to the FSR and the strain gauges, which are commercially available and well tested electromechanical sensors. Several applications of the FMG are aimed at mapping the muscles of the forearm or to categorizing gestures of the hands and limbs.

One way of improving this technology is by using a different method of manufacturing. Piezoresistive materials have been used to produce pressure sensors or mechanical stress sensors. However, these devices require multiple processes of fabrication compared to the 3D printing.

The idea of using 3D printing to develop a customizable sensor emerges from the natural usage of FMG applications, and it is aimed at broadening the usability of the signal obtained. Since the sensor is more robust and less noisy than the EMG, it needs less post-processing. By printing the sensors, the connectors are built in the same process along with the conductive lines, making the sensor implementation much more manageable than commercial force sensors.

The project will explore the use of FSR and strain gauges and analyze the advantages and disadvantages of both technologies. It will measure and test the materials selected, to determine if they are suited for the performance expected on the sensor. Finally, this work will study the performance of different sensing structures to determine the optimum design for the final 3D printed sensor.

Chapter 3

Models

3.1 Introduction

A model is a simplification of the real world, an adaptation meant as a tool to analyze the system and its behavior. The simplest model which still serves the research goal is the best model [46].

This chapter describes different models developed for the better understanding of the technologies used during the project.

Analysis of the musculoskeletal system, the materials selected and the force sensors used to acquire the signals is also developed.

3.2 Muscle Modeling

3.2.1 Musculoskeletal Model

A model of the muscles of the upper arm is necessary to know how much the muscle's cross-sectional area (CSA) is increasing and if the 3D printed sensor will elongate at the same ratio during the muscle contraction. This model should be able to demonstrate a change in cross-sectional area CSA of the upper arm, more detailed, the change of its perimeter.

Large-scale musculoskeletal models contain different parameters divided into categories. Inertia parameters (mass, rotational inertia), geometry parameters (joint rotation centers, muscle attachments and ligaments) and muscle parameters (physiological cross-sectional area, optimum length, and contraction velocity).

Since the sensor of this project is aimed to detect changes in muscle activity, the model focuses on the muscle and the geometric parameters. The mechanical properties of the skeletal muscle have been widely studied over the years to quantify its behavior with mathematical models. Fazekas et al. [47] have classified the musculoskeletal models according to the approach of study as follows:

- **Hill-type model**, which is the type of model most used in biomechanics. A. V. Hill [48] discovered the model during experimental observations. The model includes three elements; an active contractile element (*CE*) in series with a passive elastic element (*SE*) and a parallel passive elastic element (*PE*), emulating the motion of the muscle fibers and the properties of the tendon as shown in Figure 3.1.

From the Figure 3.1 it can be observed that the input to the model is the neural input (N_{in}) and the output is the total force (F_{total}). With this model Hill [48] suggested that when a neural input is maintained, the change in forces creates a change in length like a spring-like behavior [3], this gives the derivation of the spring constant as,

$$k = \Delta F / \Delta L \tag{3.1}$$

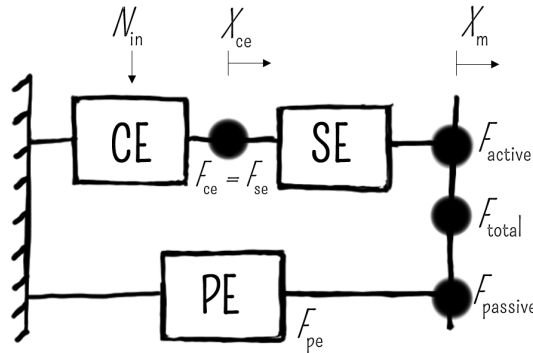


Figure 3.1: Hills model configuration illustrating the passive series element (SE) and the contractile element (CE) in parallel with the passive element (PE). The model shows the total force exerted as the summation of the force in the series element and the passive element ($F_{total} = F_{se} + F_{pe}$) [3]

As the model representation shows, ΔL is just X_m that is the summation of the displacement of CE and SE , $X_m = X_{ce} + X_{se}$.

When the neural input changes, the muscle shows a damping behavior [3]. The linearization of the change of force and length is observed in short times, such as sudden change.

- **Morphological models**, namely, designed considering the isovolumetric property of the skeletal muscle, the volume stays as force is applied and the muscle contracts. This force then depends strongly on the morphology of the muscle [47]. A morphological type of model uses the force-length relation of the muscle to predict geometrical characteristics of the muscle, and the most common model was developed by Zajac in 1989, [4] while modifying the Hills model to produce a musculotendinous model, the diagram is presented in Figure 3.2.

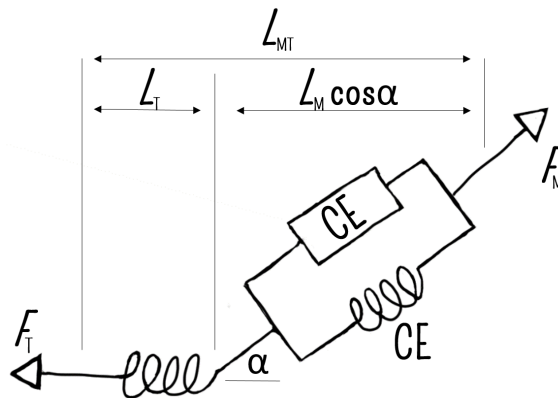


Figure 3.2: Zajac adaptation of the Hill's model related to the tendon length (L_T), the muscle length (L_M) and the musculotendon length (L_{MT}). It also considers the real pennation angle for the muscles [4]

The model presented for the muscle in this project is based on a morphological model since the objective is to determine the geometric characteristics of the muscle. Since it is also based on Hills Model, it will use the elements of that model to determine the length of the muscles involved in this project.

Muscle Force-Length Relation

An observed behavior of the muscle is the force-length relationship, which describes the phenomenon where a single or a group of muscle fibers exert different levels of maximum isometric force depending on the change in length. [Gordon et al. 1966][49].

Two underlying mechanisms affect the force-length relationship: active and passive. During the active force-length relation, as the muscle contracts, the cells forming the sarcomeres of the muscle (actin and myosin) overlap; the different degrees of overlapping lead to the different amount of force generated, as shown in Figure 3.3.

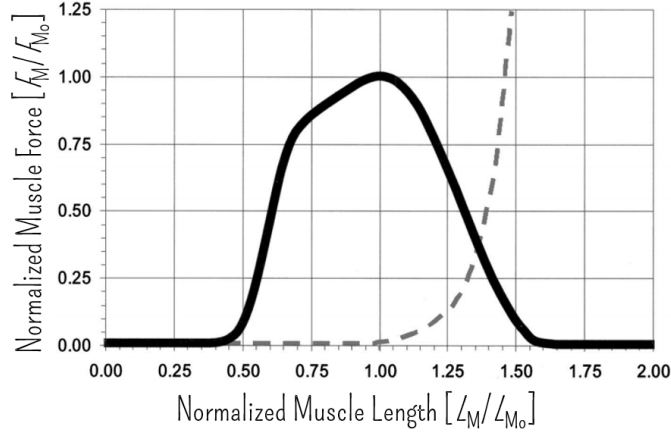


Figure 3.3: Active and Passive Force Length Relation. The plot obtained from Garner and Pandy [5] represents the behavior of the muscle isometric force. Active muscle force in a range between $0.5 L_{M0}$ to $1.5 L_{M0}$ (solid line), and passive force when muscle is stretched beyond its optimal length L_{M0} (dashed line).

The passive force-length relation reflects the elastic elements in the muscle. Therefore, the passive force can be unnoticeable during small fiber elongations, but it is important when the muscle is stretched beyond a determined length, when the passive force is produced.

Mathematical Muscle Model

Using the modified model explained by Zajac [4] and taking into account the force-length relationship for a musculotendinous system, it is possible to obtain an approximation between the muscle architecture of the biceps and the force applied during the contraction.

Garner and Pandy [5], developed a model based on Zajacs relation to finding different properties of the upper limb. This model was able to emphasize the solution in four elements: the maximum isometric force F_{M0} , the optimal muscle length L_{M0} , the pennation angle (α) of the muscle and the tendon length L_T . The diagram 3.4 shows the relation between the muscle lengths and the force generated.

The implication of the force-length relation is that the muscle is limited by a range of length to perform effectively, Zajac [4] determined the effective operating range of muscle between $0.5 L_{M0}$ and $1.5 L_{M0}$, demonstrating that the muscle cannot generate force beyond these lengths.

$$L_{MTmin} = L_T + \cos\alpha(L_{Mmin}) \quad (3.2)$$

$$L_{MTmax} = L_T + \cos\alpha(L_{Mmax}) \quad (3.3)$$

In which L_{MTmin} and L_{MTmax} are the minimum and maximum length of the entire musculotendon system analyzed. This values are calculated using the length of the tendon (L_T) and the minimum and maximum lengths of the muscle L_{Mmin} and L_{Mmax} respectively.

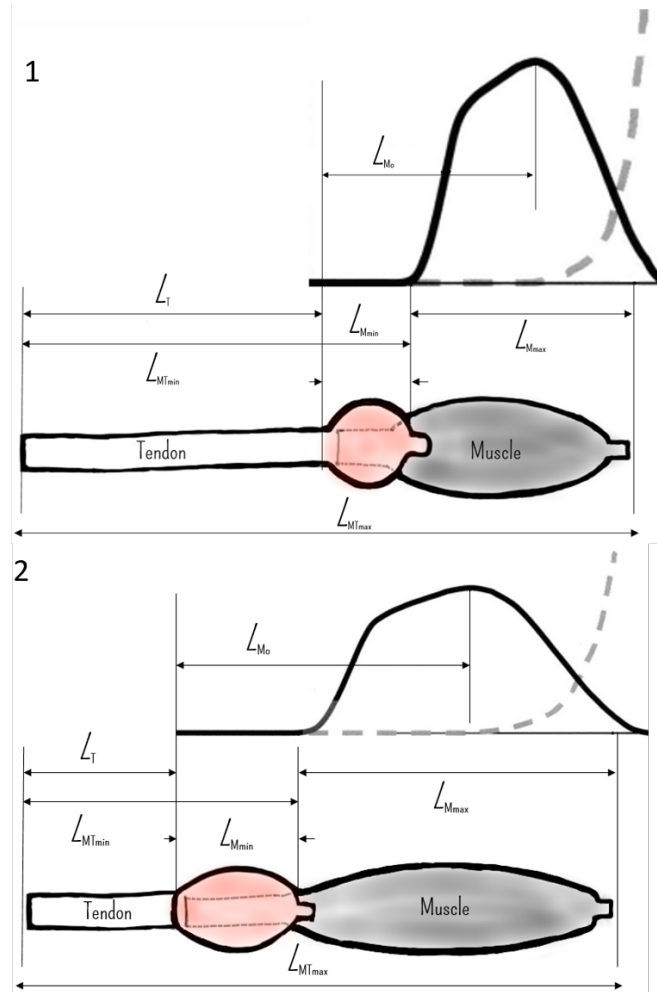


Figure 3.4: The diagram shows the importance of the slack length of the tendon, which determines the size and strength range of the muscle. While having a large slack length (1) the muscle excursion is small. On the other hand, when tendon slack is small, the muscle excursion is large. It also shows the relation to the optimal muscle-fiber length (L_{Mo}) and the physiological size of the muscle [5].

It is also possible to relate the muscle's length to the PCSA in terms of the volume known utilizing the relation showed by Garner and Pandy [5]

$$P_{CSA} = \frac{V}{L_{Mo}} \quad (3.4)$$

Where P_{CSA} is the physiological cross-sectional area obtained by dividing the volume (V) over the optimal length (L_{Mo}).

3.2.2 Circumference Analysis

Using the model of Garner and Pandy [5] it is possible to determine the length of the muscles during contraction and relate the change in length to the change in CSA of specific muscles when different forces are applied.

To relate the change in length to the change in circumference it is necessary to first relate the length to the CSA analysis. The value of circumference is the one that will show if the 3D printed

sensor can be deformed enough to produce a resistance variation.

An approximation of the muscle's structure in the upper arm can be explained with a simple diagram. Considering the shape of the upper arm as a uniform cylinder eases the analysis. This is only regarding the CSA of the muscle and not the length which is obtained in relation to the force with Zajac's model [4]. Each muscle is shaped on its own natural form. However, it is possible to study each muscle as cylinder-shaped and analyze the increase individually as shown in Figure 3.5.

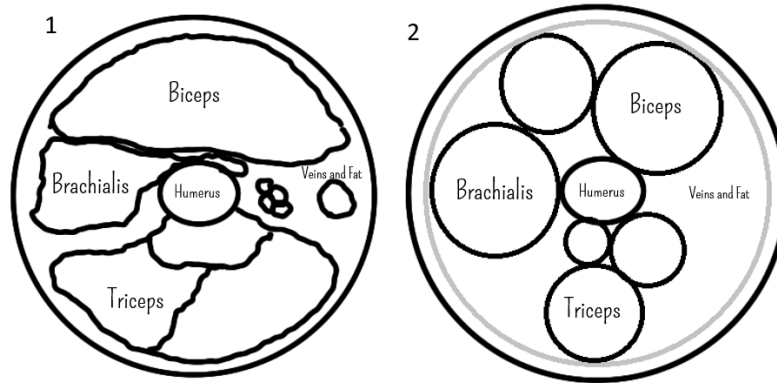


Figure 3.5: Approximation of the upper arm muscles, 1) shows an approximate axial view of the muscles surrounding the humerus (upper arm bone). 2) shows a representation of cylindrical form, two heads of the biceps, one for the brachialis and three heads of the triceps.

Poisson's ratio

Considering the muscles of the upper arm in a cylindrical form as stated in Figure 3.5, it is possible to compute the increase in diameter utilizing the Poissons ratio. When a rod is compressed or elongated by a determined force (F) the change in length (ΔL) can be related to a change in diameter (Δd), this relation is expressed in the Equation 3.5, and it is known as the Poisson's width.

$$\Delta d = -d \cdot \left(1 - \left(1 + \frac{\Delta L}{L} \right)^{-\nu} \right) \quad (3.5)$$

Given that the skeletal tissue is essentially incompressible it has a Poisson ratio between 0.45 and 0.5 as expressed by different authors [50, 51, 52].

Modeling Assumptions

The Zajac adaptation of Hill's model and the Poisson's width equation for rod deformation help to predict the increase in the size of the muscle of the arm. However, it is important to establish some assumptions that will narrow the model:

- Only the flexion at the elbow joint will be analyzed. Considering that the change in diameter of the muscles is more significant than during the extension (when only the triceps is activated).
- When the upper arm is flexing, the muscles activated are the Biceps Bracchi and the Brachialis. These are the muscles analyzed for a change in cross-sectional area.
- The pennation angle of the Biceps Bracchi and the Brachialis is no higher than 3 deg. Thus, it can be ruled out since it does not have an impact for small distances. However, a value higher than 10 deg can change the type of muscle as presented previously in Figure 2.2.

Considering that the values for PCSA or ACSA found in the literature are similar due to the small angle of pennation, using either of them will deliver similar results.

Results

Garner and Pandy [5] analyzed the muscle's architecture of the upper arm using the Zajac's model. They were able to calculate the length of the muscles on the upper limb, and some architecture as its PCSA, tendon length, volume, and the max force exerted for an estimated activation.

On the other hand, [53] utilizing the Hill's Model determined the size of the ACSA for the same muscles. The information regarding the muscle's architecture of the upper arm is shown in the Table 3.1.

	Volume (cm ³)	F_{Mo}^* (N)[5]	PCSA (cm ²)	ACSA (cm ²)[53]	Muscle Length (cm)	Tendon Length L_T	L_{Mo} (cm)
Triceps brachii	298.2[54]	2332.9	68.3[55]	27.7	26.7[56]	19.9[57]	12.1[58]
Biceps brachii	365.8[5]	849.2	31.9[55]	11.9	28.9[56]	20.5[59]	17.9[58]
Brachialis	265.9[5]	853.7	25.8[5]	13.9	20.3[53]	1.7[5]	12.3[60]

*These are the results obtained with the model of [5]

Table 3.1: Muscle architecture of the upper limb. The table presents a recompilation of different authors that obtained information of the upper body through different studies. The measurements are average data from male patients between 25-45 years old

Assuming that during the arm flexion the triceps and the humerus do not change their cross-sectional area, the analysis is applied only for the biceps and the brachialis contraction.

The maximum and minimum length values of the Biceps brachii and the Brachialis can be calculated using the relation that Zajac [4] designed. The optimal length, L_{Mo} , is taken from the Garner and Pandy model [5].

As shown in Figure 3.5 the cylinder shape of the arm is obtained by the total values of the cross-sectional area of each muscle plus the Humerus. Thus, the starting CSA at max working length will be:

$$A_{CSA,tot} = A_{CSA,Biceps} + A_{CSA,Brachialis} + A_{CSA,Triceps} + A_{CSA,Humerus} \quad (3.6)$$

This equation does not consider the fat and veins of the arm; this is because when the muscle of the arm is contracting the fat and veins are displaced from the muscle's belly which would be later the most prominent point in circumference, the point measured with the FMG sensor.

With Equation 3.5 the increment on Biceps and Brachialis diameter is independently calculated and added to the total cross-sectional area of Equation 3.6 to determine the augment in CSA.

The new total CSA represents the muscle contraction; with this value, it is possible to compute the new circumference of the upper arm.

The Figure 3.6 shows that when the biceps brachii and the brachialis are compressed the circumference of the upper arm increases. On the contrary, the muscle's cross-section decreases when the muscles are stretched, as hypothesized. After force is not exerted the muscle stops contracting which stops the increase in circumference.

According to [61] muscle tissue can exert approximately a maximal stress of 330 kPa at optimal length. With the contraction data, it is possible to estimate the optimal force applied during the change of length at maximal muscle activation, utilizing the relationship between the cross-sectional area and the force.

$$F_{Mo} = C_{max} \cdot P_{CSA} \quad (3.7)$$

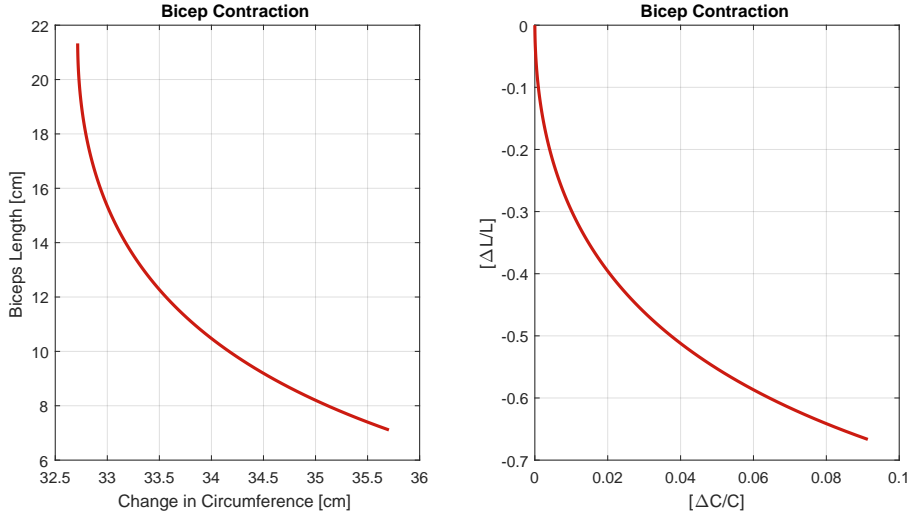


Figure 3.6: Both plots show the increase in circumference while the muscle length is decreasing, the value may differ from real due to the approximation of fat and veins in the upper arm.

Where F_{M_o} is the force exerted at optimal length, P_{CSA} is the cross sectional area and C_{max} is the muscle stress, which according to [61] the maximum muscle stress has a value ≈ 330 kPa.

After modeling the change in circumference due to length decrement, the next model focuses on the force exerted by the muscle of the upper arm during the flexion of the elbow.

3.2.3 Force Model

Muscles from the upper arm are capable of exerting a different amount of force. They produce force when performing simple tasks, to move the arm from one place to another or to lift weights. Muscles can only contract, so they come in pairs. In the upper arm, biceps brachii is the one in charge of closing the limb, and the triceps brachii is the extensor which opens the arm.

The arm can be visualized as a mechanical system to ease the analysis. The muscles have a spring-like behavior and produce a force; they are attached to the bones, not at the joint but in a specific insertion point.

The Figure 3.7 shows an upper limb in a rest position at 90 deg, with the different forces exerted by the muscles and the loads. It also illustrates the free body diagram that can be used to analyze the force exerted from the biceps to the arm; force used to maintain the position or performing different actions.

The model shows four forces applied to the forearm and the load. The forces are denominated as follows:

- F_B is the force exerted by the Biceps Brachii.
- F_E is the force from the elbow joint.
- w_a is the weight of the arm.
- w_l is the weight of the load.

Since F_B and F_E are unknown, it is necessary to take the elbow joint as the pivot to calculate F_B . The relation of the torques then states as follows:

$$d_2 w_a + d_3 w_l = d_1 F_B \quad (3.8)$$

If the angle of the forces is different than 90 deg, then it is important to consider that $\sin\theta$ is included in the relation. The equation then becomes as follows:

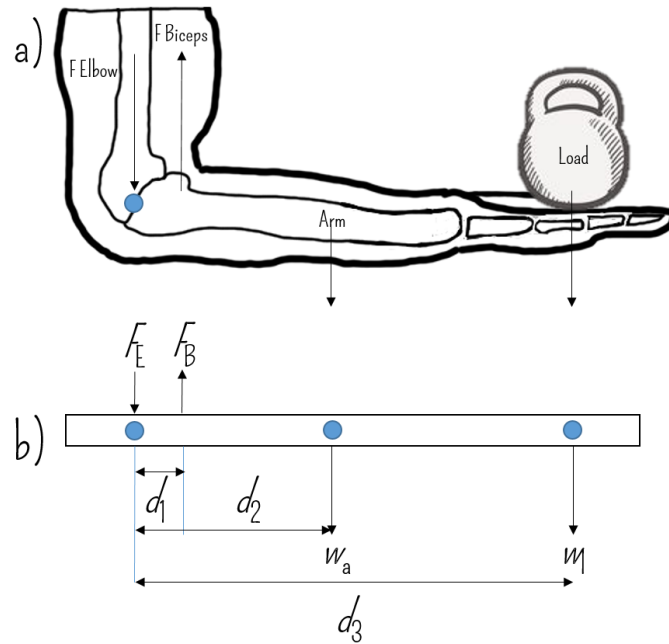


Figure 3.7: Free body diagram of the arm, while holding a load.

$$F_B = \frac{\sin(\theta_2)d_2w_a + \sin(\theta_3)d_3w_1}{\sin(\theta_1)d_1} \quad (3.9)$$

This equation makes possible to calculate the force that the biceps brachii is exerting with different weights. If the angle changes, the force exerted is also modified. The length of the biceps muscle is adjusted to the movement, and the force provided depends on the length; when the muscle is shorter, the force is smaller than when it is stretched [62].

3.2.4 Circumference as a measure for muscle contraction force

After evaluating a model of the force that the muscle can exert with a load and with an approximation of the increase in circumference due to the muscle contraction, it is possible to determine the relation between the force exerted and the change in the cross sectional area of the muscle.

For the evaluation of the muscle's length, the values considered were in the range of $0.5 L_{M_o}$ to $1.5 L_{M_o}$ of the optimal length. If the value of 330 kPa [61] of stress is used, it is possible to use the force values obtained in the previous model to determine the cross-sectional area, utilizing equation 3.7. This way, relate the force applied by the muscle when contracting to the change in circumference.

The Figure 3.8 shows a decreasing force when the circumference of the arm is increasing, which is an expected performance [63]. The muscle exerts the highest force at a maximal length, and the force decreases as the muscle shortens.

The change in circumference is proportional to the change in length. When the circumference of the arm is at maximum the muscle is contracted to its minimum optimal length, which results in a minimal force exerted.

However, it is important to mention that the force model is for an elbow flexion of an arm with a load of 3 kg. For this reason, a stress value of 330 kPa was not necessary. Instead, the ideal change in circumference was obtained with a muscle stress of ≈ 30 kPa.

The force exerted by the muscle is enough to increase the circumference of the upper arm. The next model is to determine if the material can deform to the same extent as the muscles of the arm.

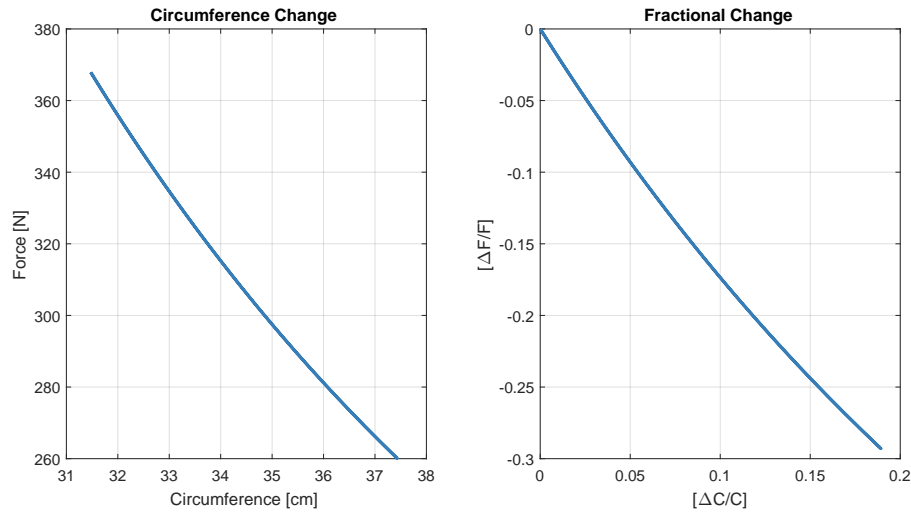


Figure 3.8: Change in force related to the increase in circumference of the upper arm. Left plot shows the absolute values and right plot shows the fractional change.

3.3 FDM Filament Model

According to the model of the previous section, the muscles of the upper arm can sufficiently expand their circumference. Then, it is necessary to model the sensing material used, to investigate its mechanical and electrical properties. This way determine if the strain gauge is able to expand at the same ratio at the muscle. The following model will represent the change in shape of the material as stretched and its electrical behavior during the deformation.

3.3.1 Material Properties

When the muscles of the upper arm are contracted, its circumference increases approximately 9% as shown in the Figure 3.6. The conductive filament in its original state has a maximum elongation of 225% according to the provider [39].

Thus, modeling the filament will show the change in resistance due to the stretching in its original conditions. The equation 3.5 from the Poisson's width can be used to compute the change in diameter of the filament.

The analysis for the model should be made on a piece of material with the same dimensions as the original filament. Thus, the material has a diameter of 1.75 ± 0.05 mm and a length of 50 mm and has a Poisson's ratio between 0.45 and 0.5 same as the dielectric material (Ninja Flex) [64].

Procedure and Results

If the elongation of the material is $\approx 9\%$, the final length will be of 54.5 mm. With this information it is possible to calculate the change in resistance utilizing the relationship between the area of the conductive material and its resistivity. The electrical resistivity is a property that quantifies how strongly a material opposes to the flow of electrical current [65]. The electrical resistance of an object depends on two factors: the material it is made of and its shape. For a specific material, the resistance is inversely proportional to the cross-sectional area and proportional to the length. Thus, the resistance is given by:

$$R = \rho \frac{L}{A} \quad (3.10)$$

Where ρ is the resistivity in $\Omega \text{ cm}$, L is the length of the gauge, and A is the cross-sectional area. The electrical resistance of the filament is expected to be greater for a more extended piece

of filament and less for a filament with a more extensive cross-sectional area. The factor that considers the nature of the material is the resistivity ρ , and at a given temperature it can be used to calculate the resistance of the filament with a defined geometry.

While the filament is stretching, the resistance is expected to increase due to increase of the length, and the reduction in the area of the filament. Additionally, there may be a contribution from the change in conductivity when the material is strained, the piezoresistive effect. In total small strains ε are found:

$$\Delta R = \frac{\partial R}{\partial L} \Delta L + \frac{\partial R}{\partial A} \Delta A + \frac{\partial R}{\partial \rho} \Delta \rho \quad (3.11)$$

$$\frac{\Delta R}{R} = \frac{\Delta L}{L} + \frac{\Delta A}{A} + \frac{\Delta \rho}{\rho} \quad (3.12)$$

$$\frac{\Delta R}{R} = \varepsilon_L + (2\nu\varepsilon_L - \nu^2\varepsilon_L^2) + \frac{1}{\rho} \frac{\partial \rho}{\partial \varepsilon_L} \varepsilon_L \quad (3.13)$$

If the material is considered incompressible, the strain is small and the piezoresistive effect is absent. It is possible to calculate the Gauge Factor (GF) from this relation, which indicates the ratio of relative change in electrical resistance due to mechanical strain as in Equation 3.14

$$GF = \frac{\frac{\Delta R}{R}}{\frac{\Delta L}{L}} \approx 2 \quad (3.14)$$

On the other side, an approach with a large strain including the piezoresistive effect, it is represented by:

$$\begin{aligned} R &= R_0 \left(1 + \frac{\Delta R}{R_0} \right) = \frac{\rho L}{\pi r^2} \\ &= \frac{\rho_0(1 + \rho_\sigma \varepsilon_L) \cdot L_0(1 + \varepsilon_L)}{\pi r_0^2(1 + \varepsilon_R)^2} \\ &= R_0 \frac{(1 + \rho_\sigma \varepsilon_L)(1 + \varepsilon_L)}{(1 - \nu \varepsilon_L)^2} \end{aligned} \quad (3.15)$$

$$\frac{\Delta R}{R_0} = \frac{(1 + \rho_\sigma \varepsilon_L)(1 + \varepsilon_L)}{(1 - \nu \varepsilon_L)^2} - 1 \quad (3.16)$$

From the latter, it is possible to plot different expressions. The Figure 3.9 shows the calculation of $\frac{\Delta R}{R_0}$ assuming a $\nu = 0.5$. The behavior observed in the plot is obtained with and without considering the piezoresistive effect. It is possible to observe a linear behavior when the material input is neglected in $\frac{\Delta R}{R_0}$.

It is possible then to use Equation 3.16 to compute the resistance change of the filament and to determine its material and geometric contribution.

Figure 3.10 shows the change in resistance of the filament decomposed. As expected the geometric input gives a $GF \approx 2$ while material input which considers the piezoresistivity of the filament for a large strain, gives a negative behavior.

According to the model, the resistance of the filament decreases due to the negative piezoresistive effect. However, this is only during small strains. When combining both inputs in the evaluation of the filament, the result shows a mixed behavior as shown in Figure 3.11.

For an elongation of 9% when the strain is small, the resistance decreases, however after the elongation of the material reaches a determined value the resistance increases again. The value where the resistance begins to increase will depend entirely on the electrical properties of the filament.

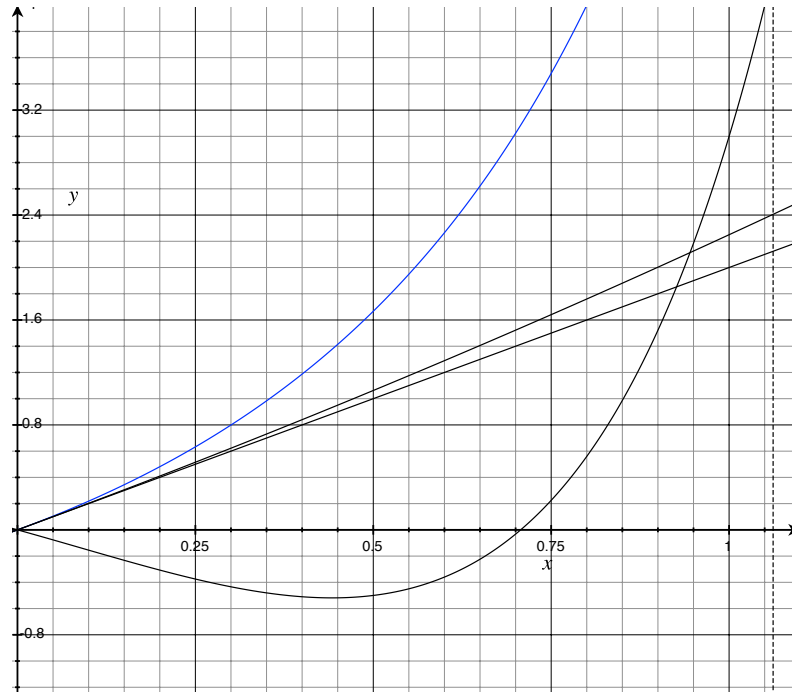


Figure 3.9: Various expressions from the Equation 3.13*, calculating $\frac{\Delta R}{R_0}$ assuming $\nu=0.5$ with and without second order term. All results are not considering the piezoresistive effect, except for the lowest curve using Equation 3.16, has a negative piezoresistive coefficient ρ_σ .

* Y axis represents $\frac{\Delta R}{R_0}$ and X axis $\frac{\Delta L}{L}$

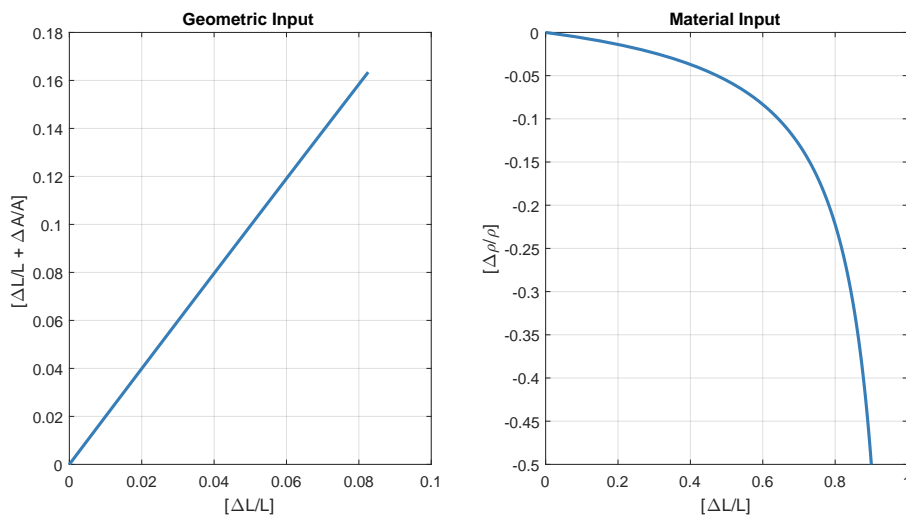


Figure 3.10: Geometric and Material inputs in the resistance value when the filament is elongated

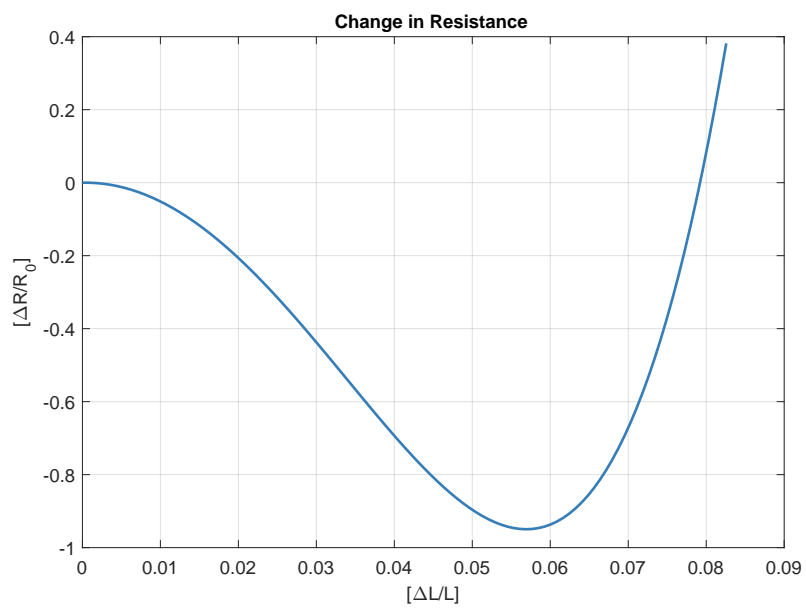


Figure 3.11: Combined contribution in resistance behavior during the elongation of the conductive material.

3.3.2 Strain Gauge Model

It is important to acknowledge that, due to 3D printing, the material will not have the same electrical properties as in its original state. Figure 3.12 shows the first design of the strain gauge to be 3D printed. Similar behavior is expected, however, since the material is exposed to high temperatures the absolute values of resistance may change.

Modeling Assumptions

The strain gauge, as shown in Figure 3.12 has 55 mm of length and 22 mm in width. The layer used to print it is of 0.15 mm width, and the thickness of the gauge is 0.5 mm, and the conductive part of the gauge is composed of three layers.

The conductive material printed on the strain gauge has a total length of 400 mm, due to the 8 lines printed, with a line width of 3 mm.

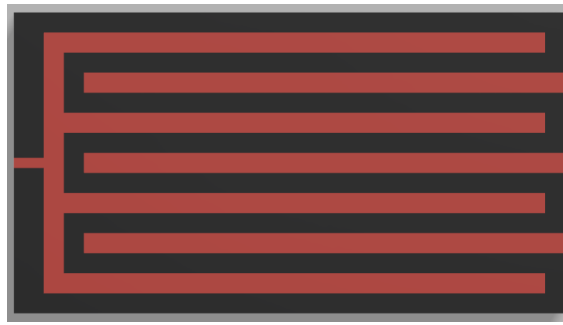


Figure 3.12: Strain gauge first model

The gauge will be analyzed using the same principle as the filament using the Poisson's strain with the equations 3.17, 3.18 and 3.19.

These equations represent the strain in the transverse direction and the strain in the longitudinal direction, as illustrated in Figure 3.13.

$$\varepsilon_L = \Delta L / L \quad (3.17)$$

$$\varepsilon_T = \Delta D / D \quad (3.18)$$

$$\nu = -\frac{\varepsilon_T}{\varepsilon_L} \quad (3.19)$$

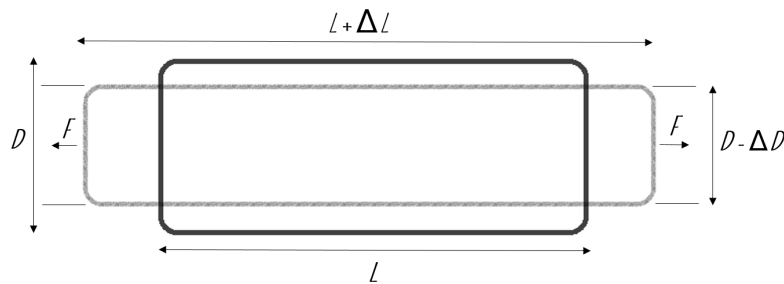


Figure 3.13: Diagram that represents the behaviour of the material while stretched based on the poisson strain.

Since the Poisson's ratio and the change in length are known data, it is possible to calculate the transverse strain. Then, the reduction in area is computed for a stretching of the strain gauge.

After calculating the change in area and length, the remaining unknown factor to calculate the resistance is the resistivity of the material.

The resistance of the strain gauge can be expressed by two different inputs if the equation is modified. The original equation for the resistance is the one showed in Equation 3.13 where ρ is the resistivity in $\Omega \text{ cm}$.

From this relation, under strain, the fractional change in R is obtained by taking the total differential [66], stated in Equation 3.11. Which lead again to the Equation 3.16 previously determined. This equation used to calculate the changes in resistance of the strain gauge considering the piezoresistive effect of the material.

Procedure and Results

After completing the analysis, Figure 3.14 shows the relation between the change in resistance and the change in length.

As expected the resistance computed has the same behavior than the filament. In this case, the plot only shows the fractional change in resistance for an elongation of 9% to predict approximately the values expected during the experiment.

The plot shows enormous changes for the small strain. This change is negative due to the material input at the beginning of the strain, and the values depend solely on the electrical properties of the material.

Since the sensing material is larger in the strain gauge than in the filament the piezoresistive effect contributes more to the resistance values than the geometric input. Thus, the negative values can be observed for an elongation of 9%.

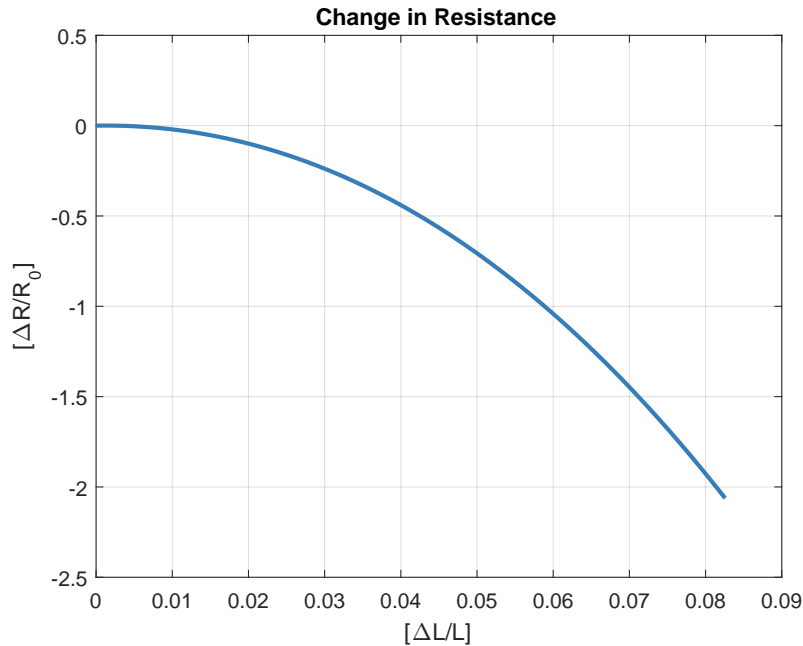


Figure 3.14: The change resistance considering the linear contribution of the of the strain gauge and the input of the material electrical properties according to Equation 3.16

The real behavior of the strain gauge depends on many different factors. Since it is a 3D printed object, the resistance is dependant on the electrical properties of the material, the type of manufacturing, and the electrical interface.

The temperature is a factor that affects the resistance in semiconductor strain gauges. However, this factor can be neglected or modified by using different arrangements in the connection of the gauge.

These features can be optimized to decrease the variations in measurement. Thus the next chapter is meant to standardize the manufacturing of the strain gauge to obtain equivalent performance through different prototypes.

3.4 Conclusion

The importance of the models takes place in the prediction of the behavior of the systems. The muscle model showed that, as expected, when the arm is shortening it produces an increment in the cross-sectional area. When the length of the muscle is reduced to the minimal optimal length, it is possible to observe an increase of 9% in the circumference of the upper arm. This percentage is useful information to calculate if the material and the 3D printed sensor can stretch at the same ratio.

The model that analyzed the relationship between the change in circumference and the force exerted by the muscles during a concentric contraction suggested that when the arm is producing the lowest force, the contraction of the muscle is more prominent. This result is due to the change in length of the muscle. This model is then representing the force exerted by the muscle through the change in circumference. This way is possible to prove that the change in circumference of the band will be able to detect the contraction of the muscle through the muscle force.

The models regarding the filament indicated the high contribution of the properties of the material to the resistance output. Geometric properties affect the measurements of the material. However, the piezoresistive effect of the filament may have higher contribution than the shape of the material at small strains.

The strain gauge model suggested that it can perform similarly to the filament. Nevertheless, since the strain gauge has more conductive lines of material, the absolute values of resistance may be higher and the input of the piezoresistive effect more dominant through relatively longer elongations.

The model of the strain gauge also suggested noticeable changes in resistance, which will ease the signal acquisition and postprocessing.

Nevertheless, despite the significant readings, the value of the resistance is high. Therefore, it is essential to improve the design of the strain gauges according to the possibilities of their geometry, to enhance the electrical characteristics of the sensor.

Chapter 4

Design

4.1 Introduction

The present chapter presents the process followed to improve the performance of the strain gauge. Currently, Figure 3.12 shows an 8-line strain gauge of 55 mm long and 22 mm of width. And most of its performance is attributed to its geometry, the resistance of the gauge depends not only on the material properties but also on its shape. The objective of optimizing the design is to reduce the absolute value of the resistance in its natural state, to allow the use of a constant current measurement without having using high voltages, and to improve the changes in the resistant when is stretched, which is the target value measured necessary to detect the muscle movement. This process will be performed while configuring the parameters of the 3D printer and testing different designs of the technologies.

4.1.1 Material

The sensor is made of two materials, one for the base, and one as sensitive material. The primary material and base of the strain gauge is the NinjaFlex which is a flexible dielectric filament made of TPU. It has a melting point between 200 °C and 230 °C and it is fabricated by the company NinjaTek.

The second material is the PI-ETPU 95-250 (ETPU) a flexible conductive filament made with a rubber-like structure with a carbon black filler bound to the base polymer. This filament is fabricated by the Palmiga Company; its melting point is between 190 °C and 220 °C.

Both materials have similar Young Modulus (≈ 12 MPa), which improves the performance of the sensor since it will deform approximately at the same ratio. The relevance of this property lies in the elastic deformation, both materials will return at its original form after elongated at approximately the same ratio.

4.1.2 Printing Specifications

The material will have the best performance when printed under the best conditions. Frequently, the provider of the material proposes specific configurations for the printer, such as temperature, layer height, the velocity of printing, among others.

Although the specifications suggested for the NinjaFlex worked correctly during the printing process, and the dielectric material was printed with good quality. When the first prototype was tested with the conductive ETPU, the resistance was higher than expected. Therefore, the following changes to the configuration were tested:

- Lower the temperature of the printing to around 200 °C.
- Reduce the velocity of printing to around 900 $\frac{\text{mm}}{\text{min}}$.

- Try different sizes for the layers to increase the cross-sectional area of each line printed.

Using a low temperature and a low velocity for the ETPU improved the lines of material, they were more continuous, showing the material less brittle after printed. Changing the size of layer did not affect the printing since the layers were small enough already. Regarding the resistance values, the conductivity of the material remained the same as before the changes.

4.2 3D Printer Configuration

The 3D printer used for this research to manufacture the sensor is a Flashforge Creator Pro [67]. Flashforge has two extruders which allow printing two-material objects easily. It is optimized with a fully enclosed chamber that eliminates temperature interference from the exterior environment and stabilizes the printing temperature for accurate prints. However, the extruder that comes with the printer is dedicated to non-flexible materials such as PLA or ABS. Thus, it was necessary to modify it to use a different extruder able to print flexible filaments.

The selected one was the Flexion Extruder [6], a high-speed printing extruder for ultra-flexible filaments, down to 60 ShoreA. It contains a brush that is constantly clearing the drive roller of plastic shavings, which allows less material to be scraped while printing and keep the teeth of the extruder sharp.

The Flexion Extruder uses a high-stiffness lever to compress the filament. The compression is controlled with a cam and adjust screw, rather than the traditional spring. This configuration increases the tension and improves the control over the tension. Figure 4.1 shows the design of a dual Flexion Extruder.

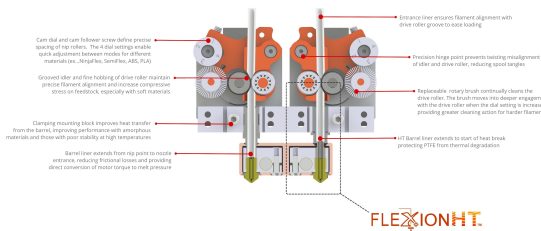


Figure 4.1: A dual Flexion Extruder that allows better control of the flexible filaments. Image obtained from [6].

3D printing could seem straightforward. However, every parameter set for printing affects the result of the object desired. 3D printing involves several features and characteristics that allow the user to customize the objects and devices further. For this purpose different specifications of the printing have to be taken into account. Various tests were performed to maximize the advantages of the 3D printing and to determine the specific configuration necessary to obtain high quality printed objects.

4.2.1 Infill

One of the essential properties of the 3D printing is the infill parameter. A 3D printer extrudes lines of material in X and Y making discrete steps in the Z direction. This procedure causes that in every layer the 3D printer has to fill the object with a specific pattern, this is called infill. There are four main shapes of infill. The grid, rectilinear, honeycomb, and triangular. Using the optimal temperature selected for both materials, different patterns of infill were tested.

The same object was printed utilizing the different types of infill. This way it was possible to verify if different patterns result in improvement of the printing quality. Figure 4.2 shows the

design printed, the orange part is the NinjaFlex, and the black part is the ETPU, four types of infill were printed in both sections at different velocities between $1000 \frac{\text{mm}}{\text{min}}$ and $2000 \frac{\text{mm}}{\text{min}}$.



Figure 4.2: Object to test the different types of infill.

The results showed that the variation of velocity do not have a significant impact on the final object. At lower velocities, the line of printing seems to have a better resolution, but the improvement is not as significant compared to the higher velocities but the time of printing is considerably more.

The honeycomb and the triangular patterns are not suitable due to the shape of the line. Since the ETPU filament will be conducting, the diagonal lines of those types of infill increase the electrical resistances of the object, thus, are less suitable for the intended objects. It was concluded that the line form created by the rectilinear infill is the most adequate for the objects printed. It helps the printer to produce a pattern of straight lines that improves the conductivity of the ETPU and merge the material layer by layer.

4.2.2 Line Width

Some objects are printed with small spaces in between the lines. The smaller the size of the nozzle the thinner lines can print. A good knowledge of the smaller size of line printable helps to avoid unconnected lines in the objects. Since the material used is conductive, the influence of the continuity of the line is rather high. It is necessary then, to maintain the lines without interruption. Thus, various sizes of line width were printed to determine the smallest continuous lines possible.

The diameter of the nozzle for printing the NinjaFlex is 0.6 mm, for the ETPU this is 0.8 mm. The 3D printer has a parameter that allows to increase the expansion of the filament when it comes out of the nozzle, denominated extrusion multiplier. If the printer is well calibrated and the extrusion multiplier is set to 1, the line printed with ETPU will be of 0.8 mm width (same size as the diameter of the nozzle), if it is set to 1.5 the line would be of 1.2 mm approximately. Since the NinjaFlex is the base material, its lines will not affect the performance of the sensor. Nevertheless, the lines of the ETPU must have an excellent line width to improve the conduction.

The primary objective is to detect the minimal amount of printing distance to provoke a separation between lines. Lines multiples of 0.8 mm were printed in a NinjaFlex base to detect optimal spacing; the line width varied from 0.8 mm to 3.2 mm with a extrusion multiplier of 1.

Figure 4.3 shows the object designed. After printing it was observed that the lines of 0.8 mm are not printed, this is due to the extrusion multiplier, even using the value of 1 the printer could not print a line of the desired width. However, lines of 1.6 mm, 4mm and 2.4mm are printed correctly and with good quality. The 3.2mm shows a small distance between the lines which indicates that they were printed separately without filling the space between them.

4.2.3 Parallel Lines

Since the conductivity of the object is dependent on the line width, it is possible that the resistance increases when the infill is not uniform. Therefore, printing small parallel lines seems like a better approach. The lines are designed to be printed slowly, straight and the same size as the nozzle

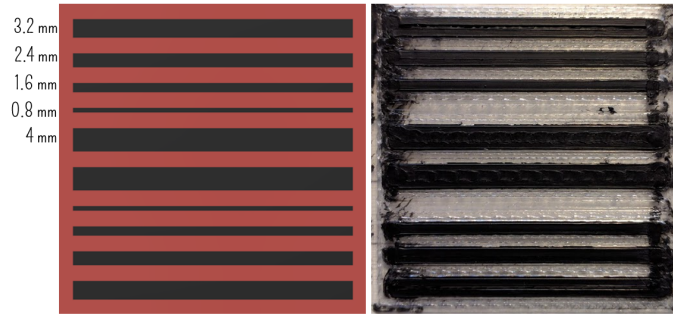


Figure 4.3: Comparison of the trial with the desired design for testing different types of linewidth.

(0.8mm for ETPU), this way the infill property of the 3D printer is avoided. The design is showed in the Figure 4.4

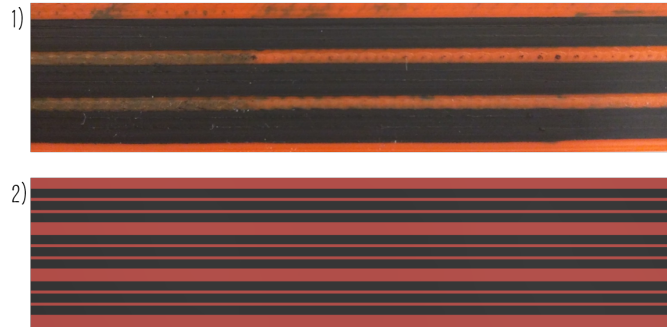


Figure 4.4: Figure of the trial lines that were tested. 1) is the printed structure and 2) is the design desired.

A group of four parallel lines forms the path of the lines. The conductivity of the lines printed cannot be interrupted due to disruptions of the infill pattern. As expected, the resistance of the lines in the object decreased and became more constant through different printed trials, showing consistency through prototypes. After establishing the configuration for high-quality printing, the next step is to design the force sensitive devices that are going to be part of the final device.

4.3 Strain Gauge

Strain gauges are a simple form of sensor, with the capability of obtaining considerable readings. It measures the strain of the device due to stress applied; stress in the form of stretching or bending to produce the deformations. As a mechanical sensor, it can be used as an indicator of force, bending, torque, pressure, acceleration, etc.

Methodology

It is necessary to set a methodology for designing; this process helps to detect the early problems and to focus on the requirements of the device. The Figure 4.5 shows the design methodology followed for each technology.

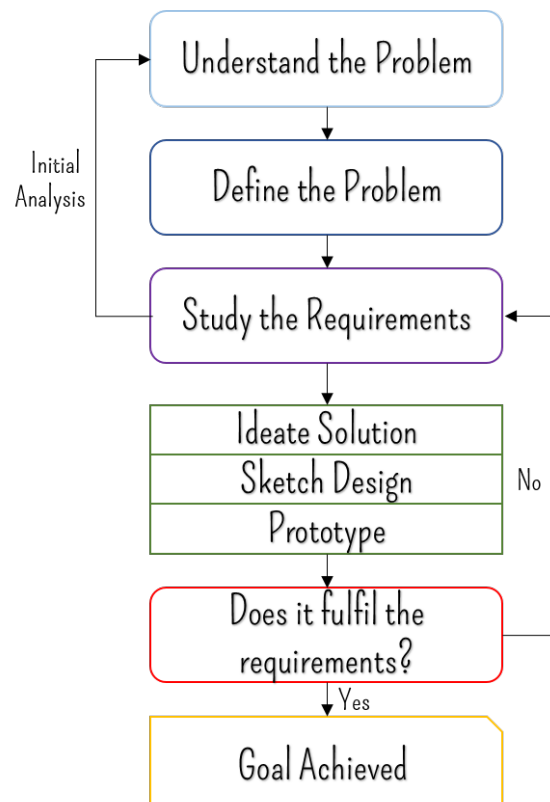


Figure 4.5: The methodology for the process of designing new objects.

Specifications and Requirements

Strain gauges could have different applications. When designed, it is possible to focus on some properties of the device to improve different qualities. Therefore, it is important to set the requirements of the system and its geometric specifications [25].

Requirements

- **Capacity to measure strain.** Although it is evident, the system should be able to measure strain under static and dynamic conditions.
- **Small size and weight.** The device should be small in size to ease its mounting, and with a low weight, so the inertia is negligible when measuring strain during dynamic conditions.
- **Temperature independence.** Even if it is a difficult requirement to achieve, it is important that small variation of temperature doesn't affect the system on a large scale.
- **Linear response to strain.** Linear relation between unit change in resistance and change in strain, providing a constant sensitivity
- **Low cost.** Since it is a 3D printed device, the cost is already low compared to the production of other strain gauges.
- **Adequate electrical connections.** The device will perform near the human skin, thus, as a safety measure, the electrical interface should be secure to avoid disconnection during movement.

Specifications

- **Adaptable to the arm.** The device has to be long enough to adapt to the arm in size and it should be comfortable to wear.
- **Flexible.** Even if the material is flexible already, the thickness of the strain gauge has to be wide enough to avoid failure but flexible to improve the measuring.
- **Low resistance values.** To be able to perform a safe reading for the user the resistance values should be low. The common way to measure a strain gauge depend on the voltage and the current applied to it. This values must not exceed the safety guidelines [27].
- **Repeatable conduction.** The lines of the sensitive material should be printed correctly. If the material is brittle or not continuous, it can produce unnecessary and inexplicable changes in resistance.

4.3.1 Prototypes

The first approach was to design a strain gauge of 30 mm long, 20 mm wide, and 3 mm of thickness with the connections on the top and bottom as Figure 4.6 shows. The lines of the resistance were in the middle of the material. The result was a resistance value of $\approx 80 \text{ M}\Omega$ and the measurement did not show repeatability. Thus this prototype did not fulfill the requirements. Since the gauge was about 3 mm thick, it had restricted flexibility while bending it. Thus, there were some modifications to the design.

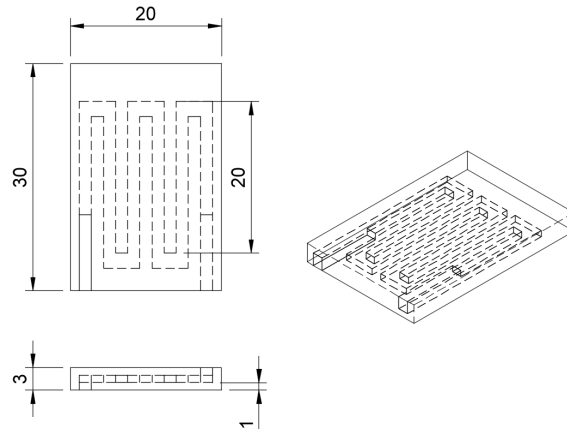


Figure 4.6: First design of the strain gauge. Dimensions in mm

The second design was slimmer than the first, the thickness was reduced to 2 mm considering both materials, the length was increased to 55 mm, and the width was also increased to 30 mm. Figure 4.7 shows the second model with improved flexibility; the first prototype had the lines correctly printed, without bleeding.¹

However, the lines were too narrow causing an increased value in resistance, and it did not show repeatability during several printings. It was necessary to redesign and to try a different approach to reduce the absolute resistance value of the strain gauge.

The second model fulfilled almost all the specifications and requirements; the only characteristic left was a better conductivity. The absolute value of resistance of a 3D printed strain gauge depends mostly on the geometry of the conductive material, and the method of printing. Since the configuration of the 3D printer was already optimized, the geometry of the strain gauge was tested to improve the results.

¹Due to the nature of the FDM's extrusion mechanism, the material is continuously near the melting point at the edge of the nozzle. This state can cause the material to leak while printing. During multi-material objects, one material can "bleed" on top of other leaving marks. This condition is called "bleeding."

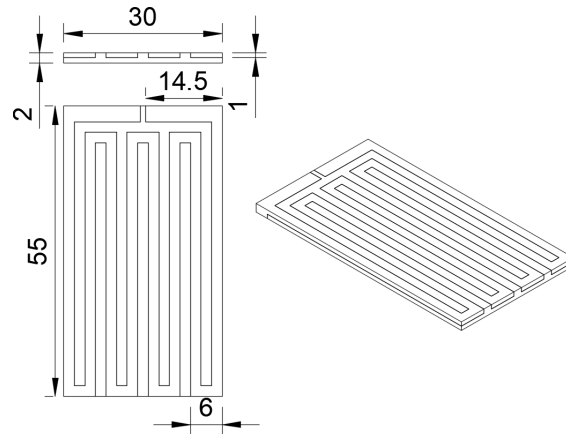


Figure 4.7: Strain gauge second design. Dimensions in mm

	1	2	3	4	5	6	7	8
$M\Omega$	16	18	6.5	8	35	40	12	16
$\Delta R/R$	≈ 0.7	≈ 0.65	≈ 1.3	≈ 1	≈ 0.8	≈ 0.75	≈ 0.5	≈ 0.55

Table 4.1: The eight different prototypes vary only in line width and line shape. All the models have the same base measurements and the same length for the sensitive material. The conductive material was printed at 1500 mm/min with a layer height of 0.15 mm for a complete thickness of 0.5 mm.

Different designs were proposed using the base dimensions of 65 mm of length, 25 mm of width and 1.5 mm of complete thickness. Table 4.1 shows eight different models of strain gauges. Its behavior was analyzed to test the requirements established for the strain gauge. The readings were performed with a 4-probe measurement at a constant 1 μ A utilizing a multimeter Keithley 2000 [68]. The values compared were the absolute resistance ($M\Omega$) and the fractional change ($\Delta R/R$) for an elongation of 9%.

- As expected the resistance values were higher in the gauges with thinner lines, due to the smaller cross sectional area.
- The round corners did affect in small proportion the resistance values; this is because the continuity of the lines in the curves is not efficient, even after printing at slow velocities.
- The shape of the gauge affects the resistance related to the length and area of the conductive material. However, the difference is not remarkable except for the 5th and 6th models which has the thinnest line width as shown in 4.1.

In the end, the model of the strain gauge number 3 was selected. Since it showed the lower value of absolute resistance and the higher change due to deformation. The final model was adapted to have connective points to ease the electrical interface. The Figure 4.8 shows the model of the strain gauge selected.

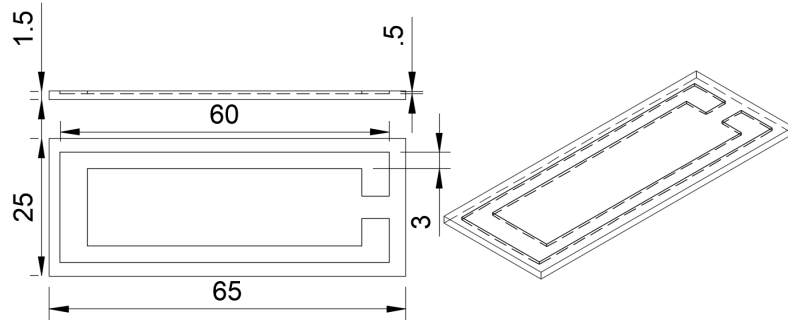


Figure 4.8: Strain gauge final design

4.4 FSR

After the strain gauge was optimized, the next step was to analyze the functioning of the FSR. The force-sensing resistor is a button-like sensor, that when pressed, makes contact and increases contact area between its layers, allowing to conduct current through its layers. The FSR is a useful type of sensor that, when well designed, can detect useful insight on the muscles during force myography, as showed by previous research [20, 44].

Requirements

The following requirements were suggested to develop a 3D printed FSR: [23]

- **Size.** The FSR will be used to detect the pressure of the more prominent part of the muscle when contracted, the belly of the muscle. The FSR should be large enough to detect the muscle movement, but small to fit the upper arm without being uncomfortable.
- **Reproducible technology.** A constant behavior is expected, the device should provide a consistent force distribution to be able to calibrate the resistance changes on the FSR [69].
- **Optimal electrical interface.** The electro-mechanical connectors should be considered at the moment of designing, so there is no excessive space used afterward.
- **Sensitivity.** The resistance of the FSR will tend to drop quickly at first and then more slowly as the spaces of the FSR are being compressed. This behavior is advantageous to cover an extensive range of force values, but also makes the FSR very sensitive to light touches. By using a voltage divider, the FSR output can be linearized, and the gain could be used to increase the FSR's effective range [70].

4.4.1 Prototypes

Considering the requirements, some prototypes were designed based on the functioning of a push button. The first design is formed by a base made of ETPU, separated by a small space of NinjaFlex, closing the device with a top part of ETPU. When there is pressure applied to the device the resistance should decrease, since the top and the bottom layer are in contact.

Figure 4.9 shows the first prototype of the FSR sensor. The design included a cup and a base of conductive material. However, due to the lack of support and the small dimensions, the top

cup failed to maintain its form. Low velocities and different types of infill were used to assist the bridging between the structures of the FSR, still a new design had to be proposed.

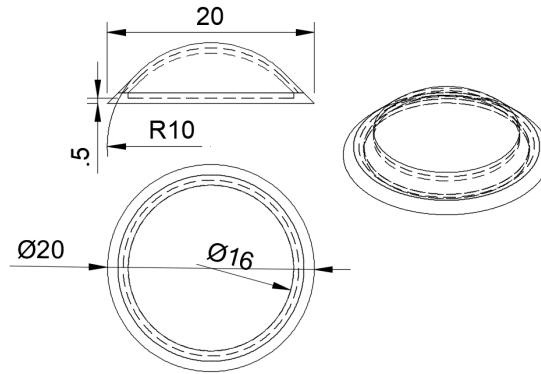


Figure 4.9: First prototype of the FSR sensor.

The second prototype was designed with a cut on the sides to allow the printing of support lines in the middle of the device. The lines were thin allowing them to be removed after printed, the cup size was increased to maintain its shape after the support was removed, and the base was bigger to provide stabilization to the area of pressure. These new features are illustrated in Figure 4.10

However, the support lines did not work as expected, and it was more difficult to remove them. The top and bottom layers were always in contact, or never released. Different positions of printing were tested without favorable results.

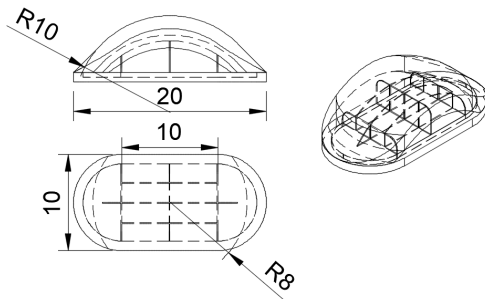


Figure 4.10: Second prototype of the FSR sensor, with support lines to be later removed

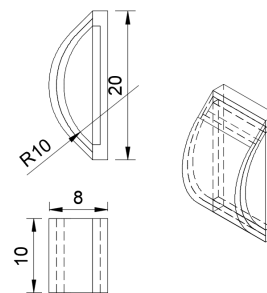


Figure 4.11: Third prototype of the FSR sensor, printed with a different orientation.

The third prototype was turned 90 deg in X-axis to manage a stable printing. This way it was possible to leave a small space inside the half-circle of the FSR.

Nonetheless, this prototype failed to achieve the dimensions, since the base of 2mm was big enough to start to feel uncomfortable when pressed against the upper arm skin. This size was without considering the electric connectors.

Some remarks are worthy of mention after testing the FSR. The force sensitive resistor is a valuable sensor that can efficiently provide relevant information about the muscle contraction. However, the many trials indicated that it was not possible to obtain designs that could be reliable fabricated by 3D printing. The printings did not have a good quality at reduced distances, and the small size of the device was an important characteristic.

Technologies Comparison

Lastly, a comparison between the two sensors was made to decide which technology would be more suitable for the final device. Table 4.2 shows the contrast between the main characteristics of the technologies.

The size and weight of both sensors were adequate. The size of the strain gauge was more adaptable to different conditions, and the first design of the FSR was small enough to be used on the skin combined with other sensors. However, the installation of the FSR was more complicated, and the conductive material would be in contact with the skin all the time; which also affects the electrical interface. Meanwhile, the strain gauge proved to have a satisfactory electrical interface, and it was quickly adapted to the band in the final sensor.

Finally, the response of both sensors was linear. The strain gauge increases as its stretched and the FSR changes its conductivity accordingly to the pressure exerted on it. However, the FSR did not show repetitive behavior during the different measurements.

	Strain Gauge	FSR
<i>Size and Weight</i>	X	X
<i>Installation</i>	X	
<i>Electrical Interface</i>	X	
<i>Linear response</i>	X	X

Table 4.2: Comparison of force sensing technologies.

The result of the comparison shows that the FSR was more suitable to provide information about the activation of a specific muscle, since it can detect light pressure applied. However, the prototype did not work as expected due to difficulties on the fabrication. The strain gauge showed information of the general activation in the muscles of the upper arm. The size of the strain gauge is more adaptable to the circumference of the arm than the FSR, and it shows changes in resistance when stretched. Finally, the electrical interface of the strain gauge was printable without the necessity of any additional procedure after printing, while the FSR prototypes did not have any proper connection for the testing.

A combination of both technologies was not considered, since using the strain gauge alone would provide enough information about the arm for this project. The FSR could be a valuable addition because it provides specific information about each muscle. However, it has to be redesigned to avoid contact of the conductive material with the skin of the subject.

The FSR alone could be an excellent tool to categorize the muscles activated while contracting the upper arm. For this reason, it could be considered in the future work as a combination of both technologies.[40, 21, 43]

4.5 Band

After having selected the main sensing technology of the device. The next step was to set some guidelines to design the final sensor.

The sensor was aimed to work on the upper arm. The muscles conforming this part of the body, are in constant movement, and therefore in continuous deformation.

Guidelines

The guidelines below are used by Gemperle et al.[71] to design wearable systems, and are an indication of the features to consider when designing a new device used in the human body.

- Placement. It is important to consider where is going to be attached the device.
- Form. Defining the shape of the device will help to improve the design.

- Human movement. Consider the dynamic structure of the human arm.
- Proxemics. Acknowledge of space of the user, space where the arm moves.
- Sizing. How is it going to adapt to different sizes?
- Attachment. Method to attach the device to the arm.
- Containment. Considering the sensors that will be included in the device.
- Weight. The weight of the device should not hinder the movement or balance of the arm.
- Interaction. The way the user interacts with the device.
- Heat. The human body is sensitive to products that create, focus or trap heat.
- Aesthetics. Shapes, textures, and colors dictate the perception of the device [72].
- Long term use. If the device is used for a extended period, consider the effect on the user's arm.

Considering the guidelines, it was possible to detail a description of the functioning and characteristics of the sensor.

- The sensor will be attached to the upper arm with a band shape made of flexible material.
- The contraction of the upper arm will increase the cross-sectional area when the length is reduced. This action will stretch the band around the arm causing a stretch in the strain gauges.
- The band should be tight enough to avoid slipping but be comfortable at the same time.
- The band should be adjustable to the circumference of the upper arm.
- After several hours of use the device can start feel uncomfortable, therefore, it is important to design the band adjustable for a better comfort.

Characteristics

The characteristics required for the band were selected after the guidelines To detect the most significant qualities that the band requires:

- Thickness. The band should be thin enough to allow its deformation when stretched along the muscle of the arm.
- Width. The width of the band depends on the strain gauge. However, extra space should not be necessary, since the strain gauge is already optimized. The slimmer the band, the better will adapt to the arm and be more comfortable.
- Adjustable. The arms are different for every user; the band must be able to adapt to the size of the arm for each subject.
- Electrical Interface. The wires connected to the band should allow free movement of the user and be easy for the researcher to adjust.
- Stain-gauge built-in. The strain gauge selected should be built in the band and not attached to it; so the deformation of the band is the same as the strain gauge, and the readings are as accurate as possible.

4.5.1 Prototypes

The prototyping started after organizing the characteristics desired. It is important to mention that the first designs of the band were made in parallel to the strain gauge analysis. Some of the first designs do not include the final version of the strain gauge presented previously.

The first proposed design was a full band with strain gauges on the external face. The band would be placed on the outside of the upper arm as an accessory and be positioned over the muscles measured. The thickness of the band was 5 mm, and it was intended to be printed in one piece.

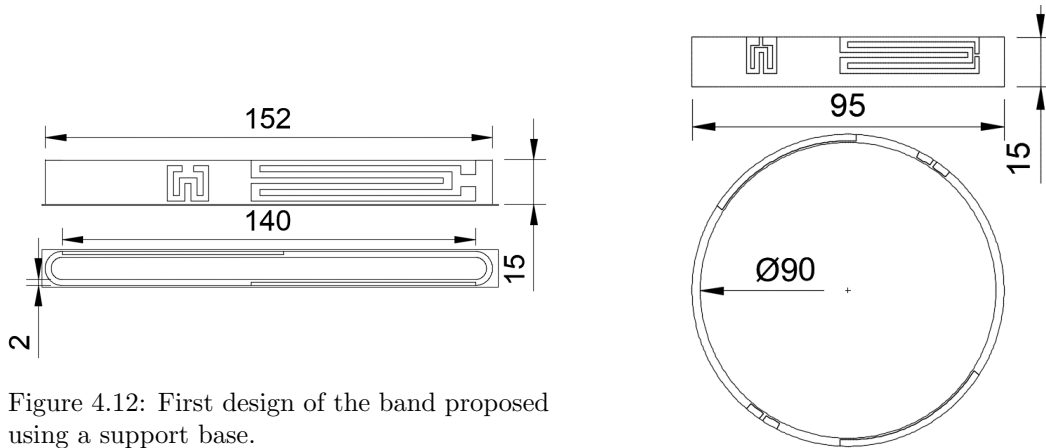


Figure 4.12: First design of the band proposed using a support base.

Figure 4.13: First design of the band proposed without support base.

The first prototype had 3 mm of width; this caused a challenging printing without supports, even at lower velocities. The gauges were also losing contact at the first layers due to bleeding of the nozzles. After noticing these errors, and due to the lack of stability while printing, the design had to be changed.

The next approach was to reduce the width of the band while adding support for the base to be printed. Besides, a change of the band's shape was implemented to reduce variations during the printing.

Figure 4.12 and 4.13 show the first prototype, using a support base on the left side and without support base on the right side. Unfortunately, in both prototypes, the band was not adjustable and impossible to fit for some users. The gauges on the side were uneven due to the position of printing, causing interruptions on the printed lines for the conductive material.

The next design was meant to be formed by two pieces to add adjustability. The Figure 4.14 shows the small band with the strain gauges built into the lines; this was to avoid the "bleeding" at the moment of the printing and to obtain a continuous line of the conductive material. The hole in one side of the object is planned to allow strapping the second part of the band. The elevations on the other superior face are intended to lock the band in different positions.

However, the thickness of the band was around 4 mm which did not allow the band to stretch or to deform; this was not noticed in the first prototype because it was printed as a circle, which could be deformed easily. The strain gauge in the middle of the band was not deforming correctly, so the values read for the resistance were not consistent after several measurements, the values varied in range of $\pm 4 M\Omega$.

The third design proposed changed the dimensions of the band. The thickness was reduced to a 1 mm, this way the band would stretch with the arm correctly. The strain gauges were printed on the top face of the band, which allows printing the lines correctly, with appropriate resistance. This change would also allow adding a connection method for the electronic interface.

The band was divided into two parts which will later be attached using metal pins. This way

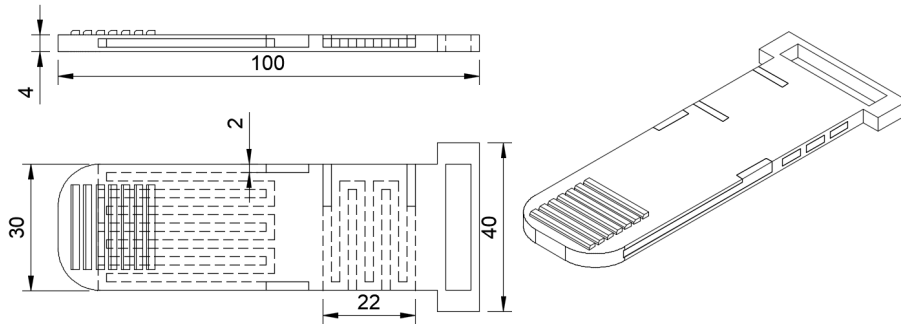


Figure 4.14: Second design of the band proposed.

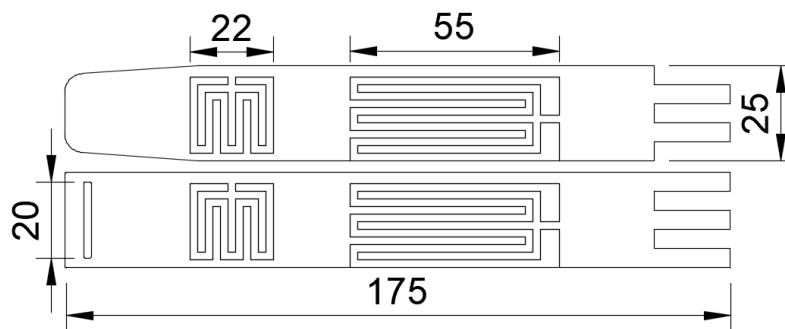


Figure 4.15: Third design of the band proposed.

the manufacturing of the two separate pieces would reduce the possibility of error, and correctly printed would increase the stability of the measurements. One part of the band comes with a hole to close the band and adjust it to the size of the user's arm as shown in Figure 4.15.

4.6 Final Design

The final design of the band includes four strain gauges of the optimized version, intended to have accurate electrical measurements. Two of the strain gauges are stretched along the band, thus, when the band is stretched the strain gauges will measure the increase in circumference due to muscle contraction. The other two gauges are in opposite direction to the band, oriented to the perpendicular part of the stretching, this way when the band is stretched the resistance values of this two strain gauges will remain almost constant. Each strap of the band contains one large strain gauge and one short perpendicular. By using a Wheatstone bridge as an electrical circuit, the use of the four strain gauges allows to compensate for temperature dependence and improve the reading to a linear, constant and stable measurement of the gauges.

The four strain gauges have four small holes to introduce electrical pins for a 4-point resistance measurement. This way the connection is stable and allows movement of the arm which eases the data acquisition during the experimentation.

One strap of the band has a hole to introduce the other part of the band. When the second part is introduced, it can be locked with a button-like system of six holes. The band is adjusted and then locked in the desired position.

The band was designed as a two-part system to allow an extra third part in the middle. Some users are more muscular than the average, which increases the size of the biceps. Hence, an extension of 3 different sizes was designed to be used if needed.

Figure 4.16 shows the final design of the band with the optimized strain gauges, and Figure 4.17 shows the measurements of the band when designed.

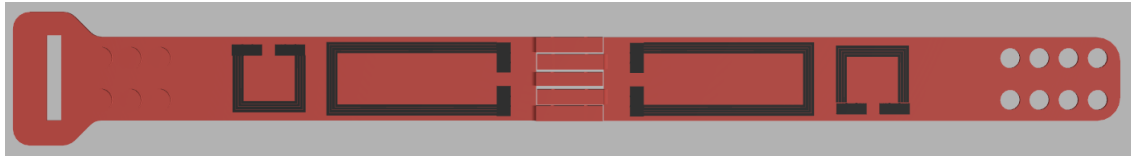


Figure 4.16: The selected design for the band contains different extensions allowing the sensor to be adapted to different users.

The final band without extension has a length of 33.2 mm, which after locked gives a circumference of 29 mm, the average size for the upper arm.

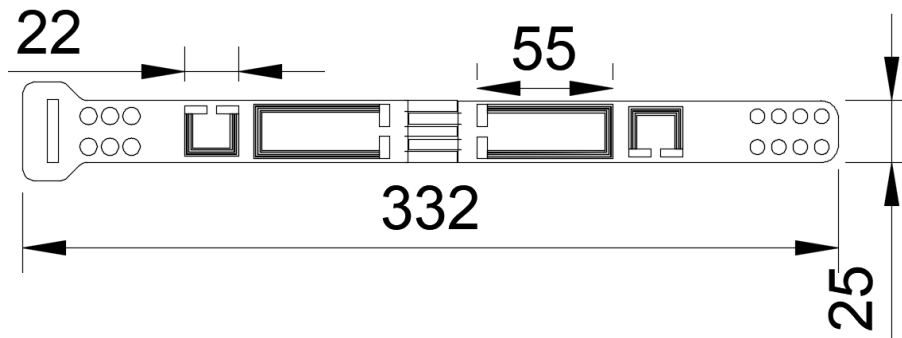


Figure 4.17: Measurements of the final band including the optimized strain gauges.

The next chapter will describe the experiments performed in the bands and the sensor technologies used.

4.7 Conclusion

Designing the FSR and the strain gauge previous to the band was a wise decision. It allowed to compare the advantages of both sensors and to optimize the mechanical and electrical characteristics individually.

The information about the human arm needed for this study could be obtained by the use of a strain gauge alone. Therefore, it was not needed to include an FSR in the final design. The band seems to deform as needed, and the next step is to test the changes in resistance due to stretching in different environments and conditions.

The strain gauge designed showed the importance of the geometric qualities of the device. It has been demonstrated that the resistance of the conductive material depends on a significant scale on the design, the width, lines, and infill of the printing. The different designs of the strain gauge suggested that the more narrow the area is, the more resistance is obtained.

The final design of the FMG sensor band reads consistent values of resistance, showing repeatability through different prototypes, and it is ready for the experimentation.

The following chapter presents the experimentation of the technologies and the clinical assessment of the FMG sensor.

Chapter 5

Experimentation

5.1 Introduction

The previous chapter gave an idea of the behavior of the technologies used in this project, this chapter will be dedicated to the experimental determination of the performance of the used material and fabricated devices, as well as with a comparison with the models introduced in the previous chapters. The experiments consist in testing the relationship between the elongation and the changes in resistance of the various systems.

5.2 Filament

The initial experiments are performed on the conductive filament, due to its importance in a 3D printed device. This material will show changes in its resistance properties when stretched. Therefore, some experiments were performed to analyze the change in resistance during the elongation of the material.

5.2.1 Setup

The first experiment is using a piece of 3D printed filament, a piece of PI-ETPU 95-250 Carbon Black (ETPU). The raw material has dimensions of 50 mm length and diameter of 1.75 mm, and it was stretched during different conditions to observe the properties of its resistance.

The filament was attached from one side to a fixed part and on the other to a sliding rail. A motor pulls the rail at $6 \frac{\text{mm}}{\text{min}}$. During the stretching of the filament, its resistance is obtained by a multimeter Keithley 2000 using a four-point measurement. The multimeter provides a constant current of $6 \mu\text{A}$. Figure 5.1 illustrates the setup where the filament was attached.

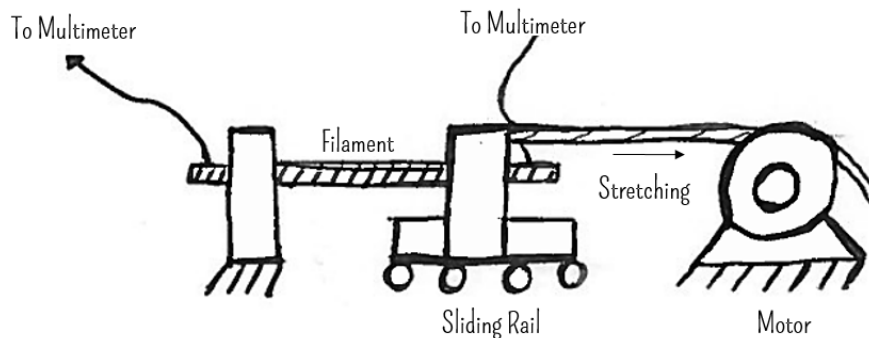


Figure 5.1: Setup used to stretch the filament while testing the resistance changes.

The following tests were performed on the filament:

- The filament is stretched 9%.
- Three samples of the filament are stretched up to the breaking point.
- Two samples of the filament with the same geometric properties are stretched and released 5 times.

These three different tests will help to understand if the filament can be elongated enough compared to the muscle's change in cross sectional area. They will show if the material properties differ from sample to sample, or if it is constant through the entire batch of material. Moreover, finally, these experiments will demonstrate the performance of the filament during extreme stretching.

5.2.2 Results

For the first experiment, the sample of the filament was stretched 9% to determine its change in resistance. It was noticed that the resistance decreased during the stretching. The model predicted an increase in resistance due to a reduction of diameter in the filament.

However, the initial absolute value of the filament was around 4.2 k Ω , and it decreased almost 25%. Figure 5.2 shows the measurement results of the filament when exposed to stretching.

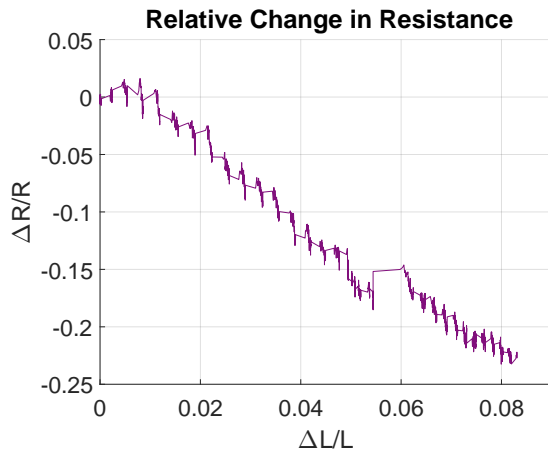


Figure 5.2: Resistance measured while filament is stretched 9%

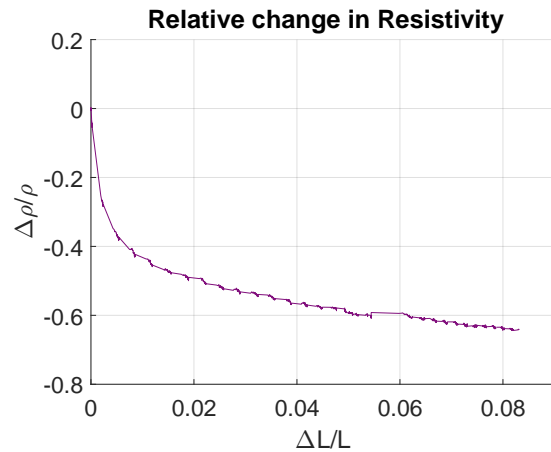


Figure 5.3: Computed resistivity of the filament tested

The decrement in resistance could be related to the input on the material's resistivity. As showed in the filament model of chapter 3 Figure 3.11. The model showed that for small strains the piezoresistive effect had more impact on the resistance of the material than the geometric change.

To corroborate if there was a negative resistivity as the assumed in the model of the filament, the resistivity was computed using the Equation 3.13. Figure 5.3 shows that the material has a negative resistivity, which decreases almost -60% for only 9% of the filament elongation, suggesting that at least for a small stretch the material's piezoresistive effect may contribute more to the resistance than the geometric input.

For this purpose the filament is after tested up to breaking point. This way it is possible to confirm if at some point the material resistance increases due to the geometric contribution.

The second experiment consisted in stretching three samples of filament under the same conditions. This test was meant to analyze the consistency of measurements through different samples of the filament. This way, it is possible to confirm that the material has the same properties in the entire spool. Figure 5.4 shows the resistance decreases when the material is stretched to around

20 mm; the filament can return to its original state after this deformation. However, when the filament is elongated up to 150 mm, it is not able to return to its original state, this is known as plastic deformation. At this point, the resistance starts to increase up to several M Ω ; nevertheless, the material will be used under elastic conditions.

There may be a narrow range where after the plastic deformation the material can have some reversible effects, however this analysis may take a deeper characterization of the filament [73]. Nevertheless, the FMG sensor will work under the same range as the upper arm; this spectrum is up to around 9% of increment, even considering a prestretching while mounting the band, Figure 5.3 suggest that the elastic deformation is up to 40%. Thus, the sensor will work only during the elastic deformation of the material to detect muscle activity.

The third experiment was meant to investigate the reversibility of resistance changes during reversible stretching. Two different samples were stretched several times to detect if the material would maintain its decrement constant; Figure 5.5 shows a drift during the measurements, while the first sample is at first presenting a fractional change of -60% during the initial stretching, after the sixth time the relative change is only over -40% .

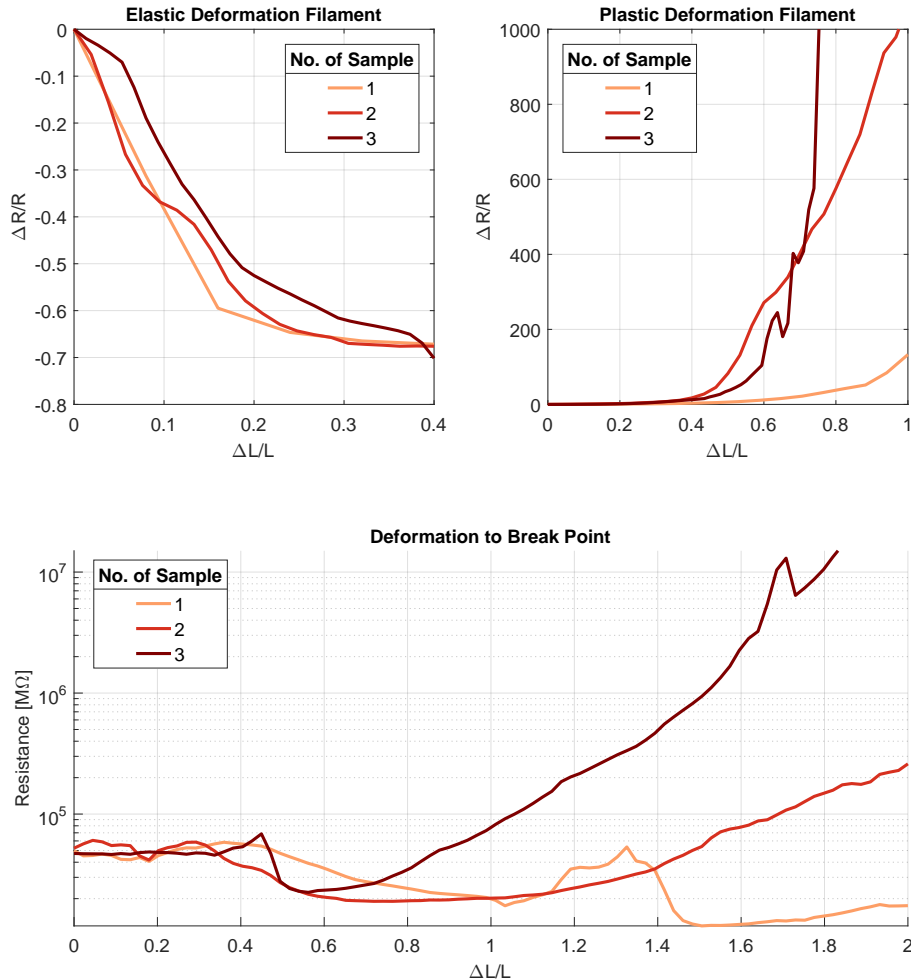


Figure 5.4: Filament measured up to breaking point

That behavior could affect the detection of muscle activity after several uses. The second sample showed a similar difference between the first and the sixth measurement. Figure 5.6 shows the end point values after stretching the filament for each sample during the six measurements. The plot shows that both sections of material have similar measurements of resistance at the initial elongation, changing at least -60% . During the following stretching, the values of both filaments

stayed within comparable ranges. At the end of the sixth measurement, the fractional change in resistance was reduced up to $\approx -42\%$ in both samples, demonstrating that both samples of material have a similar performance.

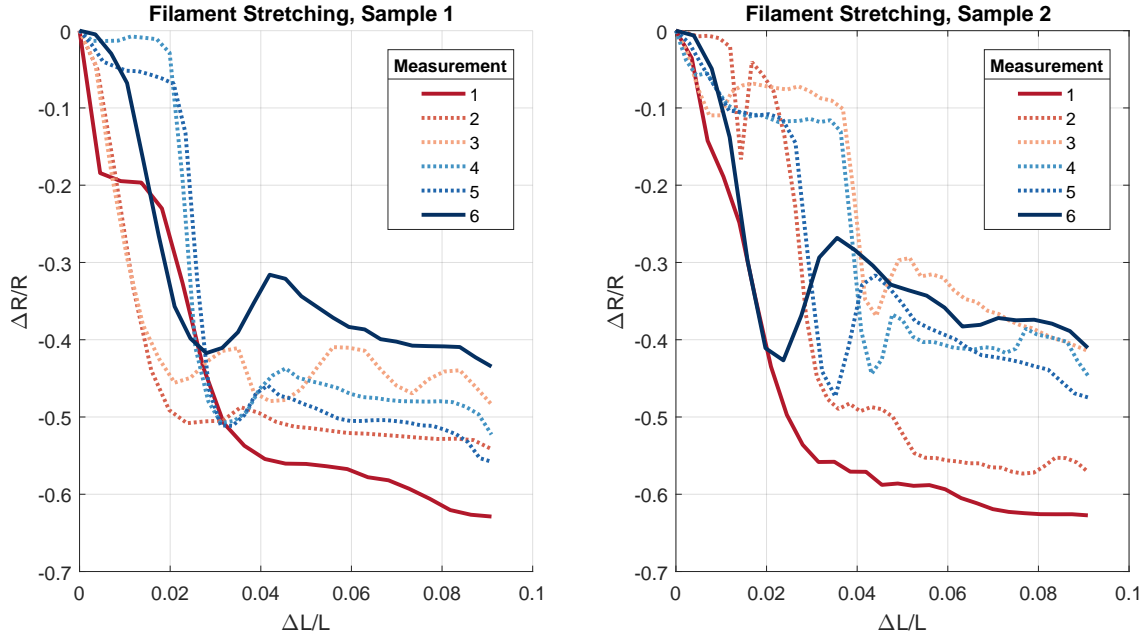


Figure 5.5: Two samples of material tested under the same conditions to determine its repeatability.

The material showed a comparable conduct during the measurement of the two samples. This result suggests that the material may have consistent properties along that specific spool. Even if there is a drift during several measurements that drift could be proportional in different samples, when having the same conditions of temperature, and mechanical stretching for each sample, at least when they are from the same batch of material.

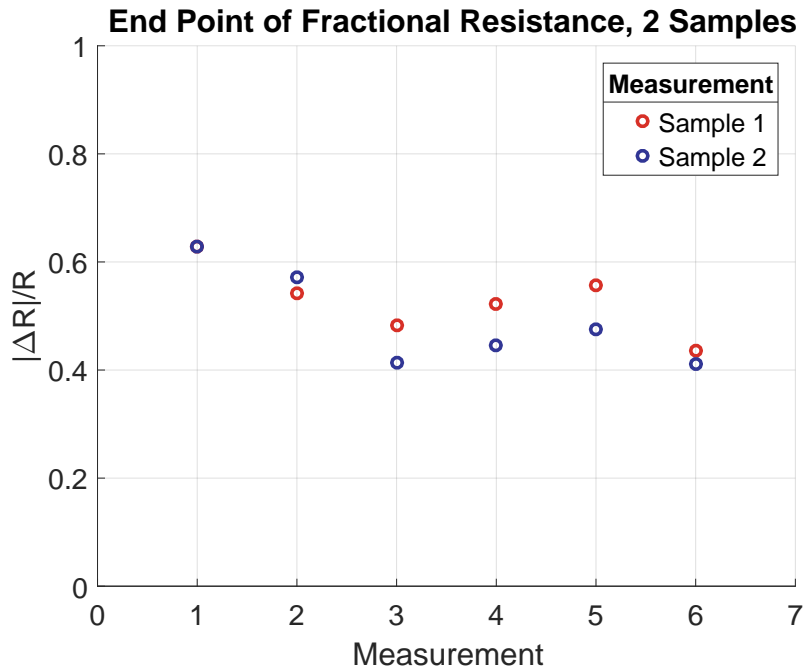


Figure 5.6: Final value of the fractional resistance for both samples of material

5.3 Printed Filament

The conductive ETPU changed its properties after being printed due to the exposure to heat. Therefore, it is necessary to test the material after printing to determine its mechanical and electrical characteristics. The information obtained will give more insight related to the eventual performance of the material in the strain gauges.

5.3.1 Setup

The printer was set to extrude 10 cm of filament at 200°C and later removed directly from the nozzle. Three samples of 50 mm long with a diameter of ≈ 0.8 mm were obtained, these samples were tested for changes in resistance while stretched; the fragments of filament were attached to the setup shown in Figure 5.1. They were stretched at 6 mm/min and measured with the same multimeter Keithley 2000 at a constant current of 1 μ A

Henceforth, the trials performed were:

- Stretch and release filament at 2 mm/min.
- Stretch and release 6 times at 6 mm/min.

This information will provide insight about the change in resistance after the material is printed, and how the temperature change affected the piezoresistive effect of the filament.

5.3.2 Results

Both tests were to detect the effect of the temperature on the electrical characteristics of the filament. After printing, the material was stretched several time, the first experiment showed that the absolute value of the resistance of the filament was higher than before printing and the second experiment tested to detect the drift on the measurement after several elongations.

As shown in Figure 5.7, the relative change in resistance was similar. The initial elongations started with significant changes up to -60% and decreased over the number of stretches. During

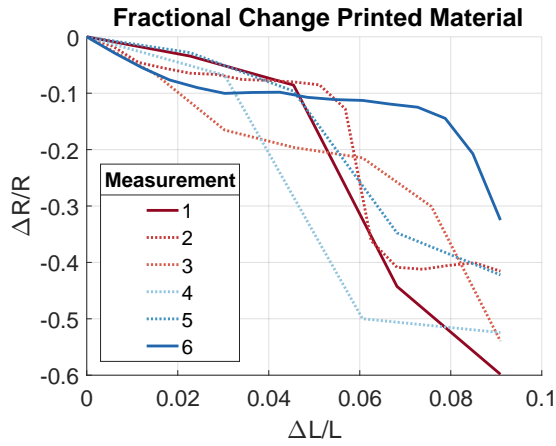


Figure 5.7: Relative resistance changes of the printed filament while stretched.

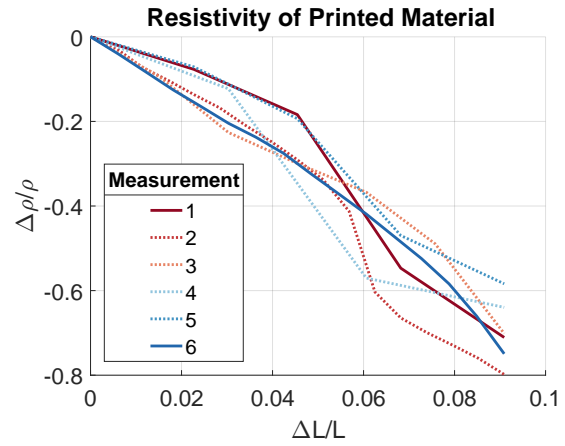


Figure 5.8: Resistivity of the material computed for the printed filament.

the final elongation, the resistance was changing around -30% . These values are consistent with the filament in its original state.

Figure 5.8 shows the resistivity computed using the Equation 3.13 for the printed filament. The material input is negative as expected, and for the 9% elongation the values are similar to the ones presented for the filament in original state.

5.4 Strain Gauge

The model of the strain gauges showed a reduction in resistance due to stretching. However, after analyzing the results of the filament experimentation, it is possible to hypothesize that the printed strain gauges will also show a decrement in resistance while stretched.

5.4.1 Setup

The setup of Figure 5.1 was modified properly to clamp the strain gauge. The dimensions of the strain gauge tested are 55 mm long, 20 mm of width and 1 mm thick. It is important to mention that the first trials were made on eight different designs to select the one with better performance, as showed in Chapter 4 Table 4.1. After selecting the strain gauge with the best design, the rest of the experiments were tested in that model.

The following tests were performed on the 8 different designs:

- Initial resistance measurement of the strain gauge designs of Table 5.1
- Fractional change for an elongation of 9%

After the selection of the strain gauge, the following tests were performed:

- Elongate three strain gauges with same dimensions and design to 9%

The tests provided insight into the properties of the design of the strain gauge selected. At the same time, it was possible to notice if the strain gauge would change its resistance enough to detect the muscle activity.

5.4.2 Results

The different designs of the strain gauge varied in geometric aspects and forms of lines; these variations produced higher or lower absolute resistance values. After measuring the value of each

	1	2	3	4	5	6	7	8
$M\Omega$	16	18	6.5	8	35	40	12	16
$\Delta R/R$	≈ 0.7	≈ 0.65	≈ 1.3	≈ 1	≈ 0.8	≈ 0.75	≈ 0.5	≈ 0.55

Table 5.1: The eight different prototypes vary only in line width and line shape. All the models have the same base measurements and the same length for the sensitive material. The conductive material was printed at 1500 mm/min with a layer height of 0.15 mm for a complete thickness of 0.5 mm.

resistance, it was noticed that, as determined in the model, the wider the lines, the lower the resistance of the gauge. Table 5.1 shows the results of the experimentation in the 8 different designs.

As it is shown, the design number 3 presented better fractional change in resistance. This factor would help to determine the muscle contraction, thus, it is important to be a large value, this way it can detect smaller deformations of the material.

After the selection, the manufacturing of the strain gauge was optimized for 3D printing using the parameters selected in Chapter 4, (infill, line width, velocity, etc..).

The next test was to stretch the strain gauge and observe its behavior during stress. Three different strain gauges with the same dimensions and model were adapted to the setup in Figure 5.1 to be stretched up to 9%.

Figure 5.9 is showing the difference in absolute values for the resistance in the different strain gauges. However, the relative change is quite similar after stretching, decreasing $\approx -7.5\%$. These values represent the expected performance of the band when attached to the arm.

The decreasing resistance suggests that the strain gauge have a similar behavior to the filament previously tested. Since the resistance is decreasing The results show a decrement in resistance most likely due to the contribution of the material piezoresistivity to the computed resistance as observed in the previous experimentation performed on the filament.

With the value of resistance measured, it is possible to use Equation 5.1 to compute the value of resistivity and observe the magnitude of the material contribution to the resistance.

$$\frac{\Delta R}{R} = \varepsilon_L + (2\nu\varepsilon_L - \nu^2\varepsilon_L^2) + \frac{1}{\rho} \frac{\partial \rho}{\partial \varepsilon_L} \varepsilon_L \quad (5.1)$$

Figure 5.10 shows the values of the change in resistivity for the three gauges tested.

This experiment showed that the strain gauge decreases its resistance when stretched. Moreover, after testing different strain gauges of the same model and dimensions, the values obtained for resistance are in the same ratio.

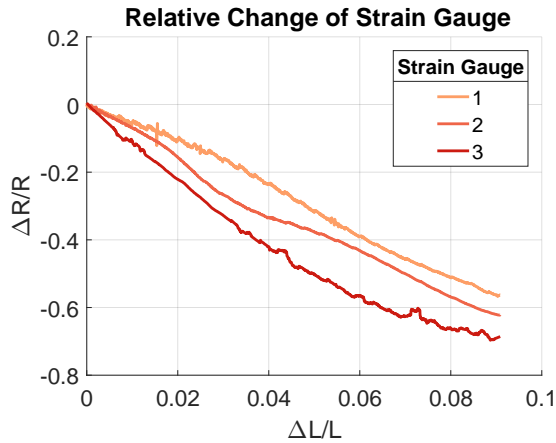


Figure 5.9: Measurement of three strain gauges with same dimensions a design. The fractional change is consistent between the three prototypes.

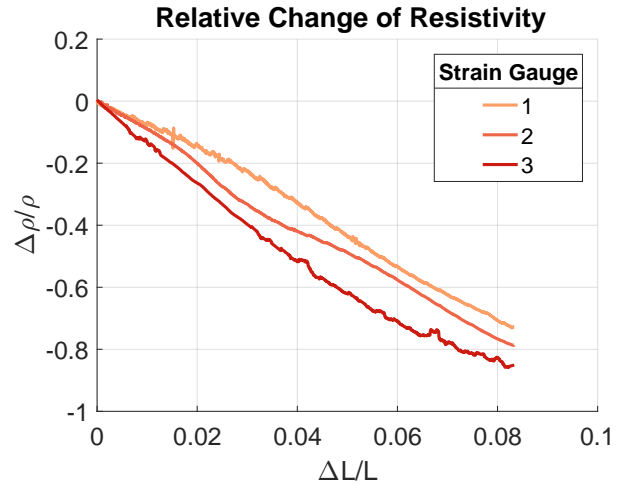


Figure 5.10: Resistivity of the material computed for the three gauges.

5.5 FMG Band Sensor

The experiments of the FMG band sensor are aimed to detect a relationship between its change in diameter and the variations in resistance that this may cause. These tests present an opportunity to check the behavior of the band in a different setup with similar conditions to the upper arm.

5.5.1 Setup

For a first approach, the band was tested attached to a PVC tube. The tube contains an air tube that expands when inflated, causing the increase in circumference of the PVC tube. This setup resembles the circumference of the arm, and when the air is pumped into the tube, the circumference raises. Since the tube is increasing uniformly, it is viable to control the size of the circumference, and ensure that the expansion will be approximate to the arm contraction.

Figure 5.11 shows the setup used for the band assessment, the FMG sensor attached to the PVC tube.

The following experiments were designed to obtain different information about the band:

- Increasing tube's circumference from 30 cm to 36 cm
- Stretch the band around the tube 6 times for 20 s until it reaches the circumference desired, and the remain 100 s at that given strain. After the stretching, release the band to test the value for hysteresis.

The muscle model showed that the muscle could increase in circumference from 32.5 cm to 35.5 cm when contracted; this is around 9%. The tube is increasing more than the expansion predicted to test the band resistance and establish the limits of its elastic deformation.

After stretching and releasing the band several times, the band could show a drift similar to the previous experiments and strain gauges. The resistance on the band could also present electrical hysteresis which means the absolute value of resistance is not returning to the original state. This hysteresis causes a drift on the measurements and can be estimated.

Stretching the band for 20 s to reach the 9% stretching and delay its return for 100 s allows examining the performance of the band during continuous stretching conditions.

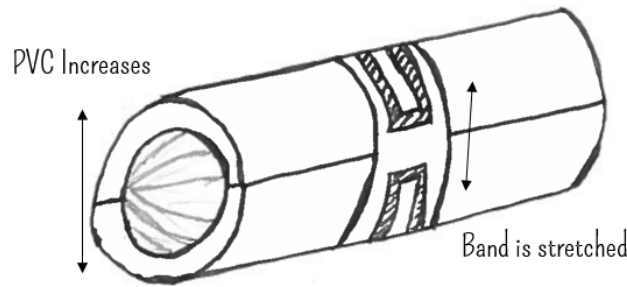


Figure 5.11: System used to test the band, the tube increases in size uniformly, allowing to test the band stretching and measure the circumference simultaneously.

5.5.2 Results

The first experiment was meant to analyze the consistency of the characteristics of the strain gauges as a part of the band. The approach was to test the resistance of the band and observe, if it was possible to obtain a significant fractional change when stretched.

Figure 5.12 show the band decreasing its resistance about 7%. The absolute values of resistance are $\approx 5\text{ M}\Omega$, but the fractional change is constant, although, it shows a small drift through measurements. Similar at the one observed when the filament was tested.

The second test was to observe the resistance on the band after stretching it 6 times. During this procedure, a drift similar as the one in the filament tests was observed; the band showed a decrement in the absolute value of resistance after each time of stretching. Figure 5.13 shows a drift of about 18% for the absolute value of resistance during the various measurements.

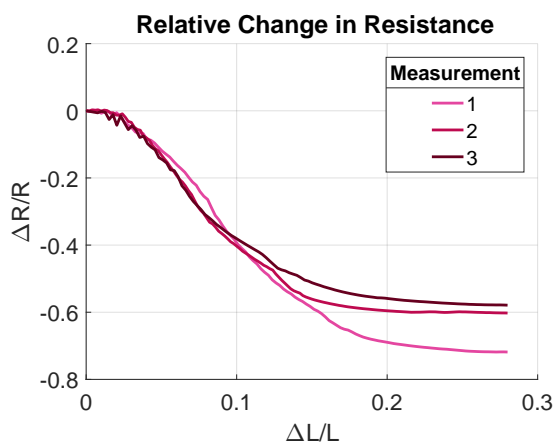


Figure 5.12: Initial measurement of the band.

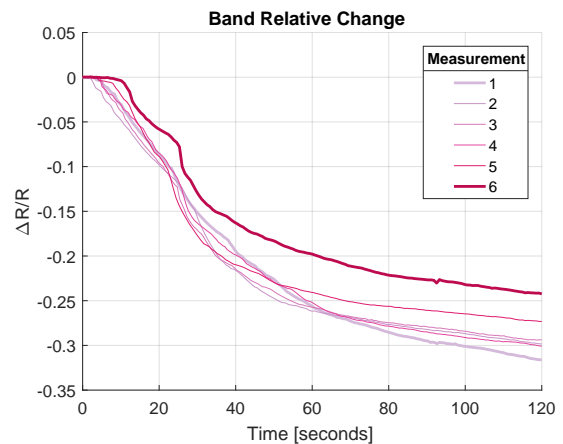


Figure 5.13: Measurement of the band stretching 6 times.

The test also showed the performance over time of the band. The sensor was stretched in the first 20s to 32 cm of diameter, and remained elongated for 100s to observe if the resistance keeps decreasing over time while stretched. The result, was a decreasing resistance, although, it was not at the same ratio, as observed in Figure 5.14.

The plot shows the ending fractional change in resistance when the band is stretched and the fractional change when the band is recovering. It seems that when the band is returning to its original state the fractional change is not the same. Also, through the different trials, the value is decreasing, although, it seems to be doing it uniformly.

The bottom part of the Figure 5.14 shows the absolute value of resistance at the beginning of

the measurement and after the recovery. The resistance is decreasing over the trials at a steady ratio.

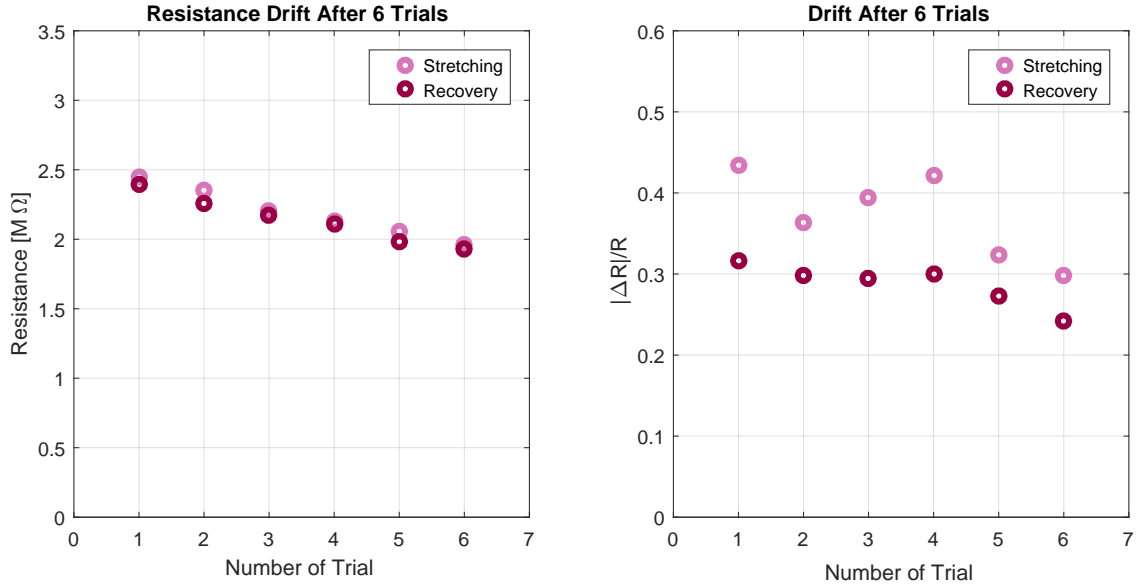


Figure 5.14: Drift analysis of the band, its absolute resistance values and the relative change.

For the final analysis using the PVC setup, the band was stretched and released while measuring the resistance to evaluate the hysteresis of the material.

Figure 5.15 shows the hysteresis of the six times that the band was stretched. The first measurement suggests that the band is recovering $\approx 2\%$ lower than its initial value. However, the last measurement, after a drift of almost 18%, shows a similar condition.

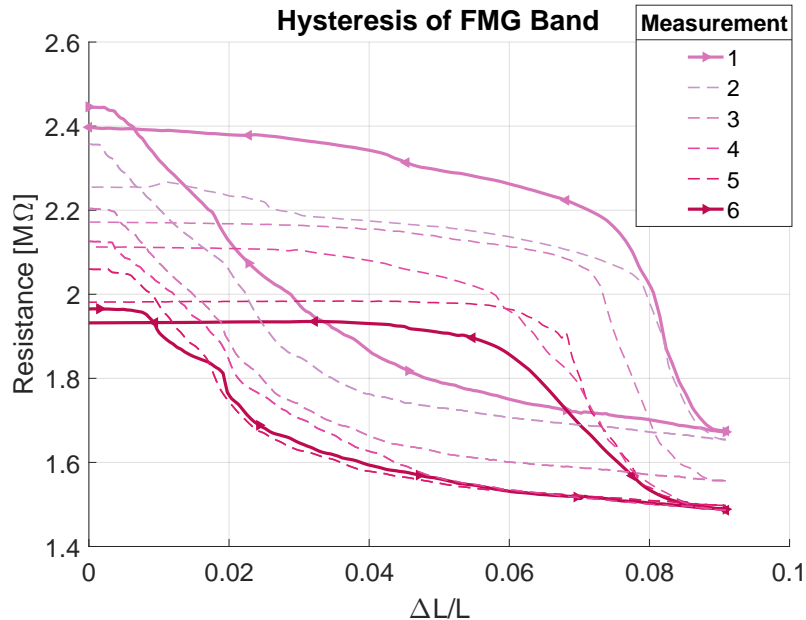


Figure 5.15: Hysteresis of the band showing the drift between the first measurement and the sixth.

The material seems to return to a lower value after each elongation; this behavior could be because of the time that the band takes to return to its original state. However, it may take more

than a few minutes for the electrical property of the material to recover from the stretching.

In any case, this is an undesirable property of the sensor, that may be investigated in future work to determine a solution.

5.6 Sensor Evaluation in Subjects

The evaluation of the sensor in subjects is meant to deliver results on the actual performance of the band and its detection of the muscle activity. The band is tested while executing different activities.

5.6.1 Setup

The band is attached to different users around the upper arm with the strain gauges placed above the Biceps Brachii. The resistances of the band is connected to a multimeter Keithley 2000 while performing a 4-point measurement. The FMG band sensor was designed to be interfaced electrically as a Wheatstone bridge, however since the ΔR values are large enough, there is no reason to use a bridge, and the resistances are measured separately.

For the evaluation of the FMG sensor, an EMG electrode will be attached to the arm slightly above the band on the Biceps Brachii allowing to measure the muscle activity of the arm simultaneously as the FMG. The data in junction will be processed by a MatLab script via USB from the multimeter and the EMG interface simultaneously.

The EMG sensor is part of the Trigno™ system, fabricated by the Delsys Inc. It is a dry, wireless electrode able to obtain EMG signals as well as motion information about the part where it is attached. For the purpose of the tests only the EMG signals will be obtained[74].

5.6.2 Experimental Protocol

Five volunteers (18+) participated in the study and signed the informed consent form. The faculty ethics committee approved the measurement protocol. The subjects were guided to perform the following tasks:

- **Isometric examination:** The subjects arm remain flexed at 90 deg, during this period, different weights are added, from 1 kg to 5 kg, while measuring the circumference of the arm, the resistance variation, and the EMG.
- **Isokinetic examination:** The subject performs a series of 3 movements at three different velocities, from the completely extended arm (≈ 180 deg) to completely flexed (≈ 45 deg), the weight increases from 1 kg up to 5 kg. The three different velocities are at 50, 60 and 70 BPM.

The total duration of the 12 trials (three isometric and nine isokinetic) are performed in less than 45 min.

5.6.3 Results

To compare the signal from the FMG and the EMG sensors, it is necessary to choose a post-processing stage of the data obtained carefully. The EMG detects the electric voltage generated by the muscle cells when these cells are neurologically activated during contraction.[18] The envelope of the signal is obtained to compare the EMG signal with the FMG measurement. The absolute value of the signal is obtained to analyze the EMG signal; this process is also known as full wave rectification. The signal is rectified to obtain the shape or ‘envelope’ of the EMG signal. When the signal is rectified, the negative swings turn into positive swings. This rectified signal is the low-pass filtered, within a range of 5 Hz to 100 Hz, the result is the envelope of the signal. A discrete version of a traditional low pass filter such as the Butterworth[75] or Chebyshev[76] filter

is applied. These are also known as 'infinite impulse response' (IIR) filters. The combination of the rectification and the (IIR) filter helps to acquire the envelope of the signal [17].

Since the EMG is a signal obtained in volts, the FMG signal was processed compiling the absolute fractional change in voltage of the data $\Delta V/V$ which is the same as the fractional change in resistance $\Delta R/R$ when a constant current of $1 \mu\text{A}$ is applied through the readings, additionally, a high-pass filtering with a corner frequency of 0.05 Hz was applied to reduce the effects of drift. Further, fractional changes were also computed for the EMG signal and adjusted to the FMG signal's magnitude. Finally, the amplitudes of both signals were equalized, this way the shape of both signals can be compared.

5.6.4 Isometric Experimentation

For the isometric analysis, Figure 5.16 shows the signals from the EMG and the FMG compared to the force model. The model was adapted for the isometric task; the test consisted in increasing the load to the grip of the subject while the arm remained contracted at 90 deg with a load of 5 kg every 8 s for a total of 35 s . The signals were post processed with the same filtering as the isokinetic analysis.

The plot shows a different behavior of both sensors than the isokinetic results. The signal of the FMG presents a peak that represents that the muscle is expanding when the load is positioned on the arm. On the other hand, the EMG signal is now more stable and consistent than for the isokinetic analysis; the measurement represents the muscle activation through the entire contraction. Both signals are similar to the behavior of the force modeled.

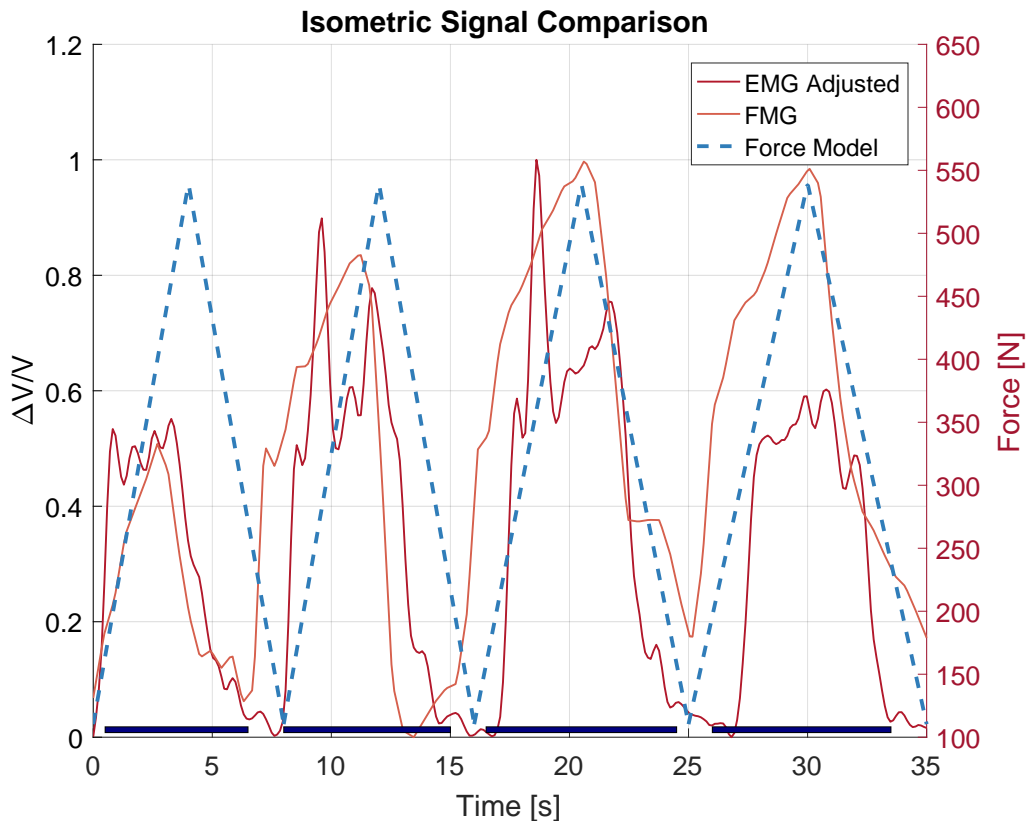


Figure 5.16: Sensor signals from Subject #2 while performing an isometric contraction every 8 sec with a 5 kg load. Blue rectangles represent the time during the upper arm contraction.

To determine the average value of the measurements the mean of the signals was obtained. The mean is the average value for a set of numbers and is defined as the sum of the sensor measurements

(A) divided by the number of measurements (n) [77]:

$$\mu = \frac{1}{N} \sum_{i=1}^N A_i \quad (5.2)$$

Figure 5.17 shows the mean results from the isometric experimentation from the five subjects, the standard deviation was also calculated to determine the spread of the measurements.

The standard deviation was computed by calculating the squared root of the variance; the variance is the concept expressing the 'spread' around the mean value μ . The standard deviation is then the square root of the summation of the mean subtracted from each value measured (A) divided by the number of measurements [77], expressed as:

$$\sigma = \sqrt{\frac{1}{N} \sum_{i=1}^N (A_i - \mu)^2} \quad (5.3)$$

After both signals are processed, the mean of the FMG shows a not consistent behavior while increasing the weight. This behavior may not be due to the sensor, since the EMG is also not detecting more muscle activity. However, both sensors could be giving false readings due to external conditions, e.g. movement artifacts, from cables or the electrodes/band. On average, the muscle activation increases when the load is increased. It is also observed that the FMG signal has a larger standard deviation than the EMG signals, this could be due to the FMG signals presenting more drift and hysteresis than the EMG signals.

This figure also represents different behavior according to the muscularity of the subject. The subjects #1 and #2 were more muscular than the subject #3 or #5, showing what could be interpreted as a less muscle activation and a smaller change in CSA. Even if at the moment of the task the subjects are lifting the same weights and exerting the same force, this may be due to the coactivation of more muscles such as the shoulder or the back, to compensate the lack of muscle fibers of the biceps. Nevertheless, this result also may not be related to the muscularity of the subject but associated to the mounting of the band. A better performance may be measured if an standardized collocation of the band was used, e.g. tightness of the band or prestraining to determine a constant initial point of measurement.

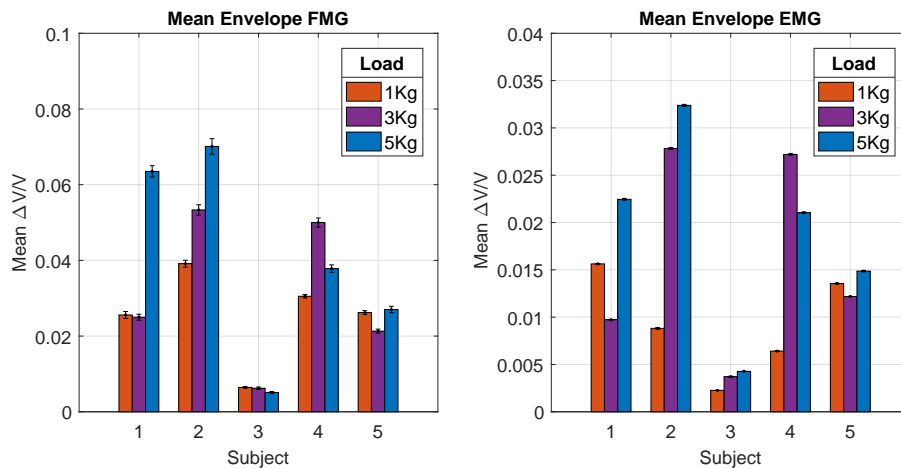


Figure 5.17: Mean of the EMG and FMG signals during isometric contraction for each subject and its standard error.

5.6.5 Isokinetic Experimentation

Figure 5.18 shows a comparison of the signals obtained from the Subject #1 when performing an isokinetic task at 60 BPM with a load of 5 kg. In the image, signals from both sensors (EMG and

FMG) are evaluated against the force model. The Force model presented in chapter 3 is used to represent the movement from extended arm to fully contracted considering the load of 5 kg and the weight of the arm. The distances of the arm are adapted according to the subject, and the weight of the arm is considered to be the average of 2.5 kg as found in the literature [62]. During the contractions, the FMG signal seems to follow the behavior of the modeled force with a greater resemblance than the EMG signal.

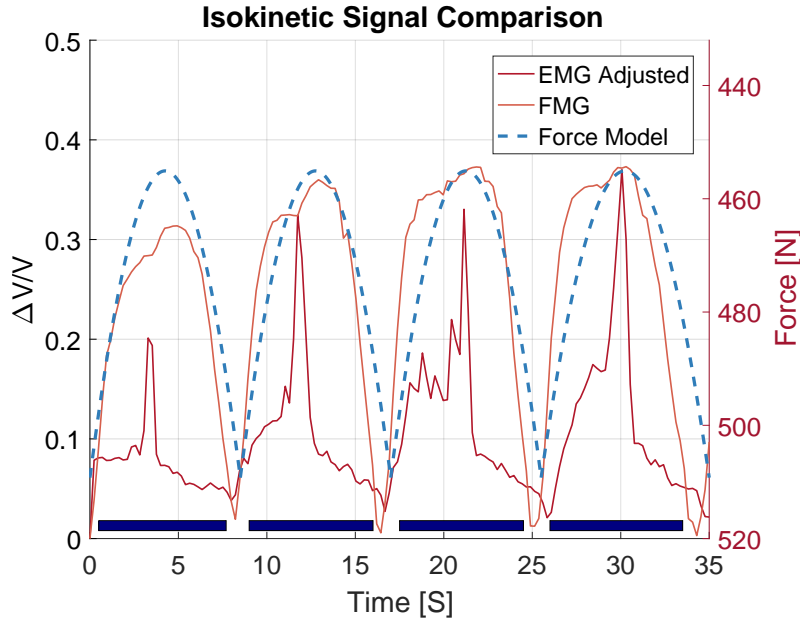


Figure 5.18: Sensor signals from Subject #1 while performing contraction every 8 sec at 60 BPM with a 3 kg load. Blue rectangles represent the time during the elbow flexion and extension.

It is important to remember that the EMG signal has a considerable sensitivity to noise and movements, and its shape may be representing the muscle activity instead of the force modeled. On the other hand, the FMG signal only represents the expansion of the cross-sectional area of the muscle, showing a more gradual change through the complete contraction. When the muscle is contracted the signal reaches the highest point, and it decreases steadily as the muscle lengthens again.

Even if the units are not the same, the pattern of the FMG sensor represents the movement of the arm correctly. When the contraction starts, the FMG sensor detects the expansion of the upper arm and the relaxation of the muscles as the tension changes.

Figure 5.19 represents the mean envelope of all the subjects while increasing the velocity of the contraction for different weights. The plot shows a apparent difference in signal for the FMG sensor but also the standard deviation is higher for the FMG than the EMG in all the measurements. The mean values of the FMG show more relation with the increment in weight over the different tasks than the EMG signals. It is normal to observe a higher detection of muscle activity when the velocity of the contraction is at 50 BPM, due to the reduced velocity of the contraction, meaning that muscle fibers are activated for an extended period, and there is more time the signal of both FMG and EMG detects the muscle contractions.

However, this plot shows a slight decrease in EMG detection when the weight is 5 kg during the three different velocities; this could mean that due to the increased weight, there is a co-activation of different muscles to compensate the lack of strength from the Biceps Brachii. This co-contraction would diminish the activation of the muscle tested. A similar muscle from the upper limb as the shoulder, the forearm or even a back muscle could be more involved in the movement reducing the recruiting of muscle fibers of the Biceps Brachii where the EMG sensor was positioned. These co-activation of muscles would not be detected by the band, since the band

is only attached to a portion of the upper arm, that includes the Biceps, the Triceps and the Brachialis. A way to detect if other muscles are also being activated when lifting larger loads, is by using additional sensors in specific targeted muscles that may be activated.

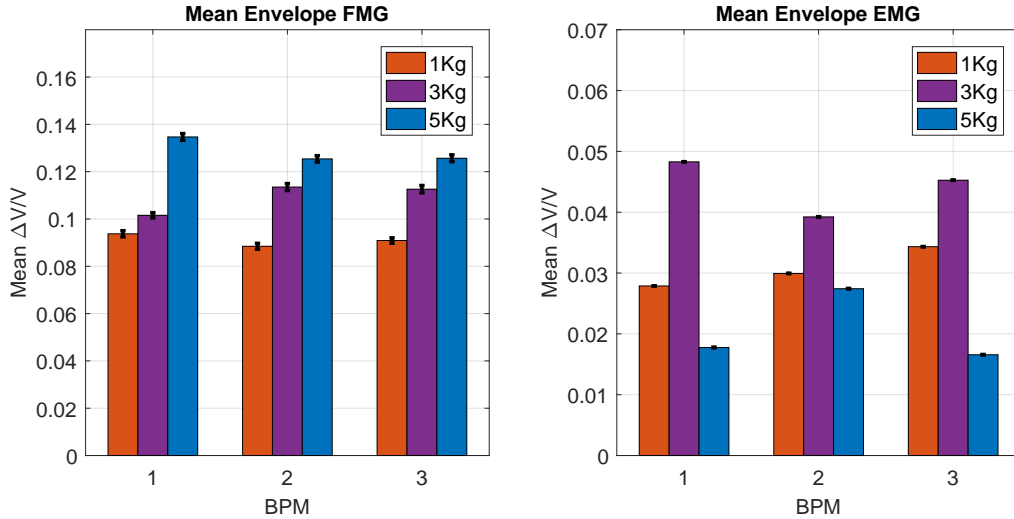


Figure 5.19: Mean of the EMG and FMG signals during isokinetic contraction for all the subjects and its standard error.

5.7 Muscle Classification

The human muscles can only contract, that is why they come in pairs with an antagonist muscle. In the case of the upper arm, the Biceps Brachii antagonist is the Triceps Brachii which helps to extend the arm after contracted. When the arm moves, there is a co-activation of the muscles, allowing the arm to move with stability through its trajectory. The FMG sensor detects the muscle contraction. However, a test was designed to evaluate if the FMG sensor is also able to classify each muscle's activation separately; this way it would be possible to categorize the muscles that are activated, as previously done by Paradiso et al. [20] and Chen et al. [42].

5.7.1 Setup

The FMG Band sensor is designed with four strain gauges allowing it to detect the stretch of the band in different positions. The band was positioned on the subjects with one strain gauge over the biceps and one over the triceps during the execution of a task involving the co-activation of the muscles.

The task consisted in the flexion and extension of the elbow joint to activate the muscles of the upper arm. The complete movement of the arm will last 10s at a velocity of 50 BPM during a total of 35s. The movement will be with a load of 3kg to perform an active contraction. Figure 5.20 shows the two positions of the arm holding the load.

Since the movement is aimed to produce a contraction in the biceps, the results should show a more significant change in the strain gauge positioned above the Biceps Brachii than the one situated over the Triceps.

Even if the strain gauges are standardized regarding its absolute value of resistance, during a second measurement the strain gauges will switch positions to discard that any difference in the outcome could be related to the strain gauge and not its position.

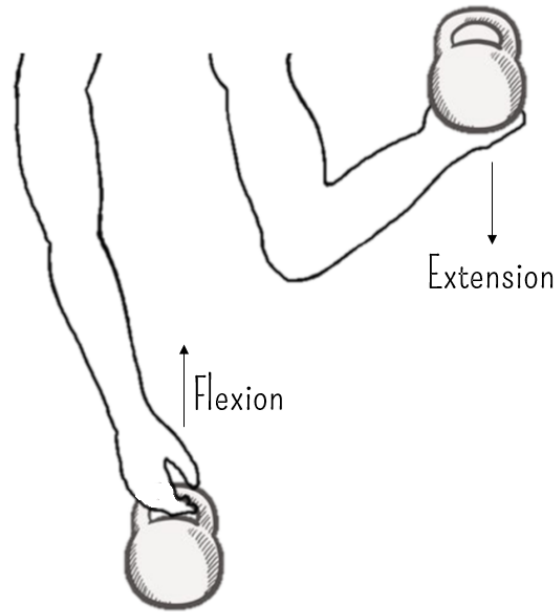


Figure 5.20: Movement to test muscle classification of the FMG sensor, flexing the elbow joint at 50BPM with a 3kg load.

5.7.2 Results

To compare the two signals the fractional change in both strain gauges was computed. In Figure 5.21 one of the measurements is showed. The strain gauge on the biceps showed a higher change than the one over the triceps. After the Triceps value is subtracted from the Biceps one, the remainder not being a flat-like result suggest that the bicep strain gauge is detecting a higher change just as hypothesized. However, since the result could be detecting only that one strain gauge is changing more due to the printed characteristics and not because of the position further analysis is needed.

In general the majority of the measurements even after changing the position of the strain gauges presented a higher change while positioned over the Biceps. The mean of the signals was computed and showed in Figure 5.22. The first plot shows the mean of the Biceps being slightly higher than the mean of the Triceps. The third plot is showing a difference between the two means of about 3% when fully contracted.

Nevertheless, 3% of difference for a fractional change of $\approx 40\%$ is a modest value. This result means that the band could detect which muscle is more contracted but is not a definitive classification. The muscles of the upper arm may be more detectable due to its size. However, to classify muscles in other parts of the body, a combination of technologies is suggested, such as using EMG, or adding more force sensors to the analysis.

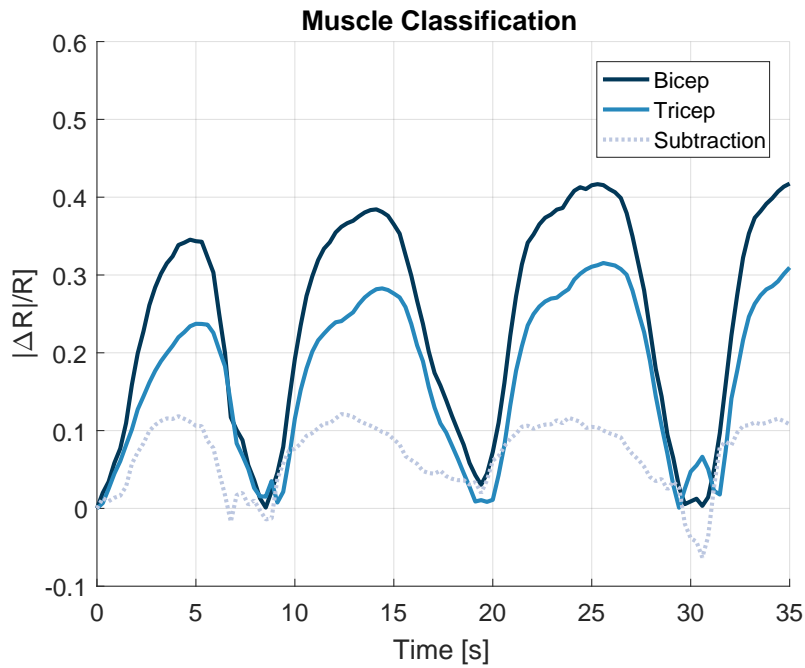


Figure 5.21: Fractional change of Biceps and Triceps movement during concentric contraction at 60BPM with a 3kg load of subject #3.

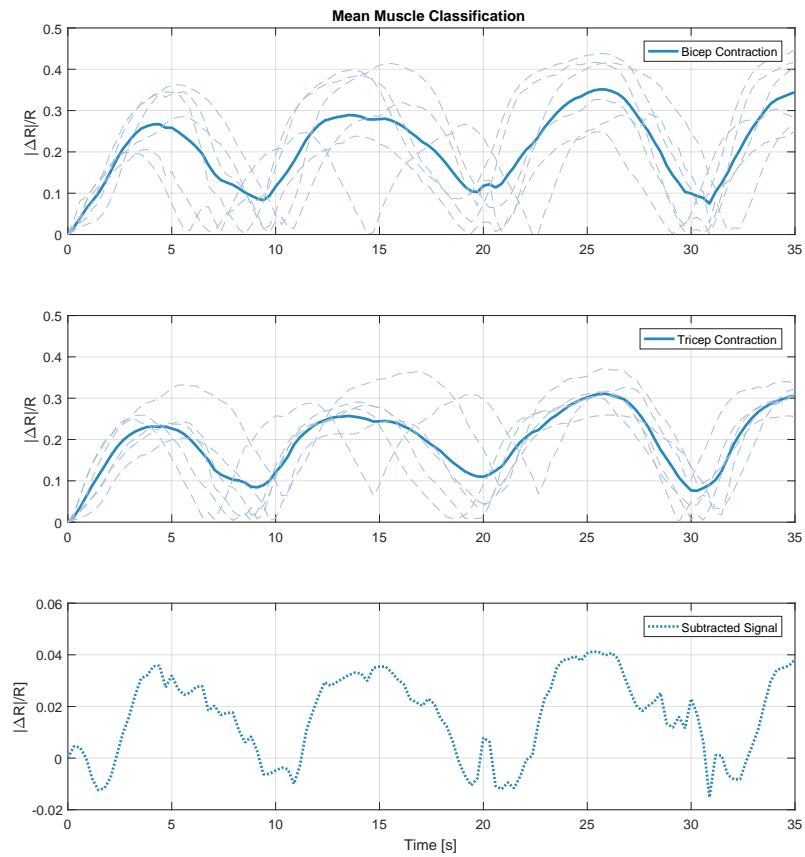


Figure 5.22: Mean values of the measured Biceps and Triceps signals, with the mean subtracted result.

Statistical Analysis of Muscle Classification

The statistical analysis aims to evaluate the two strain gauges obtained during the categorization of the muscles by comparing the measurements where the first strain gauge is positioned over the biceps brachii and the second gauge over the triceps brachii.

From this test two different signals are obtained, the shape and values of its measurements indicate that there is a difference between the mean values. However, it is important to corroborate using an statistical analysis [77].

A paired t-test was selected to test the difference between the strain gauges of the FMG Band sensor, using a significance level at $p < 0.01$ [77]. The analysis was performed for each pair of strain gauges in the five different subjects.

Subject	1	2	3	4	5
<i>P</i>-value	<0.001	<0.001	<0.001	<0.001	<0.001
Mean difference [$\Delta R/R$]	0.0510	0.0532	0.0929	0.0554	0.0692

Table 5.2: Table with the results of the paired t-test, showing the P -values for the comparison between the strain gauges of each subject while detecting biceps and triceps simultaneously.

The Table 5.2 shows that the P -value for each comparison of the strain gauges are $< .001$, in all cases the null hypothesis is rejected. Even if the signals are different statistically, it is not possible to conclude that the band can detect which muscle is being activated by using only the strain gauges; to obtain a more accurate information about the muscles contracted it is suggested to add a different sensor.

5.8 Conclusion

Each experiment was designed to obtain different characteristics of the material used and the sensors designed. The tests related to the filament showed that for a small strain the material's piezoresistive property has more contribution to the change in resistance than the changes in geometry, causing a decrement in resistance when the filament is elongated. However, this behavior changes when the material reaches a threshold or a minimum level of resistivity, and it is at this point when the resistance starts to increase according to its change in shape. Although, this threshold depends on the material properties and the way they change after being 3D printed.

The strain gauge's experiments demonstrated that after a number of elongations the absolute value of resistances starts to drift, but the fractional change remains consistent through the stretch applied; this behavior suggests that its the behavior is repeatable during the different tests performed, even after printed and tested on the band.

The band showed substantial changes in resistance while stretched. Although, the sensor is highly dependable on its geometric properties, and the elastic deformation generates a drift on the measurements that can be compensated with a high-pass filtering.

The band showed a decrease in fractional change after several stretches, showing some electrical and mechanical hysteresis, the material is not returning to its original absolute value of resistance at the same rate as it is stretched. However, after some minutes the values stabilize, and the band performs the same as during its initial state. A pre-stretching of the band could reduce the drift on the measurements and improve its accuracy since the values would be starting from a new baseline.

The band can perform an initial categorization of the muscles involved in the contraction by being placed over the muscles targeted. The difference between signals showed that muscles expand differently during specific contraction meaning that with proper processing of the signal, different muscles can be read with the sensor. However, the difference is not remarkable, and a

better classification could be performed with the assistance of additional sensors such as EMG, FSR or additional bands.

The assessment of the sensor in different subjects suggests that the band can detect the muscle activity. The similarity in behavior between the FMG signal and the force model indicates that the FMG, due to its robustness, could detect the force exerted by the muscle according to the model presented. If the behavior of the band could be compared with a more complex musculoskeletal model of the upper arm representing the change in force due to muscular activity, would be possible to test if the FMG band is reliable to detect the force exerted by the arm when contracted.

Finally, the experiment showed a relation between the size of the arm of each subject and the performance of the band, since subjects with more muscular volume showed better results during the readings. These results were not exclusive of the FMG sensor since the EMG sensor also acquired better signals, which could mean that more muscle fibers were activated through the tasks performed. Nevertheless, this relation could also be caused due to movement artifacts from the cables and the electrode which can be neglected with a design of the band able to maintain the wires in one position and a standardization of the protocol to attach the band to the body.

Chapter 6

Conclusions

The research of new technologies to detect and process biosignals is a growing field. So more devices will be soon developed towards using information from the human body to interact with the surroundings.

Developing an FMG sensor utilizing 3D printing fabrication brings a piece of information to the biomedical and the manufacturing field. The project presented in this report concerns the production of a band utilizing FMG to detect muscle contractions of the arm. The initial prototypes of this sensor mark the initial point to the new developments of sensors using FMG techniques. Even though EMG is a more established technology in the biosensors field being studied for several years, the sensor designed seem to give useful information regarding the muscle contraction with many possible advantages and the possibility of improvements.

The band is fabricated using two flexible TPU plastics a dielectric one (NinjaFlex) used as a base for the band and a conductive TPU to introduce the sensing technologies desired in the sensor. The band utilizes the strain gauge as the main sensor to detect the stretching of the band and is fully adaptable to the studied muscles of the arm. Different experiments showed that the band could detect the increase in muscle activity by measuring the resistance of the strain gauges during the increment in cross-sectional area of the arm muscles. The more the muscle is contracted, the more is the change in CSA. The FMG band was capable of fulfilling the tasks it was designed for.

Comparison of the FMG sensor readout with the EMG signals showed a high correlation between both. For a better understanding of the movements performed, the signals were studied against the force model of the movement from the arm under different loading conditions. The result of the analysis demonstrated a similarity in the behavior of the FMG sensor and the force modeled for isokinetic and isometric experimentation. The 3D printed FMG sensor establishes an advantage concerning standard FMG sensors when customization is required being able to adapt to the size and form of the users arm. The 3D printed band is more comfortable and allows to use it a longer time without inconvenience. The electro-mechanical connectors can be adapted to the band to reduce the bulkiness of the sensor and ease its electrical interface. The sensor-band can provide various gauges directly printed into the band to allow the simultaneous detection of various muscles and allows for the categorization according to the level of activation. Generally, 3D printing technology allows a cheap and faster alternative for personalized sensors with considerable advantages in the field of manufacturing and feature richness of devices.

This first prototype of the sensor developed in this thesis work raised the expectations for future devices using FMG technology. Changes in design and manufacturing can help to improve the performance and interface of the sensor. Using FMG as an alternative to sensing biosignals, allows obtaining a more robust indicator of muscle activity which reduces the post-processing work on the signal and increases the similarity with the musculoskeletal system behavior.

The FMG sensor-band may be able to measure muscles in different limbs, but much less, or not at all to measure activities of internal muscles since they do not allow to have a band around them.

6.1 Future Work

The primary purpose of this project was to confirm the use of 3D printed force sensors to detect muscle activity. Even after proof, there are different improvements to the designed model that can be suggested.

3D printing is an open hardware technology that allows improving rapidly in materials and manufacturing. The materials used for this sensors are likely to be obsolete in the next few months. More flexible materials, as well as more conductive ones, are being developed at this moment; thus utilization of different materials or a combination of those, likely generate a more accurate and comfortable device. The behavior of the conductive material is the base of the sensor since it is adapted to the skin of the user and reacts to the movements of the muscle.

With an accurate device, it is possible to adapt the sensor to different areas of the body where there are more muscles activated at the same time. One example is the forearm, even if it changes its cross-sectional area uniformly when contracted, the forearm contains all the flexor and extensor muscles that allow movement in the hands and the wrist joint. Categorizing each muscle when activated independently can develop a more useful sensor for further applications.

One of these applications is the movement classification. Detecting each muscle when activated helps to detect precise movements. For instance, the pinch strength is related to the level of muscle fibers recruitment, each movement of the musculoskeletal system has a different muscle activation, which, when detected with the proper techniques can help to classify the movements of the human body.

Improving the design of the sensor may also be helpful to counter the effects of movement artifacts, allowing the wires to be part of the band to reduce movement and therefore undesired noise in the signal.

Finally, adding a different printed sensor technology is also possible. E.g., by integrating FMG and EMG sensors in one band. Different sensors can fulfill different purposes during the detection of the muscle signals. Or even in sensing the interaction with the surroundings. 3D printing broadens the field of biosensing by allowing the devices to adapt to the shape of the human body and its environment.

Bibliography

- [1] R. L. Lieber and S. R. Ward. Skeletal muscle design to meet functional demands. *Philosophical Transactions of the Royal Society B: Biological Sciences*, 366(1570):1466–1476, 2011. vi, 6
- [2] Open Music Labs. Open Music Labs, 2016. Available at <http://www.openmusiclabs.com/learning/sensors/fsr/index.html>. vi, 9
- [3] J M Winters and P E Crago. *Biomechanics and Neural Control of Posture and Movement*. Springer New York, 2000. vi, 16, 17
- [4] Felix E. Zajac. Muscle and tendon: properties, models, scaling, and application to biomechanics and motor control., 1989. vi, 17, 18, 20, 21
- [5] Brian A. Garner and Marcus G. Pandy. Musculoskeletal Model of the Upper Limb Based on the Visible Human Male Dataset. *Computer Methods in Biomechanics and Biomedical Engineering*, 4(2):93–126, 2001. vi, vi, 18, 19, 21
- [6] DIABASE Engineering. Flexion Extruder. Available at <https://flexionextruder.com/>. vii, 32
- [7] Xianta Jiang, Lukas-karim Merhi, Zhen Gang Xiao, and Carlo Menon. Exploration of Force Myography and surface Electromyography in hand gesture classification. *Medical Engineering and Physics*, 41:63–73, 2017. 1, 9
- [8] R Drake, A W Vogl, and A W M Mitchell. *Gray's Anatomy for Students E-Book*. Gray's Anatomy. Elsevier Health Sciences, 2014. 4, 5, 6
- [9] Wendy M Murray, Thomas S Buchanan, and Scott L Delp. The isometric functional capacity of muscles that cross the elbow. 33, 2000. 5
- [10] E P Widmaier, H Raff, and K T Strang. *Vander's human physiology: the mechanisms of body function*. McGraw-Hill, 2006. 6
- [11] L. a. Spyrou and N. Aravas. Muscle and Tendon Tissues: Constitutive Modeling and Computational Issues. *Journal of Applied Mechanics*, 78(4):041015, 2011. 6
- [12] Mi Pitman. Biomechanics of skeletal muscle. *Biomechanics of the Musculoskeletal*, pages 45–68, 1989. 7
- [13] P.W. Brand, R.B. Beach, and D.E. Thompson. Relative tension and potential excursion of muscles in the forearm and hand. *The Journal of Hand Surgery*, 6(3):209–219, may 1981. 7
- [14] X. Hu, W. M. Murray, and E. J. Perreault. Muscle short-range stiffness can be used to estimate the endpoint stiffness of the human arm. *Journal of Neurophysiology*, 105(4):1633–1641, 2011. 7
- [15] V.M. Zatsiorsky. *Kinetics of Human Motion*. Human Kinetics, 2002. 8

-
- [16] X. Hu, W. M. Murray, and E. J. Perreault. Muscle short-range stiffness can be used to estimate the endpoint stiffness of the human arm. *Journal of Neurophysiology*, 105(4):1633–1641, 2011. 8
- [17] Roberto Merletti and Loredana R. Lo Conte. Surface EMG signal processing during isometric contractions. *Journal of Electromyography and Kinesiology*, 7(4):241–250, 1997. 8, 56
- [18] J.R. Cram, G.S. Kasman, and J. Holtz. *Introduction to Surface Electromyography*. Introduction to Surface Electromyography. Aspen Publishers, 1998. 8, 55
- [19] Ashkan Radmand, Erik Scheme, and Kevin Englehart. High-density force myography: A possible alternative for upper-limb prosthetic control. *Journal of Rehabilitation Research & Development*, 53(4), 2016. 8, 14
- [20] Artem Dementyev and Joseph A Paradiso. WristFlex : Low-Power Gesture Input with Wrist-Worn Pressure Sensors. pages 161–166, 2014. 8, 38, 59
- [21] Nan Li, Dapeng Yang, Li Jiang, Hong Liu, and Hegao Cai. Combined Use of FSR Sensor Array and SVM Classifier for Finger Motion Recognition Based on Pressure Distribution Map. *Journal of Bionic Engineering*, 9(1):39–47, 2012. 8, 14, 40
- [22] S I Yaniger. Force Sensing Resistors: A Review Of The Technology, 1991. 9, 10
- [23] Richard M Crowder. Sensors: Touch, force, and torque. *Handbook of Industrial Automation, RL Shell and EL Hall, Editors*, pages 377–392, 2000. 9, 38
- [24] C C Perry and H R Lissner. *The strain gage primer*. McGraw-Hill, 1962. 11
- [25] W M Murray and W R Miller. *The Bonded Electrical Resistance Strain Gage: An Introduction*. Oxford University Press, 1992. 11, 35
- [26] Aglient Technologies Inc. Practical Strain Gage Measurements. *Strain Gages*, page 102, 1999. 11
- [27] North Allen and Hubbell Incorporated. Effects of Current on the Human Body Effects of Current on the Human Body. pages 101–117, 2010. 11, 36
- [28] Mohammad Taufik and Prashant K. Jain. Role of build orientation in layered manufacturing: a review. *International Journal of Manufacturing Technology and Management*, 27(1/2/3):47, 2013. 12
- [29] J. P. Kruth. Material Incess Manufacturing by Rapid Prototyping Techniques. *CIRP Annals - Manufacturing Technology*, 40(2):603–614, 1991. 12
- [30] J.-P. Kruth, M.C. Leu, and T. Nakagawa. Progress in Additive Manufacturing and Rapid Prototyping. *CIRP Annals - Manufacturing Technology*, 47(2):525–540, 1998. 12
- [31] David Bak. Rapid prototyping or rapid production? 3D printing processes move industry towards the latter. *Assembly Automation*, 23(4):340–345, 2003. 12
- [32] S. K. Singhal, Prashant K. Jain, and Pulak M. Pandey. Adaptive slicing for SLS prototyping. *Computer-Aided Design and Applications*, 5(1-4):412–423, 2008. 12
- [33] R Melnikova, A Ehrmann, and K Finsterbusch. 3D printing of textile-based structures by Fused Deposition Modelling (FDM) with different polymer materials. *IOP Conference Series: Materials Science and Engineering*, 62:012018, 2014. 12
- [34] S. K. Singhal, Prashant K. Jain, Pulak M. Pandey, and A. K. Nagpal. Optimum part deposition orientation for multiple objectives in SL and SLS prototyping. *International Journal of Production Research*, 47(22):6375–6396, 2009. 12

- [35] Mark Richardson and Bradley Haylock. Designer / Maker : The Rise of Additive Manufacturing , Domestic-Scale Production and the Possible Implications for the Automotive Industry. (2):33–48, 2012. 13
- [36] Simon J. Leigh, Robert J. Bradley, Christopher P. Purssell, Duncan R. Billson, and David A. Hutchins. A Simple, Low-Cost Conductive Composite Material for 3D Printing of Electronic Sensors. *PLoS ONE*, 7(11):1–6, 2012. 13
- [37] NinjaTek. NinjaFlex Flexible 3D Printing Filament — NinjaTek. Available at <https://ninjatek.com/products/filaments/ninjaflex/>. 13
- [38] MakeShaper. X60 Ultra-Flexible Filament Black — Flexion Extruder. Available at <https://flexionextruder.com/shop/x60-ultra-flexible-filament-black/>. 13
- [39] Palmiga Innovation. Rubber 3D Printing - Conductive & Flexible 3D printing filament. Available at <http://rubber3dprinting.com/>. 13, 24
- [40] Sam L Phillips and William Craelius. Residual kinetic imaging: a versatile interface for prosthetic control. *Robotica*, 23(3):277–282, 2005. 14, 40
- [41] D Yungher and W Craelius. Discriminating 6 Grasps Using Force Myography of the Forearm. *Department of Biomedical Engineering, Rutgers, The State University of New Jersey*, page 2003, 2003. 14
- [42] Renato Vidoni and Carlo Menon. Force Myography to control robotic Upper extremity Prostheses : a Feasibility study. 4(March):1–12, 2016. 14, 59
- [43] Claudio Castellini and Vikram Ravindra. A wearable low-cost device based upon Force-Sensing Resistors to detect single-finger forces. pages 199–203, 2014. 14, 40
- [44] Nancy Salter. Methods of measurement of muscle and joint function. *Bone & Joint Journal*, 37-B(3):474–491, 1955. 14, 38
- [45] Zhen G Xiao and Carlo Menon. Towards the development of a wearable feedback system for monitoring the activities of the upper-extremities. *Journal of neuroengineering and rehabilitation*, 11:2, 2014. 14
- [46] F C T van der Helm. Large-scale musculoskeletal systems: sensorimotor integration and optimization. *Biomechanics and Neural Control of Posture and Movement*, pages 407–424, 2000. 16
- [47] Cs. Fazekas, Gy. Kozmann, and K.M. Hangos. *Hierarchical Modelling in Biology: Systematic Building of Limb Models*, volume 38. IFAC, 2005. 16, 17
- [48] J. W. Holmes. Teaching from classic papers: Hill’s model of muscle contraction. *AJP: Advances in Physiology Education*, 30(2):67–72, 2006. 16
- [49] A. M. Gordon, A. F. Huxley, and F. J. Julian. The variation in isometric tension with sarcomere length in vertebrate muscle fibres. *The Journal of Physiology*, 184(1):170–192, 1966. 18
- [50] Bruce Bukiet. Mathematical Analysis of Applied loads on skeletal muscles During Manual Therapy. *Journal of the American Osteopathic Association*, (June 2017), 2008. 20
- [51] S. A. Kruse, J. A. Smith, A. J. Lawrence, M. A. Dresner, A. Manduca, J. F. Greenleaf, R. L. Ehman, S. A. Kruse, J. A. Smith, A. J. Lawrence, M. A. Dresner, A. Manduca, and J. F. Greenleaf. Tissue characterization using magnetic resonance elastography: preliminary results*. *Physics in Medicine and Biology*, 45:1579–1590, June 2000. 20

-
- [52] Sebastian Papazoglou, Jürgen Braun, Uwe Hamhaber, and Ingolf Sack. Two-dimensional waveform analysis in MR elastography of skeletal muscles. *Physics in Medicine and Biology*, 50(6):1313–1325, 2005. 20
- [53] Ryota Akagi, Soichiro Iwanuma, Satoru Hashizume, Hiroaki Kanehisa, Tetsuo Fukunaga, and Yasuo Kawakami. Determination of Contraction-Induced Changes in Elbow Flexor Cross-Sectional Area for Evaluating Muscle Size-Strength Relationship During Contraction. *Journal of Strength and Conditioning Research*, 29(6):1741–1747, 2015. 21
- [54] J. E. Wood, S. G. Meek, and S. C. Jacobsen. Quantitation of human shoulder anatomy for prosthetic arm control-II. Anatomy matrices. *Journal of Biomechanics*, 22(4):309–325, 1989. 21
- [55] Philippe Favre, Ralph Sheikh, Sandro F. Fucntese, and Hilaire A.C. Jacob. An algorithm for estimation of shoulder muscle forces for clinical use. *Clinical Biomechanics*, 20(8):822–833, 2005. 21
- [56] Steven L. Peterson and Ghazi M. Rayan. Shoulder and upper arm muscle architecture. *Journal of Hand Surgery*, 36(5):881–889, 2011. 21
- [57] Jin Jong Chen. *Quantitative architectural analysis of human upper-extremity muscles*. PhD thesis, University of Virginia, 1988. 21
- [58] R.W. Bassett, A.O. Browne, B.F. Morrey, and K.N. An. Glenohumeral muscle force and moment mechanics in a position of shoulder instability. *Journal of Biomechanics*, 23(5):405 – 415, 1990. 21
- [59] Jack M. Winters and Lawrence Stark. Estimated mechanical properties of synergistic muscles involved in movements of a variety of human joints. *Journal of Biomechanics*, 21(12):1027 – 1041, 1988. 21
- [60] A A Amis, D Dowson, and V Wright. Muscle strengths and musculoskeletal geometry of the upper limb. *Engineering in Medicine*, 8(1):41–48, 1979. 21
- [61] W A Weijts and B Hillen. Cross-Sectional Areas and Estimated Intrinsic Strength of the Human Jaw Muscles. *Acta morphologica neerlando-Scandinavica*, 23(3):267–274, 1985. 21, 22, 23
- [62] John R. Cameron John R. Cameron, James G. Skofronick, Roderick M. Grant. Muscle and Forces. *Physics of the Body*, pages 37–84, 1999. 23, 58
- [63] William K. Durfee and Karen I. Palmer. Estimation of Force-Activation, Force-Length, and Force-Velocity Properties in Isolated, Electrically Stimulated Muscle. *IEEE Transactions on Biomedical Engineering*, 41(3):205–216, 1994. 23
- [64] Edwin A. Peraza Hernandez, Darren J. Hartl, Ergun Akleman, and Dimitris C. Lagoudas. Modeling and analysis of origami structures with smooth folds. *CAD Computer Aided Design*, 78:93–106, 2016. 24
- [65] F C T van der Helm. Large-scale musculoskeletal systems: sensorimotor integration and optimization. *Biomechanics and Neural Control of Posture and Movement*, pages 407–424, 2000. 24
- [66] John G. Webster, John W. Clark, Michael R. Neuman, Walter H. Olson, Robert A. Peura, Frank P. Primiano, Melvin P. Siedband, and Lawrence A. Wheeler. Medical instrumentation: Application and design. *Control Engineering Practice*, page 296, 2010. 29
- [67] FlashForge Corporation. Creator Pro 3D Printer FlashForge 3D Printers, 2016. Available at <http://www.flashforge.com/creator-pro-3d-printer/>. 32

- [68] Keithley Instruments. Model 2000 Multimeter User's Manual, 2003. 37
- [69] Interlink Electronics. Interlink Electronics Inc., FSR integration Guide and Evaluation parts catalog with suggested Electrical interfaces. *Version 1.0, 90-45632 Rev. D, 2007.*, 1.0,:1–26, 2007. 38
- [70] U. Thongudomporn, P. Smithmaitrie, V. Chongsuvivatwong, and A.F. Geater. Design and evaluation of a Force Sensing Resistor based bite force measuring device. *International Journal of Biomedical Engineering and Technology*, 4(1):78–87, 2010. 38
- [71] F. Gemperle, C. Kasabach, J. Stivoric, M. Bauer, and R. Martin. Design for wearability. *Digest of Papers. Second International Symposium on Wearable Computers (Cat. No.98EX215)*, pages 116–122, 1998. 40
- [72] J. Craik. *The Face of Fashion: Cultural Studies in Fashion*. Routledge, 1994. 41
- [73] Z. Budrovic. Plastic Deformation with Reversible Peak Broadening in Nanocrystalline Nickel. *Science*, 304(5668):273–276, 2004. 47
- [74] Delsys Inc. Delsys Trigno Wireless EMG, 2017. Available at <http://www.delsys.com/products/wireless-emg/>. 55
- [75] Li Zhongshen. The design of butterworth lowpass filter based on matlab [j]. *Heilongjiang Electronic Technology*, 3:017, 2003. 55
- [76] John D Rhodes and SA Alseyab. The generalized chebyshev low-pass prototype filter. *International Journal of Circuit Theory and Applications*, 8(2):113–125, 1980. 55
- [77] James F Zolman. *Biostatistics: experimental design and statistical inference*. Number QH323. 5. Z64 1993. 1993. 57, 62

Appendix A

Experimental Protocol

Measurement Proposal

Assessment of 3D printed FMG sensor

Principal researcher: Gijs Krijnen (gijs.krijnen@utwente.nl)

Researcher: Eric Perez (e.a.perezlorea@student.utwente.nl)

Introduction

Currently, the most used sensor to detect muscle signals from the human body are the Electromyography (EMG) Sensors; they are reliable, cheap and easy to use. Finding new alternatives to improve the signal acquisition and ease the signal processing is one of the objectives of the biomedicine nowadays. 3D printing technology has revolutionized the manufacturing field, allowing the users to obtain customized devices with comfortable and useful designs. Utilizing the 3D printing expands the field of techniques used to produce and manufacture sensors. One of them is the Force Myography (FMG), exploiting the flexible polymers is possible to manufacture force sensitive sensors (FSS), furthering its applications and interfacing with actuators and transducers.

Goal and Research Questions

This research focuses in to develop an FSS to detect the muscle contraction as an alternative to EMG sensors by means of FMG.

Research Questions

- Is it possible to relate the change in resistance of the sensor with the increase in cross section of the upper arm?
- Are the signals from FMG comparable to the ones obtained from EMG?
- Does the type of contraction be related to the variation of resistance of the sensor?
- Is repeatability present during the measurements?

Subjects

For this research subjects, adults (18+) can volunteer, subjects can withdraw from the research at any moment without stating any reason.

Exclusion Criteria

Subjects with reported injuries or disease to their arms, cognitive disabilities or history of skin allergies or sensitivity to cosmetic products cannot participate in this study.

Materials

- Printed FSS Band
- EMG sensor and Electric Interface
- Multimeter Keithley Model 2000
- Wires/Clamps
- Laptop Computer
- Weights (1kg to 5kg)

Measurement Setup

Printed FSS Band

The band showed in Figure 1 is the sensor used during the procedure. The band is printed using two flexible materials, conductive TPU (Black) and dielectric TPU (Orange or Transparent). The band is self-secured with the included strap. The sensor was manufactured utilizing an FDM 3D multi-material printer. The flexible thermoplastic polyurethane (TPU) utilized is NinjaFlex, manufactured by NinjaTek, Manheim, USA. The black material used in the band is a flexible electrical conductive TPU filament PI-ETPU 95-250 fabricated by Palmiga Innovation, Sweden.



Figure 1 FSS Band manufactured with flexible TPU, conductive (Black) dielectric (Orange).

EMG Sensors

Ag/AgCl Electrodes will be used to determine the EMG signals. The electrodes will be connected to the upper part of the bicep muscle, just above the correct positioning for the band. A reference electrode will be connected at the elbow or at the wrist bone of the same arm where the skin is thinner, and the bones are more prominent.

Multimeter

To acquire the data a multimeter Keithley Model 2000 shown in Figure 2 will be used to perform a 4W measurement, applying a constant current to the conductive material while measuring the change in voltage due to elongation. The data will be processed by a MatLab interface to acquire the voltage during the procedure. The MatLab program will monitor the voltage changes while the sensor is being stretched.



Figure 2 Multimeter Keithley Model 2000 used to measure the change in resistance.

EMG Interface

The electrodes of the EMG will be connected to an electrical interface that processes the signal and sends it via USB to a computer. A MatLab software will process the information and show the data necessary. The script is designed to obtain both signals (FMG and EMG) simultaneously.

Measurement Procedure.

During the measurements, muscle contraction will be tested. A sensor-band will be attached to the upper arm of the subject. Since the base of the material is NinjaFlex (a dielectric TPU), there is no direct contact with any conductive part of the sensor. The band will be connected to a digital multimeter Keithley Model 2000 that will provide no more than $1 \mu\text{A}$ to the band, varying the voltage in a range between 5V and 1V depending on the resistance change, this value is harmless for the human body, however in case of any discomfort the procedure can be stopped immediately.

The protocol of measurements is divided into two parts and states as follows:

Isometric Measurement

During the isometric measurement, the subject's arm will remain flexed at 90° supporting a weight bar. The measure will start without the weight and it will be changing to three different weights, 1kg, 3kg and 5kg.

Isokinetic Measurement

During the isokinetic measurement, the user will perform a series of 3 movements at 3 different velocities, from the completely extended arm ($\approx 180^\circ$) to completely flexed ($\approx 45^\circ$), the weight will increase from 1kg up to 5 kg.

Trial measurements can be performed in order to understand correctly the task and to test the measurement system before the procedure. The multimeter will be set up with a MatLab interface recording the measurements while performing the tasks.

The procedure will be performed in adults (18+) without any skin allergies or sensitivity to cosmetic products. Subjects are free to quit the research at any time without stating a reason.

Data acquired

The data will be acquired by a Multimeter Keithley Model 2000 and processed by an interface utilizing MatLab. The data will be saved utilizing the subject number without any personal data. The file .mat will contain information about the current applied to the device, the voltage read and the time of the measurements.

Risks

During measurements, a voltage is applied to the conductive material, even if the material is not in direct contact with the skin and it's a harmless value in case of any discomfort the measurement is stopped immediately.

The skin of the subject will be only in contact with the NinjaFlex material which is not likely to result in irritation in solid form or any other potential health effects¹.

[1] "Safety Data Sheet NinjaFlex 3D Printing Filament", 2016 <https://ninjatek.com/wp-content/uploads/2016/05/SDS-NinjaFlex-rev0.pdf>

Appendix B

Ethical Committe Documents

Information Letter

Assessment of 3D printed FMG sensor

Dear reader,

In this letter, we would like to inform you about the research you have applied to participate in. The experiment entitled "Assessment of 3D printed FMG sensor" is part of the proposed research "3D printed sensor to detect muscle contraction by means of Force Myography", and is focused on the measurement of muscle activity.

Note: As a volunteer, you are free to withdraw from the study without any reason stated at any time.

Objective of the study

Muscle contraction is present in every movement of the human body, managing the signal by means of any acquisition device increases the purposes of its use in different actuators. The 3D printed sensor used in this evaluation detects by means of FMG the signal of the muscle.

The aim of this research is to evaluate the performance of the 3D printed sensor in different subjects to determine its reproducibility regarding the results and its reliability.

Description of the experiment

During the study, measurements of your muscle contraction will be tested. In this measurements, a sensor-band will be attached to your upper arm. The band will be connected to a digital multimeter Keithley Model 2000 that will provide no more than 1 μ A to the band, varying the voltage in a range between 5V and 1V DC depending on the resistance changes, this value is harmless for the human body and the base of the band is made of dielectric material which means no current will be in direct contact with your skin. However, in case of any discomfort, the procedure can be stopped immediately.

The measurements consist of two parts: isometric and isokinetic. During the isometric measurement, the arm will remain in a flexed position around 90° supporting a weight that will increase three times. The isokinetic measurement will be 3 measurements increasing weight at 3 different velocities, moving the arm from a non-bent (180°) to a completely-bent (45°) position.

There is a programmed rest between both measurements up to 5 minutes, and the band can be readjusted to avoid misreading the signal.

On the other hand, EMG electrodes will be allocated near the band to read the muscle's signal and a reference electrode near the elbow or the wrist bone depending on your comfort.

Risks

During measurements, a voltage is applied to the conductive material, even if the material is not in direct contact with the skin and it's a harmless value in case of any discomfort the measurement will stop immediately.

Subjects

For this research subjects, adults (18+) can volunteer, subjects can withdraw from the research at any moment without stating any reason.

Exclusion Criteria

Subjects with reported injuries or disease to their arms, cognitive disabilities or history of skin allergies or sensitivity to cosmetic products cannot participate in this study.

Data acquired

The data will be acquired by a Multimeter Keithley Model 2000 and processed by an interface utilizing MatLab. The data will be saved utilizing the subject number without any personal data. The file .mat will contain information about the voltage applied to the device, the current read and the time of the measurements.

Questions?

If you have any questions regarding the procedure, please do not hesitate to contact the researchers by asking in person or via email to Eric Perez (e.a.perezlorea@student.utwente.nl) or Gijs Krijnen (gijs.krijnen@utwente.nl).

Kind regards,

Eric Perez
NIFTY Group
University of Twente
e.a.perezlorea@student.utwente.nl
Tel: +31 (0) 6482244209

Informed Consent

Assessment of 3D printed FMG sensor

I hereby declare that I have been informed in a manner which is clear to me about the nature and method of the research as described in the information letter.

I am 18 years or older, and I have been informed about the requirements regarding skin allergies and/or sensitivity to cosmetic products. My questions have been answered to my satisfaction. I agree of my own free will to participate in this research.

I reserve the right to withdraw this consent without stating any reason, and I am aware that I may withdraw the experiment at any time. If my research results are to be used in scientific publications or made public in any other manner, then they will be made completely anonymous. My personal data will not be disclosed to third parties without my express permission.

If I request further information about the research, now or in the future, I may contact: Eric Perez (e.a.perezlorea@student.utwente.nl) or Gijs Krijnen (gijs.krijnen@utwente.nl).

If you have any complaints about this research, please direct them to the Acting Secretary of the Ethics Committee of the Faculty of Electrical Engineering, Mathematics and Computer Science (EWI) at the University of Twente, Drs. Jorien van Loon, P.O. Box 217, 7500 AE Enschede (NL), telephone: +31 (0) 53-4893748.; email: j.vanloon@utwente.nl.

Name of the Subject: _____

Date: _____ Signature: _____

I have provided explanatory notes about the research. I declare myself willing to answer to the best of my ability any questions which may still arise about the research.

Name of researcher: _____

Date: _____ Signature: _____

Appendix 6. Checklist for submitting a research proposal to the Ethics Committee

(See Chapter 3)

Checklist for the principal researcher when submitting a request to the EC or the EC member for an assessment of the ethical permissibility of a research proposal

1. General

1. Title of the project:
2. Principal researcher (with doctoral research also a professor):
3. Researchers/research assistants (PhD students, students etc. where known):
4. Department responsible for the research:
5. Location where research will be conducted:
6. Short description of the project (about 100 words):
7. Expected duration of the project and research period:
8. Number of experimental subjects:
9. EC member of the department (if available):

2. Questions about fulfilled general requirements and conditions

1. Has this research or similar research by the department been previously submitted to the EC?
 Yes,
 No
If yes, what was the number allocated to it by the EC?
Explanatory notes:
2. Is the research proposal to be considered as medical research (Also see Appendix 4)
 Yes
 No
 Uncertain
Explanatory notes:
3. Are adult, competent subjects selected? (§3.2)
 Yes, indicate in which of the ways named in the general requirements and conditions this is so
 No, explain
 Uncertain, explain why
Explanatory notes:
4. Are the subjects completely free to participate in the research, and to withdraw from participation whenever they wish and for whatever reason? (§3.2)
 Yes
 No, explain why not
 Uncertain, explain why
Explanatory notes:
5. In the event that it may be necessary to screen experimental subjects in order to reduce the risks of adverse effects of the research: Will the subjects be screened? (§3.4)
 Screening is not necessary, explain why not
 Yes, explain how
 No, explain why not
 Uncertain, explain why
Explanatory notes:

6. Does the method used allow for the possibility of making an accidental diagnostic finding which the experimental subject should be informed about? (§3.6 and Appendix 4)
- No, the method does not allow for this possibility
- Yes, and the subject has given signed assent for the method to be used
- Yes, but the subject has not given signed assent for the method to be used
- Uncertain, explain why
- Explanatory notes:
7. Are subjects briefed before participation and do they sign an informed consent beforehand in accordance with the general conditions? (§3.2, §3.3, §3.7, §3.8)
- Yes, attach the information brochure and the form to be signed
- No, explain why not
- Uncertain, explain why
- Explanatory notes:
8. Are the requirements with regard to anonymity and privacy satisfied as stipulated in (§3.8)?
- Yes
- No, explain why not
- Uncertain, explain why
- Explanatory notes:
9. If any deception should take place, does the procedure comply with the general terms and conditions (no deception regarding risks, accurate debriefing) (§3.10)?
- No deception takes place
- The deception which takes place complies fully with the conditions (explain)
- The deception which takes place does not comply with the conditions (explain)
- If deception does take place, attach the method of debriefing
- Explanatory notes:
10. Is it possible that after the recruitment of experimental subjects, a substantial number will withdraw from participating because, for one reason or another, the research is unpleasant? (§3.5)
- No
- Yes, that is possible
- If yes, then attach the recruitment text paying close attention to what is stated about this in the protocol.
- Explanatory notes:

3. Questions regarding specific types of standard research

Answer the following questions based on the department to which the research belongs.

11. Does the research fall **entirely** under one of the descriptions of standard research as set out in the described standard research of the department? (Chapter 4)
- Yes, go to question 12
- No, go to question 13
- Uncertain, explain what about, and go to question 13
- Explanatory notes:
12. If yes, what type of research is it? Give a more detailed specification of parts of the research which are not mentioned by name in this description (for example: What precisely are the stimuli? Or: What precisely is the task?)
13. If no, or if uncertain, give as complete a description as possible of the research. Refer where appropriate to the standard descriptions and indicate the differences with your research. In any case, all possible relevant data for an ethical consideration should be provided.

Checklist

1. General

1. *Title of the project*

3D Printed sensor to detect muscle contraction by means of Force Myography

2. *Principal Researcher (with doctoral research also a professor)*

Gijs Krijnen (gijs.krijnen@utwente.nl)

3. *Researchers/research assistants*

Eric Perez (e.a.perezorea@student.utwente.nl)

4. *Department responsible for the research*

EWI/ EE / RAM

5. *Location where research will be conducted*

University of Twente

6. *Short description of the project*

Using the versatility of the 3D printing, it is possible to design devices to work as an alternative of the currently developed. Force Myography as an alternative sensing to recognize movement is relevant due to its robustness while detecting signals. The goal of this research is to assess the functioning of the 3D printed sensor designed. The sensor was printed utilizing a multi-material FDM 3D printer utilizing flexible polymers, one of that conductive material. The band-like structure is placed around the upper arm while the user produces different movements, the analysis in a change of current will determine the usefulness of the sensor.

7. *Expected duration of the project and research period*

The research period will take around one hour, the duration of the project will be until September 2017.

8. *Number of experimental subjects*

5 to 10 subjects.

9. *EC Member of the department (if available)*

No EC member available at RAM

2. Questions about fulfilled general requirement and conditions

1. No

2. No

3. Yes, the subjects are healthy, adult (18 years or older) and mentally competent volunteer, who voluntarily participates in the trial. Subjects will not have a history of skin allergies or sensitivity to cosmetic products. And they will be informed of the procedure while signing an informed consent and reading the information letter.

4. Yes

5. Screening is not necessary; the subjects will be asked before if they fulfill the skin requirements.

6. No

7. Yes

8. Yes

9. No deception takes place

10. No

3. Questions regarding specific types of standard research

11. No, go to question 13

12. –

13. The attached document will describe the research.